

Development of a Dual Ionization Source Time-of-Flight Mass Spectrometer for Gas Chromatography

Dissertation

Zur Erlangung des akademischen Grades
Doktor der Naturwissenschaften (Dr. rer. nat.)

Vorgelegt von

Steffen Bräkling

Bergische Universität Wuppertal
Fakultät für Mathematik und Naturwissenschaften
Physikalische und Theoretische Chemie

Wuppertal, November 2022

Erklärung

Ich versichere, dass ich die von mir vorgelegte Arbeit selbständig und andere als die angegebenen Hilfsmittel nicht benutzt sowie jede wörtlich oder inhaltlich übernommene Stelle kenntlichgemacht habe.

Wuppertal, 11.11.2022

Steffen Bräkling

Acknowledgement

In the first place, I want to thank everyone who accompanied me during my studies and on the way to completing this dissertation. Of particular note:

Dr. Sonja Klee for initiating this project and for supervising this thesis.

Dr. Hendrik Kersten for his valuable inputs and support while supervising this work.

Prof. Dr. Thorsten Benter for the support during this work and the chance to be part of his group.

TOFWERK and employees for the extensive support of this project.

The European Union's Horizon 2020 research and innovation program under the Marie Skłodowska-Curie grant agreement No 764991 is gratefully acknowledged for the financial support.

Abstract

Non-targeted analysis (NTA) using gas chromatography (GC) coupled to mass spectrometry (MS) is not widely established, compared to methods using liquid chromatography (LC) as the pre-separation. This can mainly be explained by the instrumentation and ionization mechanism used: along with the many advantages of using electron ionization (EI), a major drawback is the frequent absence of the molecular ion. The generation of the molecular ion or equal information (e.g., the protonated molecule) is necessary for unknown compound identification, but often requires additional experiments and measurements using other ionization techniques. This work describes the development, characterization, and use of a time-of-flight mass spectrometer (TOFMS) operating two ion sources simultaneously: an EI- and a chemical ionization (CI) source. The instrument was designed for use in combination with a GC. The GC effluent is split equally to both ionization sources. Compounds eluting from the GC can be measured within a distinct time window with both ionization techniques, during a single chromatographic separation step. In most cases, this results in the instantaneous acquisition of CI information in addition to the EI information. The EI and CI data collected thus are highly complementary. Together, they deliver both the common EI fragment spectrum (useable for library comparisons), and precursor ion information from e.g., the protonated molecule using CI. Due to the mass accuracy of the TOF mass analyser, the determination of empirical sum formulas of measured compounds becomes feasible. The CI source was specifically developed for this purpose. In contrast to conventional CI sources, a hydrogen plasma at 13 mbar is used for ion generation prior to the addition of reagent gas, thus obviating the need for a filament. This CI source allows for improved long-term stability and sensitivity compared to conventional low pressure CI sources. The ion source can be operated using various reagent gases, offering a very controlled variation of ionization selectivity and harshness due to a three-stage design. The improved performance of the system for compound identification in NTA is demonstrated by means of exemplary material outgassing measurements of an artificial leather part used within car interiors. Several example scenarios for improved compound identification using both EI and CI are presented for compounds that would otherwise yield equivocal and uncertain results in an EI only approach. Especially the availability of rapidly interchangeable CI reagents is of great value in the analysis of unknown samples. By design, the new system does not compromise standard methods, mainly

designed for EI, and is therefore compatible with most normed measuring regulations such as ISO16000-6:2011^[1] and ISO 12219-3:2012^[2].

Table of Contents

1 Aim of this work	1
2 Introduction and theoretical background	2
2.1 Gas chromatography coupled to mass spectrometry.....	2
2.2 Ionization sources	3
2.2.1 70 eV electron ionization	3
2.2.1.1 Mass spectral libraries.....	4
2.2.2 Soft ionization sources for GC-MS.....	5
2.2.2.1 Chemical ionization	5
2.2.2.2 Thermodynamics of proton-transfer reactions	7
2.2.2.3 The role of contamination in CI sources	8
2.2.2.4 Kinetics of proton transfer reactions	9
2.3 Non-targeted analysis.....	9
2.3.1 Non-targeted analysis using GC-MS.....	10
2.4 Measurement of the accurate molecular mass and TOF mass analyzers	11
3 Structure of this work.....	13
4 Experimental part.....	16
4.1 Mass spectrometer.....	16
4.2 Acquisition and post processing software.....	17
4.3 Gas chromatography and sampling.....	17
4.4 GC transfer.....	17
4.2 Chemicals.....	19
5 Cumulative part.....	20
5.1 Hydrogen plasma-based medium pressure chemical ionization source for GC-TOFMS .	20
5.1.1 Abstract	20
5.1.2 Introduction.....	21
5.1.3 Experimental	23
5.1.4 Results and discussion.....	26
5.1.4.1 Reagent ion distributions.....	26
4.1.4.2 The active reagent ion for the N ₂ system with low water content.....	29
5.1.4.3 Protonation vs photoionization and the role of the segmented quadrupole.....	31
5.1.4.4 Analyte fragmentation behavior.....	33
5.1.4.5 Chromatographic performance and sensitivity.....	35
5.1.4.6 Range of ionizable compounds	38
5.2.5 Conclusion	42

5.2 Parallel operation of electron ionization and chemical ionization using a single TOF mass analyzer	43
5.2.1 Abstract	43
5.2.2 Introduction	44
5.2.3 Experimental	45
5.2.4 Results and discussion.....	48
5.2.4.1 Chromatographic data alignment and GC column split characterization.....	48
5.2.4.2 Analytical performance	51
5.2.4.3 Spectrum quality for compound identification.....	51
5.2.4.4 Improved identification using EI and CI information	53
5.2.5 Conclusion and outlook.....	58
5.3 GC-CI&EI-TOFMS using permeation tube facilitated reagent ion control for material emission analysis.....	59
5.3.1 Abstract	59
5.3.2 Introduction	60
5.3.3 Experimental	61
4.3.3 Results and discussion.....	63
4.3.3.1 Reagent supply unit – control of the reagent ion distributions.....	63
5.3.3.2 Reagent supply unit – control of selectivity and degree of fragmentation.....	65
5.3.3.3 Enhanced compound identification with complementary EI and CI information.....	68
4.4 Conclusion.....	77
6 Summary	79
7 Literature	81
8 Appendix	96
8.1 Supporting information: Hydrogen plasma-based medium pressure chemical ionization source for GC-TOFMS.....	96
8.2 Supporting Information: Parallel operation of electron ionization and chemical ionization using a single TOF mass analyzer.....	106
8.3 Supporting Information: GC-CI&EI-TOFMS using permeation tube assisted reagent ion control for material emission analysis.....	113

List of Figures

- Figure 4.1.1: Schematic set up of the dual ionization source TOFMS during (A) EI mode and (B) CI mode.....16
- Figure 4.4.1: GC transfer design to the EI source including the flexible heated transfer line and the heated vacuum feedthrough.....18
- Figure 5.1.1: Schematic of the chemical ionization source mounted to the first pressure stage of the mass spectrometer including the segmented quadrupole of the first MS pressure stage (cf. MS interface section).....25
- Figure 5.1.2 Reagent ion distribution as function of ionization source pressure for the reagent gases (A) nitrogen, (B) isobutane and (C) methane.....27
- Figure 5.1.3: (A) Relative $[M+H]^+$ signal intensities of benzene and toluene sampled using GC separation at different ionization source pressures with N_2 with low water content as reagent gas. Signals were normalized to the benzene signal. Expected ratios calculated via reaction rate constants are plotted as dotted lines. Rate coefficients were taken from^[103,104]. (B) Reagent ion spectra using nitrogen with low water content as reagent gas at ion source pressures of 2 mbar and 13 mbar.....30
- Figure 5.1.4: (A) Protonated and (B) photoionized analyte in dependence of the first quadrupole RF voltage at different ionization source pressures. A continuous sample flow of 0.5 sccm of a 10 ppmV xylene gas mixture with N_2 as reagent gas was used.....32
- Figure 5.1.5: Pressure dependent α -pinene fragmentation behavior for (A) nitrogen, (B) isobutane and (C) methane as reagent gases. The measurements were performed with repeated GC injections of α -pinene. For comparable signal intensities, 100 pg and 2.5 ng on column injections were used for nitrogen and isobutane/methane as reagent gases, respectively.....33
- Figure 5.1.6: (A) Chromatographic peaks of multiple 100 pg benzophenone injections recorded over a period of six days. Each day represents an average of three injections. (B) Mass spectrum of a 100 pg benzophenone injection with nitrogen as reagent gas at 13 mbar ion source pressure.....35

Figure 5.1.7: TICs of 2.5 ng splitless injections of an EPA 8270 LCS mix using (A) nitrogen, (B) isobutane and (C) methane as reagent gas, respectively. The pie charts illustrate the amount of detected (blue) and not detected compounds (red).....	38
Figure 5.2.1: Schematic depicting of the dual ionization source GC-MS setup and normalized Total ion counts of the CI and EI signals during switched operation. A switching rate of 10 Hz is shown resulting in a 5 Hz temporal resolution for each ion source.....	46
Figure 5.2.2: (A) normalized extracted ion chromatograms (EIC)s of the $[M+H]^+$ signals from CI and the fragment at m/z 74 from EI for 1 ng on column of C_4 - C_{24} saturated carbon FAMES. (B) normalized mass-signal distributions of the FAMES standard, sampled from the CI and EI source, respectively. Intensities are indicated by the marker size.....	48
Figure 5.2.3: (A) Time deviation between CI and EI chromatogram for each FAME. (B) Measured column split ratios between CI and EI source for each FAME. In both data sets, three replicates were averaged, and the error bars indicate the respective standard deviation.....	50
Figure 5.2.4: (A) Mass accuracy of the $[M+H]^+$ signals from the CI source and (B) the accuracy of the natural isotopic abundance on the first isotopic peak $[(M+1)+H]^+$. (C) Fragment library matching scores (Match) and reversed matching scores (R Match) of the ion distributions from the EI source.....	52
Figure 5.2.5: Total ion chromatograms (TIC)s of (A) a custom-made carbonyl compound mix and (B) the headspace of a perfume sample.....	54
Figure 5.2.6: Enlarged chromatograms and mass spectra for three substances of the carbonylic standard mix. Chromatographic peaks of 100 pg on column (50 pg per ion source) of (A) 2-dodecanone (B) dodecanal and (C) 2-tridecanone, simultaneously recorded in CI and EI mode. Comparison of the acquired EI and CI mass spectra of (D) 2-dodecanone and (E) dodecanal and (F) 2-tridecanone.....	55

Figure 5.2.7: (A) Enlarged chromatogram of the brand perfume headspace sample. All EICs of the detected masses below the chromatographic peak at 1184 s retention time are depicted. The trace of the dominant protonated molecule in the CI mode at m/z 253 is shown in red. (B) Corresponding EI and CI mass spectra of the chromatographic peak at 1184 s.....	57
Figure 5.3.1: flow scheme of the instrumental MS set up.....	62
Figure 5.3.2: Reagent ion distributions generated using (A) RG1, (B) RG2, (C) RG3 and (D) RG4. (E) averaged proton affinity in dependence on the water permeation tube temperature. (D) Switching time between dry nitrogen as reagent gas and water doped nitrogen.....	65
Figure 5.3.3: (A) Number of detected compounds from the artificial leather emission, depicted for EI and each CI reagent. All signals above a threshold of 1 µg/m ³ toluene equivalent were used for this evaluation. The marker size represents the normalized intensities of the signals. For each ionization method the number of detected compounds is given within the Figure. (B) Comparison of survival yields of the intact parent ions using EI and the different CI reagents, exemplarily shown for compounds 3-methylpentadecane, diethyl phthalate and 1,2-propylenglycol diacetate.....	66
Figure 5.3.4: (A) Extracted ion chromatograms (EIC) of different alkane mass traces ionized with the CI reagent system RG1. (B) Enlarged EICs of two closely eluting signals at ~34.9 min. (C) CI and EI mass spectrum of the chromatographic signal at 31.87 min (compound 1) (D) CI and EI mass spectrum of the chromatographic signal at 31.91 min (compound 2).....	69
Figure 5.3.5: (A) CI (RG4) and EI mass spectra of the chromatographic signal at 38.60 min (compound 3) (B) CI (RG2) and EI mass spectra of the chromatographic signal at 44.80 min (compound 4). The molecular structures in each spectrum are derived from the respective MS information. In EI details on certain hydrocarbon branches are not available and assigned with C _x H _y , respective.....	71

Figure 5.3.6: The CI and EI mass spectra used for similarity search approaches were recorded at (A) 38.66 min (compound 5) and (B) 39.49 min (compound 6) retention time. The depicted substances in the EI mass spectra are the compounds predicted by the NIST hybrid search, but do not match the CI information.....73

Figure 5.3.7: CI and EI spectra of (A) compound 7 and (B) compound 8 at retention times 29.37 min and 30.24 min, respectively. In both cases no reasonable EI library search result is obtained but the corresponding CI spectra provide the molecular formula.....76

Figure 8.1.1: Reagent gas spectra at 13 mbar ion source pressure for (A) nitrogen, (B) isobutane, (C) methane as reagent gas.....96

Figure 8.1.2: Fragmentation behavior of o-xylene on the quadrupole RF amplitude for different pressures. The ratio of the $[M-H]^+$ (fragment) and the $[M+H]^+$ increases with higher RF and lower pressures. A continuous sample flow of 0.5 standard cm^3/min of a 10 ppmV xylene gas mixture with N_2 as reagent gas was used.....97

Figure 8.1.3: Range of linearity for benzophenone, naphthalene, anisaldehyde, 2-decanone, 2,6-di-tert-butylamine, and α -pinene using nitrogen as reagent gas. Left: Entire linearity range probed, right: expanded lower mass region.....98

Figure 8.1.4: Range of linearity for benzophenone, naphthalene, anisaldehyde, 2-decanone, 2,6-di-tert-butylamine, and α -pinene using isobutane as reagent gas. Left: complete linearity range, right: expanded lower mass region.....98

Figure 8.1.5: Range of linearity for benzophenone, naphthalene, anisaldehyde, 2-decanone, 2,6-di-tert-butylamine, and α -pinene using methane as reagent gas. Left: complete linearity range, right: expanded lower mass region.....99

Figure 8.1.6: CI Mass spectra of benzophenone, naphthalene, anisaldehyde, 2-decanone, 2,6-di-tert-butylamine, and α -pinene using nitrogen as reactant gas at 13 mbar.....99

Figure 8.1.7: CI Mass spectra of benzophenone, naphthalene, anisaldehyde, 2-decanone, 2,6-di-tert-butylamine, and α -pinene using isobutane as reagent gas at 8 mbar.....100

Figure 8.1.8: CI Mass spectra of benzophenone, naphthalene, anisaldehyde, 2-decanone, 2,6-di-tert-butylamine, and α -pinene using methane as reagent gas at 13 mbar.....	101
Figure 8.2.1: Time response of the switching ion optics between the CI and EI source. Single spectra were averaged to 500 Hz.....	106
Figure 8.2.2: Instrumental arrangement.....	106
Figure 8.2.3: Linear regression of CI and EI retention times.....	107
Figure 8.2.4: Peak shape comparison of different compounds of the FAMES GC standard. The relative peak width difference is measured at full width half maximum (FWHM) of the corresponding peaks.....	108
Figure 8.2.5: Nine repeated GC injections of benzophenone and octafluoronaphthalene for IDL calculations.....	108
Figure 8.2.6: Chromatograms of co eluting compounds (trans-2,cis-6-nonadienal (C ₉ H ₁₄ O) and citronellal (C ₁₀ H ₁₈ O)).....	110
Figure 8.2.7: Chromatogram of a 2.5 ng spitless injection of an EPA 8270 LCS mix....	110
Figure 8.2.8: Enlarged chromatogram of the EPA 8270 LCS mix.....	110
Figure 8.2.9: EI and CI mass spectrum of a chromatographic peak within the perfume sample at 1035 s.....	111
Figure 8.3.1: Dependence of the reagent ion distribution on the water filled permeation tube temperature.....	113
Figure 8.3.2: CI chromatograms of the artificial leather emission measured with dry N ₂ (RG1), H ₂ O doped nitrogen at a permeation tube temperature of 85 °C (RG2), H ₂ O doped nitrogen at a permeation tube temperature of 115 °C (RG3), and H ₂ O/NH ₃ doped nitrogen at permeation tube temperature of 85 °C (RG4). The simultaneously recorded EI chromatograms were identical for each CI reagent run and are therefore displayed just once.....	114
Figure 8.3.3: Mass spectra of diethyl phthalate, 1,2-propylenglycol diacetate and 3-methylpentadecane recorded with EI and each CI reagent system.....	115

Figure 8.3.4: Retention time index function of the alkane standard for retention indice assignment.....116

Figure 8.3.5. NIST hybrid similarity search results for compound 6 shown in Figure 5.3.6B. The measured spectrum is shown in red compared to the library spectrum in blue. Peaks present in the library spectrum but not in the measured spectrum are indicated in grey. The pink colored peaks assign signals that are present in the measured spectrum but not in the library spectrum and that additionally show a mass difference of 14 (CH₂-group) with respect to the peaks indicated in grey.....116

Figure 8.3.6: Isotopic pattern of C₆Cl₂H₁₁O₂.....117

Figure 8.3.7: (A) Deconvoluted extracted ion chromatograms of triacetin showing a strong coelution on m/z 145.050 and m/z 116.062. (B) These mass signals are therefore lost in the processed and deconvoluted mass spectrum compared to the library spectrum.....117

List of Tables

Table 2.2.1: reagent ions and proton affinities for common PCI reagents.....	8
Table 5.1.1: Limit of detections and protonated molecule yields for different compounds using nitrogen, isobutene, and methane as reagent gases, respectively.....	36
Table 5.1.2: Number of detected compounds in the EPA 8270 LCS mixture, classified by functionality.....	41
Table 5.2.1: First compound suggestions of the fragment spectra library search in combination with the CI information for the mass spectra shown in Figure 5.2.7B.....	58
Table 5.3.1: Results for a similarity search approach using EI and complementary CI information for the spectra in Figure 5.3.6.....	75
Table 8.1.1: Compounds present in the EPA 8270 LCS mix, proton affinities, and the m/z of the base peak observed nitrogen, isobutane and methane as reagent gas.....	102
Table 8.2.1: Compounds of the C4-C24 even carbon FAMES GC standard mix.....	107
Table 8.2.2: Compounds of the custom carbonyl mix.....	109
Table 8.2.3: Sum formulas generated with the common hetero atoms and an allowed mass difference of ± 10 ppm for the measured exact values of m/z 185.1907 and m/z 199.2052, respectively.....	109
Table 8.2.4: First compound suggestions of the fragment spectra library search in combination with the CI information for the mass spectra shown in Figure 8.2.9.....	111

List of Abbreviations

A	anion
APCI	atmospheric pressure chemical ionization
APPI	atmospheric pressure photo ionization
API	atmospheric pressure interface
CI	chemical ionization
CT	charge transfer
CID	collisional induced dissociation
DBE	double bond equivalent
ECNI	electron capture negative ionization
EI	electron ionization
EIC	extracted ion chromatogram
ESI	electro spray ionization
FI	field ionization
FAME	fatty acid methyl ester
GB	gas phase basicity
GC	gas chromatography
GCxGC	comprehensive two-dimensional gas chromatography
HRP	helical resonator plasma
HS	headspace
ICR	ion cyclotron resonance
ID	inner diameter
IDL	instrument detection limit
IE	ionization energy
IMS	ion mobility spectrometry
LC	liquid chromatography
LOD	limit of detection
M	molecule
MS	mass spectrometry
MCP	multichannel plate
NCI	negative chemical ionization
NTA	non-targeted analysis
OD	outer diameter

OFN	octafluoronaphthalene
PA	proton affinity
PAH	polycyclic aromatic hydrocarbon
PCA	principle component analysis
PCI	positive CI
PI	photo ionization
PTR	proton transfer reaction
RF	radio frequency
RG	reagent gas
RSD	relative standard deviation
TIC	total ion chromatogram
TOF	time-of-flight
VOC	volatile organic compound

List of Physical quantities

$\Delta G_R^0(T)$	gibbs free energy
ΔH_R^0	reaction enthalpy
σ	standard deviation
v	velocity
E_{kin}	kinetic energy
e	charge of an electron
m	mass
m/z	mass to charge ratio
R	(mass) resolution
sccm	standard cubic centimeter per minute
T	temperature
U	voltage/potential difference
U_{pp}	amplitude of RF voltage
z	number of charges
k	reaction rate constant

1 Aim of this work

Gas chromatography (GC) coupled to mass spectrometry (MS) using 70 eV electron ionization (EI) is a widely used method for targeted chemical analysis. The very reproducible and instrument independent 70 eV EI mass spectra are of great value and necessary for chemical analysis in many analytical standard methods. However, this method is not always sufficient, especially for non-targeted analysis (NTA) approaches. Information about the intact precursor ion and the resulting empirical sum formula are often required but can be lost in EI mass spectra. To overcome this lack of information, “softer” ionization mechanisms such as field ionization (FI)^[3,4], soft EI^[5,6] and chemical ionization (CI)^[7] are used in addition to EI. To employ these techniques, further chromatographic experiments for each ionization technique are needed in most cases. In addition to a complex chromatographic data alignment, some of these techniques show low sensitivities^[8]. A different approach is the use of atmospheric pressure interfaced MS using ionization techniques such as atmospheric pressure chemical ionization (APCI)^[9,10] or atmospheric pressure photo ionization (APPI)^[11,12]. Although higher sensitivities can be achieved for some compounds, small and non-polar molecules are not always feasible to analyze. In addition, mass spectral libraries for fragmentation methods such as collisional induced dissociation (CID) as used for APCI^[13] are not as comprehensive as the EI libraries^[14]. Therefore, the aim of this work is the development and the characterization of a time-of-flight (TOF) mass spectrometer delivering complementary information about the precursor ions using CI, whilst also detecting the 70 eV EI mass spectra during a single chromatographic separation step. This set up maintains the EI mass spectra, necessary for targeted analysis, while expanding the use of GC towards NTA. Due to the lack of CI sources suitable for the development of this instrument, this work also encompasses the development and characterization of a new hydrogen plasma-based CI source.

2 Introduction and theoretical background

2.1 Gas chromatography coupled to mass spectrometry

When it comes to the targeted chemical analysis of complex mixtures of volatile and semi-volatile compounds, GC coupled to mass spectrometry is often the method of choice for qualitative and quantitative analysis. GC-MS has been used for decades and is still the standard method for several analyses e.g., ISO16000-6:2011^[1] and ISO 12219-3:2012^[2]. The coupling of the GC to an EI source interfaced MS is usually assumed when talking about GC-MS. Molecules within a sample, introduced to the GC, are evaporated, sampled onto the chromatographic column, and separated by their boiling point and degree of interaction (mainly polarity) with the stationary phase of the chromatographic column. The compounds subsequently elute from the GC, while commonly temperature ramping the GC oven. The mass analyzer measures the mass to charge ratio of the previously ionized, and often fragmented molecules. The mass to charge ratio of the precursor ions/molecular ions, but also the fragment ions, can give important information about the actual measured substance^[15]. In the ideal case, a clean, non-disturbed mass spectrum for each compound can be acquired due to the GC pre-separation. In addition to the mass spectra, the retention time information of the compound is a valuable tool for compound identification, particularly for isomers and homologues of a certain compounds class that show similar 70 eV EI mass spectra as alkanes. GC offers a high peak capacity and separation power. If needed, the peak capacity of the chromatogram can be increased even further using two-dimensional GC (GCxGC)^[16,17]. Mass spectrometry on the other hand offers a very sensitive and highly linear detector for GC, adding a mass dimension to the GC separation. The use of this instrumentation, mainly in combination with a linear quadrupole MS, represents a very powerful and cost-effective tool for targeted, so called known known and known unknown compound analysis. Library EI mass spectra and the retention time information/retention indices (RI) for GC separation columns of different polarities are available for a vast number of compounds (c.f. Section 2.2.1.1). Those can be used for comparison, and consequently for compound identification. However, beside the advantages of EI several drawbacks as the loss of the molecular ion can emerge (c.f. Section 2.2.1). Although 70 eV EI is most commonly used, the use of GC is not restricted to this ionization technique. An overview about the most common ionization sources in combination with GC is given in Section 2.2.

2.2 Ionization sources

Only charged molecules/ions are affected by the electrical field of the mass analyzer, separating them by their mass to charge ratio. Therefore, the ionization of the sample is a key procedure within any mass spectrometer. The choice of the ionization technique strongly depends on the application, the sample introduction, and the analyte characteristics e.g., gaseous, liquid, solid. Therefore, a huge variety of ionization techniques have been developed. In GC analysis the target molecules entering the ion source are generally gaseous with masses rarely above 800 Da. The advantages and drawbacks of the most common techniques in combination with a GC as EI and CI are discussed in detail below.

2.2.1 70 eV electron ionization

Electron ionization is commonly used for compound ionization prior to the mass analysis in combination with a GC. The carrier gas flow from the GC is low enough to maintain the required vacuum conditions for EI. Electrons are emitted thermionically in high vacuum from a resistively heated filament. The emitted electrons are accelerated to 70 eV. The 70 eV electrons interact with the neutral analyte molecules entering the ion source and transfer a portion of their energy to the neutral analyte molecules. If the transferred energy is above the ionization limit of the analyte, an ionization process can occur. The ionization using EI leads to the formation of radical cations. In general, the EI ionization process shows the highest efficiency at 70 eV electron energy^[18]. The high energy intake results in an ionization via different reaction channels resulting in a multitude of different processes and ion types (molecular ions, fragment ions, multiply charged ions, metastable ions and rearrangements^[19,20]). Especially fragmentation reactions are pronounced in EI. Since each molecule has a unique structure and therefore unique fragmentation pathways, a unique EI mass spectrum is expected when using EI^[14]. This, together with the high reproducibility and instrument independence of the resulting mass spectrum, renders EI suitable for comparisons with mass spectral libraries such as the NIST/EPA/NIR mass spectral library^[21]. Due to the nature of the process, the fragmentation pattern of EI mass spectra measured decades ago show astonishing similarities to more recently generated EI spectra^[14]. If the measured compound has been measured before and was included in the library, the probability is high that a compound can be identified using a matching EI fragment spectrum. However, fragmentation reactions follow certain low energy pathways. If some bonds are weaker than others they can cause dominant peaks of

fragment ions within the mass spectrum and therefore, compounds with similar structures can end up with equivalent mass spectra^[14,21]. Additionally, the compound identification can become difficult if compounds are not listed within the libraries using 70 eV EI. The molecular ion can give, in addition to the fragment ions, valuable information about an unknown compound as the empirical sum formula. The fragmentation in EI, however, can become so dominant that the molecular ion of certain compounds can disappear completely within the mass spectrum. Therefore, EI can be considered as a relatively “hard” ionization process. The loss of the molecular ion and unspecific fragmentation can together increase the probability of a false positive compound identification. Yet, EI still represents the gold standard in combination with GC due to its high sensitivity, a fast time response and straightforward data analysis and interpretation.

2.2.1.1 Mass spectral libraries

Next to quantitative chemical analysis, mass spectrometry is also commonly used for qualitative analysis of complex chemical mixtures. The determination of compound identities is mainly done by comparisons to reference standard measurements or to mass spectral libraries. The most comprehensive mass spectral library is the NIST/EPA/NIR library containing over 3×10^5 EI mass spectra and over 1×10^5 retention indices (RI) from several compound classes such as metabolites, flavors/fragrances, drugs and metabolites pesticides, industrial chemicals, toxins and petrochemicals^[22]. Mass spectral libraries are also available for tandem mass spectrometry covering an order of magnitude less fragment mass spectra, although steadily growing^[22].

A measured (EI) spectrum compared to the libraries is returned with a list of suggestions yielding a similarity score and an identification confidence^[14]. Due to the reproducible fragmentation in EI this ionization method is particularly appropriate for spectra library comparisons. However, possible misidentifications (false positives and false negatives) are difficult to avoid^[14]. False positives mainly originate from structural similarities resulting in very similar fragmentation pathways. Thus, vast numbers of compounds yielding matching factors above 800, which is considered a “good match”^[23], can appear for e.g., monoterpenes such as alpha-pinene^[14]. False negative annotations appear when differences between library and measured spectra become too great. There are several reasons for such a variability in the spectra, such as contamination peaks within the mass spectra, low signal to noise ratios, different instrument configurations, instrument saturation and different temperatures. The influence of the temperature on the EI mass

spectrum is impressively demonstrated using EI in supersonic expansions^[24]. In addition, examples are presented in the literature reporting chemical reactions in advance to the ionization^[25]. A detailed summary is given by Stein^[14].

Moreover, there is also always the possibility that the exact compound and corresponding spectra is simply not within the library. This can strongly hinder the correct identification using mass spectral libraries, especially in fields where new compounds are rapidly appearing, such as with illicit drug identification^[26,27]. In these cases, advanced library search algorithms as the simple similarity search^[28] and the hybrid similarity search^[26], combining fragment matching and neutral-loss matching for a final score can be used. These approaches can generate high match factors for compounds that differ just slightly from library entries e.g., by the insertion or deletion of chemical groups that do not affect the fragmentation mechanism. The latter requires the knowledge about the molecular mass of the analyte.

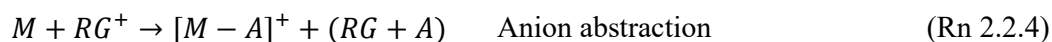
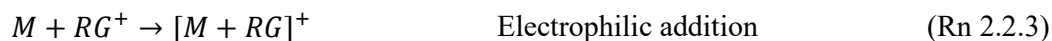
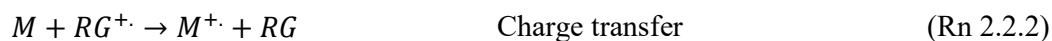
2.2.2 Soft ionization sources for GC-MS

As described in Section 2.2.1, compound identification using EI is strongly dependent on the entries within the mass spectral databases. If a compound is not listed within the library different identification approaches must be applied for compound identification. Identifying the molecular ion and therefore the sum formula of the molecule, preferably using accurate mass measurements, is essential. However, as also mentioned in Section 2.2.1, the molecular ion can disappear in EI due to excessive fragmentation. One approach yielding an increased abundance of molecular ions is to decrease the electron energy from 70 eV to 12-15 eV^[5,6]. This can enhance the relative intensity of the molecular ion peak. However, the decrease in electron energy has drawbacks, notably a reduced ionization efficiency. In addition, a spectrum without a molecular ion will not convert to a spectrum with a dominant molecular ion. Instead, molecular ions with low abundance in 70 eV EI are enhanced^[29]. Due to these reasons several other “soft” ionization sources have been introduced such as FI^[3,4], CI^[7], photo ionization (PI)^[17,30], APPI^[11,12] and APCI^[9,10]. All those techniques show a decreased fragmentation behavior, and therefore a higher probability of yielding precursor ions in the mass spectrum.

2.2.2.1 Chemical ionization

The most used “soft” ionization technique in combination with GC is chemical ionization. The first fundamental work for the development of CI were done by Tal’rose and

Frankevitch^[31], before being introduced by Munson and Field^[7]. Since then a multitude of chemical ionization techniques working at pressures from the low mbar range to atmospheric pressure have been introduced such as atmospheric pressure chemical ionization (APCI)^[9] and proton transfer reaction mass spectrometry (PTR-MS)^[32]. However, a classical CI source, mainly used for GC applications, differs only slightly from an EI source^[33]. The principle of CI is to ionize the analyte using ion-molecule reactions rather than directly using highly energetic electrons. Therefore, the ionization volume is filled with the reagent gas. The reagent gas is ionized using highly energetic electrons and in addition shields the neutral analyte molecules from these electrons^[34]. Since an effective number of collisions are required for ion molecule reactions to take place, the pressure within the CI source is typically in the low mbar range. Several ion molecule reactions are possible in positive CI (PCI) to transfer the charge from the reagent gas RG to a neutral molecule M , always dependent on the used reagent gas^[34,35]:



where A is the anion. Therefore, the chosen reagent gas plays a major role in CI^[35]. The most common reagents are methane (mainly proton transfer), isobutane (mainly proton transfer) and ammonia (proton transfer, electrophilic addition). The formation of protonating reagents such as CH_5^+ and $C_2H_5^+$ from methane, by auto-protonation, commonly appearing in classical CI sources is well studied^[7,36]. Ionization behaviors for many substance classes have been studied in detail especially for methane as reagent gas^[7,37-41]. Isobutane as reagent gas shows even less fragmentation due to a higher proton affinity (PA)^[42] compared to methane (c.f. Section 2.2.2.2), but is very prone to ion source degradation^[43,44]. Ammonia shows an even higher PA and is therefore even more selective than isobutane^[42]. However, in addition to protonation, ammonia shows enhanced tendency of electrophilic addition reactions^[45,46]. For molecules which still fragment using proton transfer, the intact NH_4^+ -cluster with the molecules can become feasible. Moreover, a multitude of other, rather uncommon reagents are available for PCI summarized by Viramani et al.^[47].

It is worth mentioning that common CI sources also offer the possibility of negative mode ionization using negative CI (NCI) and electron capture negative ionization (ECNI). Especially electron poor compounds containing e.g., halogen or nitro-group substituents, such as many pesticides^[48] and explosives^[49] are very selectively and sensitively ionizable by negative mode reaction mechanisms. However, since NCI and ECNI are not used during this work negative ionization is not further discussed.

2.2.2.2 Thermodynamics of proton-transfer reactions

Whether or not an analyte is ionized by the reagent depends on several physico-chemical parameters of the reagent and analyte. Since proton transfer is the most common reaction used for chemical ionization the thermodynamics of this reaction type are discussed briefly. The relative gas phase basicity of the neutral analyte and the reagent ions determine whether a proton is transferred to the analyte or not. The gas phase basicity for a molecule is defined for following reaction:



The Gibbs free energy change $\Delta G_{\text{Rn2.2.5}}^0(T)$ for the protonation of a molecule M by H^+ in the gas phase at a certain temperature T is considered as the gas phase basicity (GB(M,T))^[42].

$$GB(M, T) \equiv -\Delta G^0(T) \quad (2.2.1)$$

A proton transfer from the reagent ions to the neutral analyte will occur when the process is exergonic, i.e., if $GB_{\text{RG}} < GB_{\text{M}}$. However, the entropy changes for proton transfer reactions are rather small^[42] and in addition, the relative PA shows a low temperature dependence compared to the relative GB^[42]. Therefore, the PA and thus the exothermicity of the reaction is mostly used for reactivity evaluation^[50]. A protonation of the analyte by the protonation reagent RH^+ can be expected when:

$$PA_{\text{M}} > PA_{\text{RG}} \quad (2.2.2)$$

The lower the PA of the reagent gas, the broader are the ionization capabilities. The reaction enthalpy ($\Delta H_{\text{Rn2.2.1}}^0$) of the protonation is the difference between the

corresponding PAs of the reagent gas and the analyte and can be considered as the excess energy of the proton transfer reaction that is absorbed by the analyte $[M+H]^+$ in its degrees of freedom. However, a high excess energy of the ionization step can cause fragmentation of the analyte ions^[51–53]. Therefore, the choice of an appropriate reagent system is essential. PAs of common protonation reagents are given in Table 2.2.1.

Table 2.2.1: reagent ions and proton affinities for common PCI reagents

Reagent gas	Reagent ion	Proton affinity (kJ/mol) ^[42]
H ₂	H ₃ ⁺	422.3
N ₂	N ₂ H ⁺	493.8
H ₂ O	H ₃ O ⁺	691.0
CH ₄	CH ₅ ⁺	543.5
C ₄ H ₁₀	C ₄ H ₉ ⁺	802.1
NH ₃	NH ₄ ⁺	853.6

2.2.2.3 The role of contamination in CI sources

Methane represents the most common CI reagent in classical CI (excluding APCI and PTR). As shown in Table 2.2.1 the PA of CH₄ is relatively low. The advantage of a reagent gas with low proton affinity is the broad ionization capability, as discussed previously. However, impurities in the ionization source with higher PAs can deplete these highly acidic reagents completely. Since the overall PA of the reagent gas system is shifted to higher values this effect is usually not desired. Water is the most abundant contamination in vacuum systems and therefore plays a major role as an impurity in CI ion sources. Studies using methane as reagent gas were performed by Munson and Field, and showed the complete depletion of the CH₅⁺ ions by H₃O⁺^[54]. The same result applies for H₃⁺ and N₂H⁺. This effect is even more pronounced at elevated pressures and increased collision numbers such as in APCI. Here, elevated water cluster distributions dominate the mass spectrum^[55]. However, this effect can be also used for diversification of reagent ions systems, particularly in combination with hydrogen for classical low pressure CI sources. As shown in Table 2.2.1, H₃⁺ is highly acidic and therefore can protonate numerous other species that can in turn be used as protonating reagents. Studies using mixtures of hydrogen with bulk gases such as N₂, CO₂, N₂O, and CO are presented in the literature^[51–53].

2.2.2.4 Kinetics of proton transfer reactions

Protonation reactions are relatively fast and occur at reaction rates close to the capture collision rate of $\geq 10^{-9} \text{ cm}^3 \text{ molecules}^{-1} \text{ s}^{-1}$, if exothermic^[56]. The chemical kinetics for the generation of product ions (P^+), including the protonated molecule and fragments, as for example given in reaction Rn 2.2.1 can be demonstrated using the following equation:

$$\frac{d \sum [P^+]}{dt} = k * [M] * [[RG + H]^+] \quad (2.2.3)$$

where k is the reaction rate constant for reaction Rn 2.2.1. In a chemical ionization source, the reagent ions are available in a huge excess concentration ($[[RG+H^+]] \gg [M]$) and stay relatively constant ($[RG+H^+] = \text{const.}$) resulting in a pseudo first order reaction. Therefore, the analyte ion formation is directly proportional to the gas phase concentration of the analyte and the reaction rate constant. This behavior is especially used in PTR-MS^[56-58]. If the reaction rate constant of the CI reaction is known and a single species such as H_3O^+ represents the main ionizing species in a defined reaction time this information can be used for the quantitative calculation of analyte concentrations from the signal intensity. Consequently, (protonation) reactions of analytes with large rate constants produce higher signals than those with lower constants for an equal analyte concentration.

2.3 Non-targeted analysis

Nature provides a vast number of possible molecules and chemical structures. In addition, the commercial production of organic chemicals results in the release of complex and potentially harmful chemical mixtures that impact human health and almost all environmental compartments. The diversity of possible organic pollutants is analytically challenging. Especially in fields where new chemicals are rapidly emerging, classical targeted analysis approaches are often insufficient^[26,27,59]. NTA approaches aim to identify unknown molecules not included in any database or regulation, in contrast of screening the samples only for targets known or suspected to be in a sample. First approaches of unknown identification in the environment using NTS started to appear in the 1970s using mainly GC-MS^[60,61]. Many of in these studies newly identified compounds as polycyclic aromatic hydrocarbons, dioxins, pesticides, alkylphenols and volatile aromatic hydrocarbons are now under official control^[62]. This shows the importance of NTS for the detection and characterization of new pollutants and

subsequently their regulation especially for compounds exposed to humans^[63] and the environment. The recent developments in NTA in the environmental sector are strongly driven by the field of water research^[62,64]. However, NTA approaches are used in various fields as food analysis^[65,66], atmospheric science^[59,67], drug abuse^[26,27] and metabolomics^[68,69].

2.3.1 Non-targeted analysis using GC-MS

When it comes to NTA, there are much higher performance requirements of the instrumentation e.g., high resolution, soft ionization and more sophisticated software compared to targeted analysis. This is due to the fact that a comparison of the measured fragment spectra and retention time with a reference standard is not always feasible. The use of GC-MS lags behind MS coupled to liquid chromatography (LC) for which NTA approaches are already widely established^[62,64,65]. This is due the reduced chemical coverage of GC (especially for aquatic and biological samples) but primarily due to the MS instrumentation used, specifically GC coupled to unit resolution mass spectrometers, generating fragment spectra often without high resolution molecular ion information^[62]. LC however, is mostly coupled to atmospheric pressure interfaced MS equipped with an electrospray ionization (ESI) source or atmospheric chemical ionization (APCI) source attached to high resolution mass analyzers. These ionization techniques, compared to EI, dominantly produce protonated molecules, or adducts revealing information about the intact molecule. Structural information is gained using dissociation processes subsequently to the ionization process, such as CID. Indeed, these instruments can be also coupled to GC for NTA using e.g., APCI^[13,70,71]. However, if the molecular ion shows strong fragmentation or adduct formation following to the ionization, a clean and intense fragment spectrum is not always available. In addition, the advantages of EI compared to CID (e.g., the very comprehensive mass spectral libraries such as the NIST/EPA/NIR library, the instrument independence of the fragmentation process and the high ion yield using 70 eV EI) are lost. Many standard norms are designed for EI and due to the low selectivity of EI not easily interchangeable with other ionization techniques^[1,2]. Nevertheless, for NTA the molecular ion is essential, especially when compounds show unspecific fragmentation or are not listed in the spectra libraries. Ion sources combining the capability of EI and e.g., FI were already presented in the 1960s^[72]. Experiments using FI simultaneous to EI were done by Hejazi^[73] et al. using two different mass spectrometers coupled to a single GC. Eschner et al.^[16] used PI next to EI in a single ion

source. The set up in ref [16] allowed for fast switching between both ionization techniques to even resolve GCxGC experiments analyzing diesel fuel. In contrast to CI, PI and FI can be operated in the same pressure region as EI and thus permit a single ion source design. However, FI shows low sensitivities^[8], while PI often requires sophisticated high power laser systems to achieve high sensitivities^[17,74]. The use of EI in addition to CI for NTA was shown by Portolés et al.^[75] performing subsequent GC experiments with each ionization technique and enabling the identification of unknown compounds within water samples. Although combination ion sources capable of using CI and EI in consecutive experiments are presented previously^[76], the use of CI and EI simultaneously using a single mass spectrometer such as is described in this work has not previously been reported in the literature. A single ion source design switching fast enough between CI and EI to scan GC peaks with both techniques seems impractical due to the required rapid pressure adjustments. Using subsequent measurements for EI and CI respectively is time consuming and can result in tedious data alignment or even sample degradation. Therefore, an instrument operating two ion sources for the simultaneous detection of the EI fragment spectra in addition to the CI information is desirable.

2.4 Measurement of the accurate molecular mass and TOF mass analyzers

As stated before, the measurement of the accurate mass of a molecule is essential for compound identification of unknowns. Because of the varying binding energies of atomic nuclei, atoms of a given element have a unique mass defect. This is due to the correlation of the energy during nucleation and the mass given by $E = mc^2$. The mass defect is the difference between the nominal, integer mass, and the exact accurate mass of an atom or molecule^[77]. Since every atom and therefore every molecule shows a unique mass defect, the sum formula of a measured molecule becomes accessible. A higher certainty in sum formula calculation can be achieved with higher mass accuracy. In addition, selection rules e.g. the isotopic pattern, can be used to increase identification confidence^[78]. The difference of the measured mass to the theoretical mass is mainly given as a relative deviation in parts per million (ppm).

$$\frac{\delta m}{m} = \Delta\left(\frac{m}{z}\right) / \left(\frac{m}{z}\right) \quad (2.4.1)$$

However, not all mass analyzers can deliver such data. For example, linear quadrupole MS, often used in combination with GC, exhibit a relatively low mass resolving power

and therefore mass accuracy^[79,80]. In general, the mass accuracy of a mass analyzer system is closely related to its mass resolving power. Although there are several mass analyzers offering a high mass resolution and therefore a high mass accuracy such as Orbitraps, ion cyclotron resonance (ICR) MS and sector field MS, TOF mass analyzers show a good compromise between acquisition speed and mass resolution/accuracy (in this work $R \sim 5000$ and $\frac{\delta m}{m} < 5 \text{ ppm}$). The mass separation using a TOF mass analyzer relies on different velocities v for ions of different mass m and number z of charges e for a given kinetic energy E_{kin} imparted by moving through a potential difference U ^[81].

$$v = \sqrt{\frac{2E_{kin}}{m}} = \sqrt{\frac{2ezU}{m}} \quad (2.4.2)$$

A beam of ions entering the (orthogonal)-TOF mass analyzer is accelerated orthogonal to the initial ion motion into the mass analyzer by an electrical pulse. The ions are separated in a field free drift region under collision free conditions before impacting the detector, commonly a multichannel plate (MCP). The flight time can be converted into the ion mass to charge ratio due to the correlation given in Equation 2.4.2. For longer ion flight distances, higher mass resolutions can generally be achieved. However, using pulsing rates up to 25 kHz a TOF mass analyzer can display a whole mass spectrum within a fraction of a second and is therefore suitable for applications requiring a fast time resolution e.g., hyphenation to fast GC, GCxGC and ion mobility spectrometry (IMS).

3 Structure of this work

To accomplish the goals of this work described in Section 1, different objectives including the development of a chemical ionization source suitable for GC-MS analysis, the characterization of the developed dual ionization source TOFMS coupled to a GC, with special attention to the analytical performance and the evaluation of the instrument for non-targeted analysis were pursued. The results are presented within three peer-reviewed/for peer-review submitted publications prepared during this work. Those publications are shortly summarised in the following:

As described in Section 2.2.2, several types of “soft” ionization sources, including CI, are implemented in different ways e.g., as classical CI, APCI or PTR. All these ion sources comprise several advantages and disadvantages. To overcome the main disadvantages of certain CI sources such as short filament lifetimes, short maintenance cycles, reagent ion accessibility and temperature limits, the development of a new CI source for GC applications is presented in Section 5.1. The CI source is in depth characterized in terms of selectivity, sensitivity, stability, analyte fragmentation behavior and the performance in combination with a GC. In contrast to classic CI sources, generating reagent ions using highly energetic electrons and operating in the low-pressure regime of a mass spectrometer, the developed ion source operates on an atmospheric pressure interface. Reagent ions are produced using a hydrogen plasma ignited by a helical resonator at 13 mbar generating H_3^+ as primary charge carrier in an initial stage. The plasma is ignited by a radio frequency (RF) applied by the helical resonator power supply placed on a 12.7 mm OD glass tube. In this configuration the plasma area is not in contact to any electrodes and therefore shows no wear as shown by reproducible measurements over several days. The subsequent addition of reagent gas such as nitrogen in a second stage leads to the formation of the final CI reagent, ionizing the analyte in a third stage. The three-staged design allows for a distinct separation of ion generation, reagent ion formation and analyte ionization. In depth studies were performed adding nitrogen, isobutane and methane to the H_3^+ gas stream. Reagent ion distributions and fragmentation effects were investigated in detail. Especially the use of nitrogen as reagent gas, leading to the formation of N_2H^+ and N_4H^+ as protonating species, shows high analytical value with limits of detection down to 0.4 pg on column and broad ionization capabilities due to their low proton affinity. Therefore 74 of 78 compounds of an EPA 8279 LCS mix were detected using nitrogen as reagent gas while e.g., isobutane showed a more selective,

but also “softer” ionization behavior ionizing 41 of 78 compounds. During the development, special attention was paid to the chromatographic performance to ensure symmetrical peaks even for high boiling compound. This was achieved using a completely heated flow path within the GC transfer, ion source and partly within the ion optics.

The development and characterization of a GC-EI&CI-TOFMS instrument using the previously presented CI source in combination to a commercially available EI source on a single mass spectrometer is presented in Section 5.2. The instrument records mass spectra from both ionization sources during a single chromatographic experiment. Typical figures of merit are presented in addition to the characteristics of the GC hyphenation. The analytical performance of the dual ionization source TOFMS, operating both CI and 70 eV EI in parallel, is presented. The GC flow was split using a deactivated Y-splitter delivering ~50 % of the GC effluent to each ion source, respectively. Due to a fast and distinct switching within the ion optics of the dual ionization source TOFMS, the different ion populations were led alternately to the TOF mass analyzer. During this work switching rates of 10 Hz were used to resolve the chromatographic peaks with both ionization sources in parallel. Time deviations between the chromatographic peaks acquired with the CI and EI source, respectively are < 100 ms. It was shown that the obtained fragment spectra, using the 70 eV EI, match the most common fragment libraries, obtaining high match factors of ~850 – 950 for a fatty acid methyl ester (FAMEs) standard. The CI yields mass spectra containing abundant signals of the precursor ions, as expected. In combination with accurate mass measurements (< 5ppm) and the depiction of the isotopic pattern of the precursor ion, this data improves the generation of an empirical sum formula and therefore the identification probabilities in combination to the 70 eV EI spectra using the NIST/EPA/NIR fragment spectra library for several examples. The complementarity of the CI and EI data are shown for a custom standard mixture containing several ketones and aldehydes. An example from a head space sample of a brand perfume showing the unambiguous identification of a fragrance compound using both the EI and CI information is presented.

Finally, the use of the dual ionization source TOFMS system for a non-targeted analysis is presented Section 5.3. The experiments were carried out for material emission studies of car interior parts, in particular artificial leather. For this an improved reagent gas supply unit based on permeation tubes was deployed and shortly characterized, varying between

N_2H^+ / N_4H^+ , H_3O^+ , $[(\text{H}_2\text{O})_n+\text{H}]^+$ and NH_4^+ as reagent ions. This set up avoids the need for compressed gas cylinders of flammables e.g., methane and isobutane. Reagent ions can be alternated between consecutive GC experiments without hardware changes using this reagent gas supply unit. While N_2H^+ / N_4H^+ showed an excellent broad range selectivity, the survival yield of the precursor ions increased towards NH_4^+ . The head space of the artificial leather sample was collected on Tenax® desorption tubes and sampled to the GC using a thermal desorption sampling system. The complexity of the emission chromatograms was used to demonstrate the benefits of combining both EI and CI information for different compound identification scenarios. The precursor ion information gained via CI in addition to the 70 eV EI mass spectra allowed for complete reconstruction of molecules and avoidance of false positives using common fragment library comparisons. This is particularly beneficial for compounds resulting in unspecific fragmentation pattern using 70 eV EI. Additionally, the sum formula information enables identification of compounds not listed in fragment spectra libraries using similarity search approaches^[26]. Specifically, the knowledge of controlled and well characterized CI mechanisms reduced the uncertainties in the identification of unknown compounds. Moreover, the system is improving upon standard methods e.g., ISO2219-3:2012^[2] and ISO16000-6:2021^[1] by not compromising the original EI information required for targeted analysis and many norm methods by also gaining high resolution CI information.

4 Experimental part

4.1 Mass spectrometer

All experiments were performed using the, during this work, developed dual ionization source TOFMS. The instrument is characterized in detail in Section 5.2. The instrument combines two different interfaces, coupled to a single TOF mass analyzer, hosting an EI and a CI source, respectively.

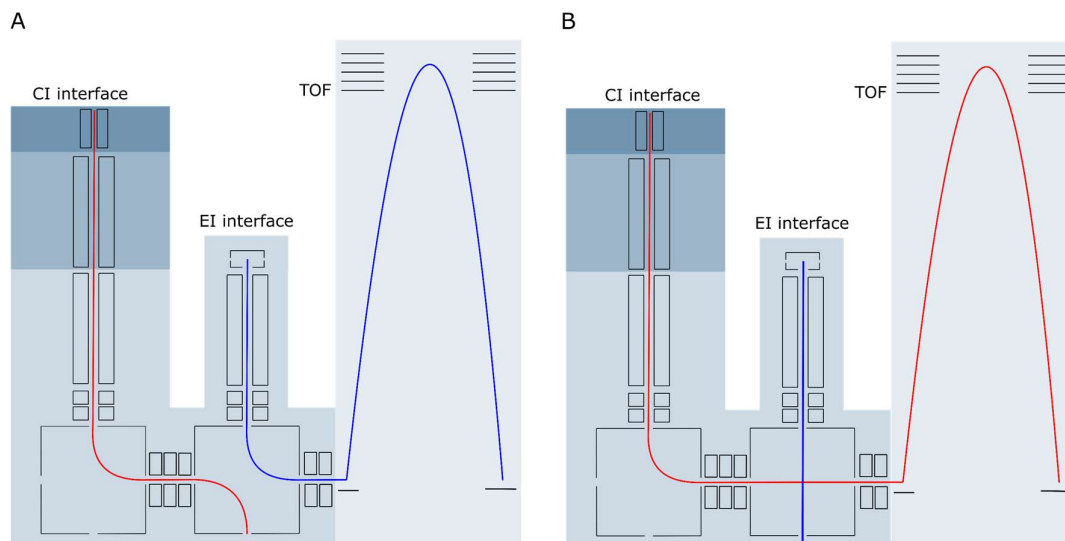


Figure 4.1.1: Schematic set up of the dual ionization source TOFMS during (A) EI mode and (B) CI mode.

The CI interface displays an atmospheric pressure interface including several differential pumping stages and corresponding ion optical transfer devices e.g., transfer quadrupoles. The EI interface is embedded in the last pumping stage upstream to the TOF mass analyzer. Custom designed quadrupole ion deflectors are used to parallelize the ion beams, generated by the ion sources, towards the TOF mass analyzer. By rapidly switching the voltages of the second quadrupole ion deflector, the ion beams are either deflected or passed straight through this ion optical device as indicated in Figure 4.1.1. Thereby, either the CI or the EI ion beams are sampled to the TOF mass analyzer. This allows for a clear differentiation of both ion types during the acquisition of the corresponding mass spectra. For experiments operating both ion sources simultaneously, the switching rate of the quadrupole ion deflector was set to 10-15 Hz leading to a data acquisition of 5-7.5 Hz for each ion source, respectively. The used TOF mass analyzer was an HTOF (TOFWERK, Thun, Switzerland) operated with a resolution between 4000 and 5000 and a sampling rate of 25000 mass spectra per second within a mass range of

m/z 3 - 450. A commercial EI source (Star beam EI source; TOFWERK, Thun, Switzerland) was utilized. The CI source is described in detail in Section 5.1.

4.2 Acquisition and post processing software

TOFDAQ recorder (TOFWERK, Thun, Switzerland) was used for data acquisition and storing the data as hdf5 files. The hdf5 file format supports a four-dimensional data structure (in this case time, segment, mass, intensity). The data acquired during the EI and CI phase, respectively are saved to different segments within the hdf5 file format. High resolution data were mainly handled using TOFware (Tofwerk, Thun, Switzerland) while chromatographic deconvolution of EI and CI spectra were performed via Analyzer Pro XD (SpectralWorks, Runcorn, UK).

4.3 Gas chromatography and sampling

For all experiments an Agilent 7890A GC (Agilent technologies, Santa Clara, CA, USA) was used. The GC conditions including, GC columns, oven temperature programs, inlet temperatures, sampling devices and conditions are given for each experiment separately. During this work several sampling methods were used as liquid injection, head space sampling using a manual headspace sampler (Ellutia, Ely, UK) and thermal desorption (Gerstel TDS3, KAS4; Gerstel, Mülheim an der Ruhr, Germany).

4.4 GC transfer

The connection between the GC and the ion sources of the mass spectrometer is essential to preserve the chromatographic performance of the GC. Conventional GC transfer lines are designed as stiff and well insulated heated metal tubes representing a continuously heated connection between both instruments. Since the ion sources of the operated mass spectrometer are spatially distanced but should be coupled to the same analytical separation column special attention was paid to the GC transfer development. In addition to the flexibility of the transfer lines in terms of bending radius, a quick connection system for easy installation, column positioning and ventless separation column exchange was implemented. The transfer design leading the GC effluent to the EI source is shown in Figure 4.2.1. The coupling between the GC and the MS consists mainly of two different parts: the heated transfer line and the heated vacuum feedthrough. Both parts are connected using a SilcoNert® coated (SilcoTeck GmbH, Bad Homburg, Germany) 1/32" internal/external union with a 0.25 mm bore (Vici, Huston, TA, USA). The heated vacuum feedthrough is directly installed on the MS interface. Within the heated vacuum

feedthrough, a methyl/phenyl deactivated fused silica capillary of 0.25 mm ID (BGB Analytik, Bökten, Switzerland) is installed as inlet capillary directing the GC effluent into the EI source. The heated transfer line is connected to the heated vacuum feedthrough using the mentioned 1/32" internal/external union. To avoid cold spots, the connection is stabilized using the transfer line connection clamp as shown in Figure 4.2.1. The heated vacuum feedthrough acts as flow restriction and maintains a low pressure within the mass spectrometer even when the transfer line and GC are removed. This allows the instrument to be maintained without venting the MS system or the need to re-align the GC column within the ionization source. A more detailed characterization of the vent free capillary feedthrough system is given in ref [82]. The transfer line represents a 0.25 mm ID stainless steel tubing with a deactivating coating (UltiMetal stainless steel capillary tubing; Agilent technologies, Santa Clara, CA, USA). The stainless-steel tubing was insulated using a 0.5 mm ID fiber glass hose (Techflex, Kürten, Germany). For resistive heating a nickel heating wire with diameter of 0.3 mm and a resistance of 1.3 Ω /m was wound around the insulated capillary with a pitch of ~ 0.5 turns/mm. A Pt-100 temperature sensor 2.1 mm x 3.9 mm (width x length) (Heraeus, Hanau, Germany) was taped onto the heating wire for temperature regulation.

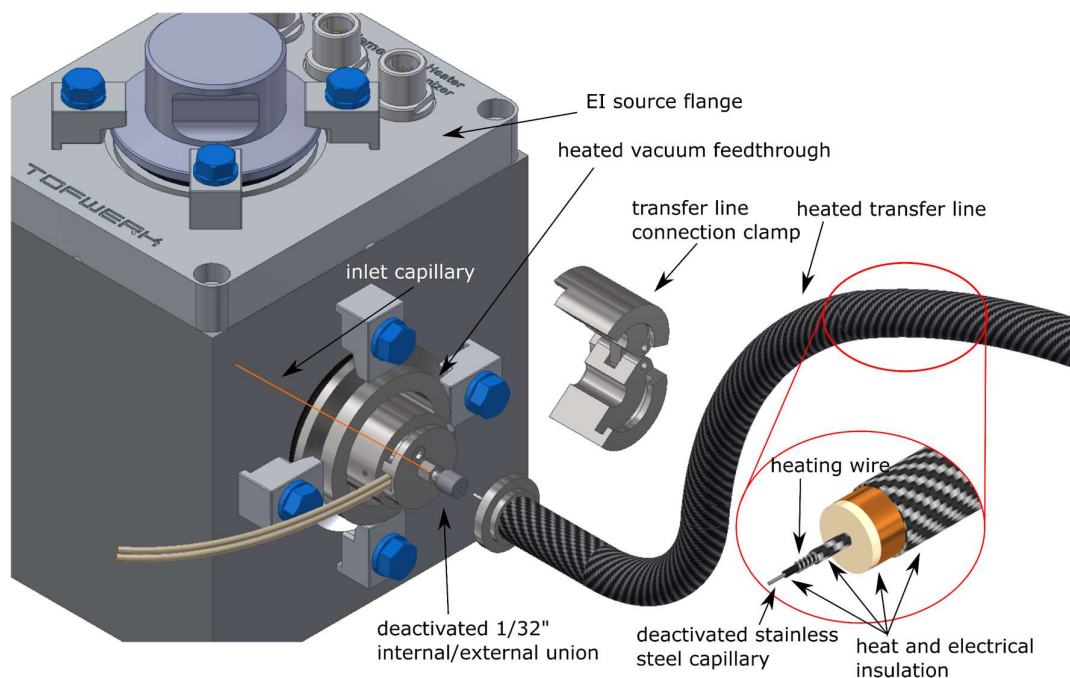


Figure 4.2.1: GC transfer design to the EI source including the flexible heated transfer line and the heated vacuum feedthrough.

Additional layers of heat insulation were added (cf. Figure 4.2.1) resulting in a transfer line with 2.5 mm diameter and a bending radius of > 15 cm. With this, an operation at 280 °C results in a power consumption of 28 W. The same transfer line design was used for the GC coupling of the CI source. In the CI case, however, the heated transfer line was directly connected to the ion source inlet. The GC separation column was coupled to the transfer line either by a straight MXT union connector for single ionization source mode or a MXT Y-split connector (Restek, Bellefonte, PA, USA) in dual ionization source mode.

4.2 Chemicals

All used chemicals were ordered in high purity > 95 % from different suppliers. Gases were all used in a purity of ≥ 99.999 % either purchased from Carbagas (Bern, Switzerland) or in the case of Hydrogen produced by a Hydrogen generator Trace (Peak Scientific, Glasgow, UK). Detailed declarations are given for each section in separate.

5 Cumulative part

5.1 Hydrogen plasma-based medium pressure chemical ionization source for GC-TOFMS

Steffen Bräkling^{1,2}, Kai Kroll², Sonja Klee¹, Thorsten Benter², Hendrik Kersten²

¹ TOFWERK, 3645 Thun, Switzerland

² Department of Physical and Theoretical Chemistry, University of Wuppertal, 42119 Wuppertal, Germany

Reprint with permission from *J. Am. Soc. Mass Spectrom.*, **2022**, 33, 3, 409-509. Copyright 2022 American Chemical Society.

<https://pubs.acs.org/articlesonrequest/AOR-NQ3WCVEZYTXS8ZFXKMWZ>

5.1.1 Abstract

The construction, critical evaluation, and performance assessment of a medium-pressure (2 - 13 mbar), high temperature chemical ionization (CI) source for application in GC-MS is described. The ion source is coupled to a commercial time-of-flight (TOF) mass analyzer. Reagent ions are generated in a two staged process. The first stage uses a filament free, helical resonator plasma (HRP) driven ion source for H_3^+ generation. Reagent gases e.g., nitrogen, isobutane and methane are added in a second stage to the H_3^+ stream, which leads to the formation of final protonation reagents. The GC effluent is added subsequently to the reagent ion gas stream.

Designed for the hyphenation with gas chromatography, this GC-CI-TOFMS combination produces GC limited Gaussian peak shapes even for high boiling point compounds. Limits of detection for the compounds investigated are determined as 0.4 pg - 1.2 pg on column with nitrogen, 0.6 pg - 12.6 pg with isobutane, and 2 pg - > 25 pg with methane as reagent gas, respectively.

An EPA 8270 LCS mix containing 78 main EPA pollutants is used to evaluate the selectivity of the different reagent ions. Using nitrogen as reagent gas, 74 of 78 compounds are detected. In comparison, 41 of 78 compounds and 62 of 78 compounds are detected with isobutane or methane as CI reagent gas, respectively.

5.1.2 Introduction

Gas chromatography (GC) coupled to mass spectrometry (MS) is one of the most common hyphenated techniques in analytical chemistry in use for decades. The design of the ion source requires careful attention to a multitude of parameters for an acceptable overall analytical performance. Particularly with regard to sensitivity, selectivity and chromatographic fidelity, an appropriate ionization scheme, a proper pressure and flow balance, and a careful choice of high temperature mounts are required.

Chemical ionization (CI) was introduced as an alternative for electron ionization (EI). The latter is regarded as the gold standard for GC-MS. Due to the pronounced and reproducible fragmentation of precursor ions it allows for reliable fragment library searches^[23,83,84]. EI has the disadvantage that it sometimes loses the molecular ion information^[13,17,75]. CI normally delivers such molecular ion information. Generally, in CI the generation of a large excess of reagent ions is responsible for analyte charging. One of the most important issues to be addressed in CI concerns the reagent ion distribution, since the relative proton affinity (PA) and ionization energy (IE) of the reagent ions and analytes define 1. whether a compound is amenable to this ionization scheme and 2. the maximum excess energy remaining after the charging event within the vibrational modes of the analyte, possibly causing fragmentation^[31]. Hence, CI always requires a fine balance between selectivity, degree of fragmentation, and sensitivity.

The first “classical” CI source was introduced by Munson et al. in 1961^[7] which essentially represents a modified EI source. Reagent gas pressures up to 1 mbar^[35,44] ensure mean free paths in the millimeter range and thus lead to sufficient bimolecular collisions for reactions between the EI induced reagent ion and the analyte. In particular acidic, protonating reagents play a major role in positive CI, such as $\text{CH}_5^+/\text{C}_2\text{H}_5^+$ (methane), and C_4H_9^+ (isobutane), with sometimes rather complex underlying ionization mechanisms^[35]. In classical CI the entire chemistry from reagent gas ionization, reagent ion formation and analyte charging occur in one spatially confined volume, which renders control on the reagent ion distribution rather difficult. In many cases the collision rate at 1 mbar is not sufficient to collisionally disperse excess precursor ions energy which results in increased fragmentation. Additionally, traditional EI driven CI sources often suffer from reduced filament lifetimes and residue build-up due to ionization source “fouling”^[43,44]. Many ion source designs for GC using chemical ionization with separated regions for reagent ion formation and analyte ionization, working in various pressure

regions, were introduced since then e.g., atmospheric pressure chemical ionization (APCI)^[9,10] and proton transfer reaction mass spectrometry (PTR-MS)^[85].

In this work reagent ions are generated in a two staged process. H_3^+ as one of the strongest gas phase acids is used to initiate the reagent ion formation from a suitable reagent gas. H_3^+ is generated by flowing ultra-pure H_2 through a radio frequency (RF) plasma, driven by helical resonator plasma (HRP) supply^[86], replacing the operation of a filament along with its drawbacks. The low proton affinity of H_2 enables the protonation of a broad range of molecules with H_3^+ . Even bulk gases such as nitrogen can be protonated and used by subsequent addition as final reagent ion for analyte ionization^[42,52,53,87]. The pressure is maintained in the range of 2-13 mbar, i.e., is slightly higher than in classical CI. In addition, the dwell time for neutral analytes to react with a defined reagent ion population is significantly increased as compared to classical CI, which enhances sensitivity. However, the ion-molecule chemistry of this system is not yet fully equilibrated, such as in APCI^[88-90]. Consequently, the presence of water does not result in formation of an equilibrated cluster distribution acting as a thermodynamic reagent ion sink leading to loss in ionization range. Even a considerable H_3O^+ population can be generated as the protonating reagent without the need of elevated electrical field strengths as in PTR-MS^[32,58,91,92]. This minimizes feasible collisionally induced dissociation (CID) steps of the charged precursor ions^[93]. Furthermore, the reagent ion generation and analyte protonation regions of the source are spatially separated, providing much better control of active protonating species, in contrast to classical CI, where reagent and analyte ions are generated in the same rather confined reaction volume. The main goals for the presented chemical ionization source are 1. the generation of controllable reagent ion systems for different reagent gases leading to virtually non-selective protonation, e.g., via N_2H^+ or H_3O^+ ions as well as selective protonation, e.g., via C_4H_9^+ ions; 2. establishing abundant $[\text{M}+\text{H}]^+$ signals for the analyte compounds of interest; 3. maintaining the chromatographic performance for the entire GC-EI-MS analyte range; and 4. establishing competitive sensitivities with limits of detection (LODs) in the femto- to low picogram (on column) region.

The selectivity of the different reagent ions is demonstrated using an EPA standard mixture containing 78 environmental pollutants. The diversity of compounds in this mixture provides a good measure for the different reagent ion coverage and overall source

performance. A similar approach was chosen by Kauppila et al.^[94] for a comparison between direct and dopant assisted APPI and APLI, respectively.

5.1.3 Experimental

MS Interface. The ionization source is connected to the first differential pressure stage of an originally atmospheric pressure interfaced time of flight (API-TOF) mass analyzer (TOFWERK, Thun, Switzerland). A vacuum pump (Fossa FO 0035A Busch Vacuum Solutions, Maulburg, Germany) controls the flow/pressure in this first vacuum region. Ions are guided downstream into the next pressure stage with a segmented quadrupole. The ion source is coupled upstream to the ion guide using an additional enclosure, cf. Figure 5.1.1. The latter is optimized for passive heat conduction through the ion source. The TOF was operated at mass resolving power of $R \sim 5000$ Th/Th at 183 Th. The mass range was configured to acquire ions in the mass range from ~ 10 - ~ 450 Th. Individually recorded mass spectra at 25 kHz repetition rate were averaged to 5 spectra per second (5 Hz acquisition rate).

Ionization source design. A schematic of the ionization source is shown in Figure 5.1.1. The set up can be divided into three stages, each marking a different ion chemical process. The first stage controls the generation of H_3^+ from a hydrogen fed helical resonator plasma^[86]. The formation of abundant H_3^+ ions through this plasma setup was shown previously^[95]. The helical resonator itself was placed on a ½-inch OD glass tube connected to the stainless-steel ion source housing. The H_2 supply was connected to the glass tube via a ½ inch Swagelok Teflon fitting. The frequency of the plasma power supply was adjustable between 11 MHz and 16 MHz. If not stated otherwise, the hydrogen flow was kept at 100 standard cm^3/min to minimize back diffusion of reagent gas. The spontaneous ignition of the hydrogen plasma was possible in a pressure region between 0.2 mbar and 15 mbar. The plasma supply applied < 2 Watt at optimum operation for all investigated pressures. The ionization source pressure was adjusted with a manual valve regulating the pumping speed of the connected rough pump. The pressure was recorded with an absolute capacitive vacuum gauge CMR 362 (Pfeiffer vacuum, Asstar, Germany).

The second stage is located downstream of the active plasma region, where nitrogen (99.999 %), methane (99.9995 %) or isobutane (99.95 %) (cf. Chemicals section) were added as reagent gases into the H_3^+ enriched gas flow. This stage is responsible for

generating the respective reagent ions and allows to switch between highly acidic compounds, such as N_2H^+ , and less acidic compounds such as C_4H_9^+ . Experiments with lower purity nitrogen revealed the possible usage of H_3O^+ as reagent ion without any issues arising from formation of larger proton bound water clusters. As depicted in Figure 5.1.1, the reagent gas flow circumvents the inner glass tube until it diffuses into the H_2 flow within the actively heated ionization source region. The source housing temperature was kept at 300 °C. If not stated otherwise, the reagent gas flows were adjusted to 200 standard cm^3/min . In all experiments, the reagent gas flows were always kept twice as high as the H_2 flow. Due to the low hydrogen pumping speed of many vacuum pumps, this is the minimum ratio between hydrogen and reagent gas to ensure acceptable pressures in the TOF mass analyzer.

In the third stage, the GC effluent is added orthogonally to the reagent ion flow for protonation, followed by a voltage free drift region that ends in the first pumping stage of the mass spectrometer. The GC column protrudes 3 mm into the main gas flow. The original quadrupole in the first vacuum region is a standard component of the API-TOF mass analyzer. For this work, it was modified with an axially surrounding aluminum enclosure, which turned this quadrupole into an essential part of the ion source, featuring improved mixing, focusing and partly ion activation. The direct contact of the enclosure with the heated ionization source housing maintained a high temperature reaction pathway throughout the first vacuum region of the mass spectrometer. In this way, GC peak tailing effects caused by condensation of high boiling compounds and thus long residence times of non-ionized analytes in the first vacuum chamber were minimized. A gas temperature of ~160 °C was measured at the quadrupole entrance and ~130 °C at the exit. Holes in the end plate of the ion guiding quadrupole established the gas flow of all three stages through the entire source. The axial voltage gradient along the quadrupole was kept low (< 10 V) to avoid elevated reduced electrical field strength in addition to the focusing RF field.

Kalrez 4079 O-rings seals (Angst+Pfister, Geneva, Switzerland) and Valcon Polyimide ferrules (VICI Valco instruments, Huston, Tx, USA) were used in the ionization source. Typically, GC applications require temperatures up to 350 °C within these regions to maintain the chromatographic fidelity over the whole GC analyte spectrum. Commonly used sealing materials, such as FKM/FFKM O-rings, PEEK and Kapton, are not suitable in such high temperature regimes. Even showing a good form stability at such

temperatures, outgassing of these materials strongly interferes with the analysis^[12]. O-ring sealed areas are spatially separated from the heated ionization source body to keep outgassing effects to a minimum. Temperatures at O-ring sealing sites were measured to be $< 150\text{ }^{\circ}\text{C}$.

For the MS voltage tuning and mass calibration, 0.5 standard cm^3/min of a 10 ppmV mixture of benzene, toluene and xylene in helium (see Chemicals section) were added to the nitrogen flow.

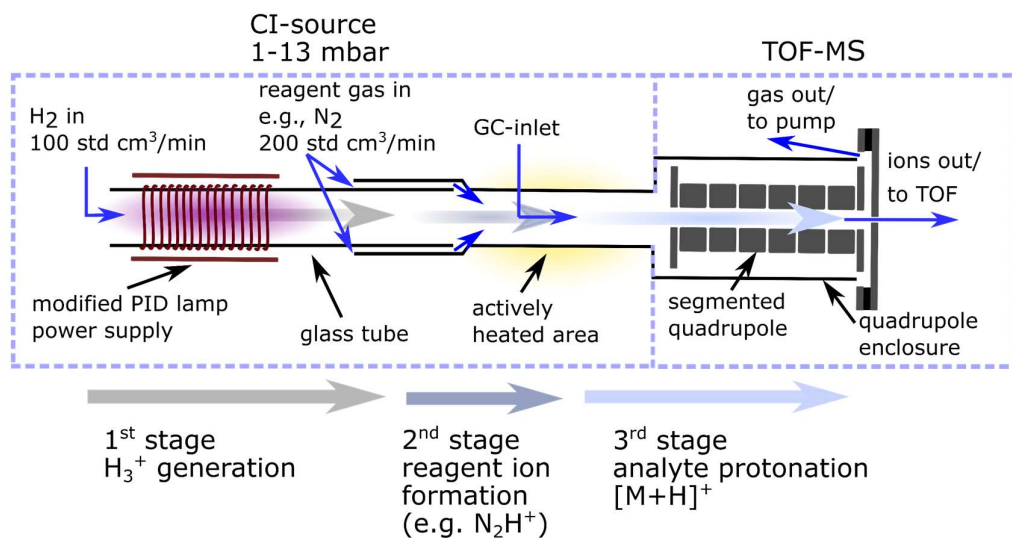


Figure 5.1.1: Schematic of the chemical ionization source mounted to the first pressure stage of the mass spectrometer including the segmented quadrupole of the first MS pressure stage (cf. MS interface section).

GC Interface. The ionization source was coupled to an Agilent 7890A GC (Agilent technologies, Santa Clara, CA, USA) equipped with a liquid injection inlet and a Rxi-5ms column (30 m, 0.25 mmID, 0.25 μm , Restek, Bellefonte, PA, USA). The GC coupling to the ionization source was accomplished with a custom heated transfer line operating at $280\text{ }^{\circ}\text{C}$. The GC separation was done with the following temperature program: 1 μl splitless autosampler injection (inlet temperature $280\text{ }^{\circ}\text{C}$), temperature hold for 2 min at $43\text{ }^{\circ}\text{C}$, temperature ramp to $250\text{ }^{\circ}\text{C}$ at $20\text{ }^{\circ}\text{C}/\text{min}$ rate, temperature ramp to $300\text{ }^{\circ}\text{C}$ at $30\text{ }^{\circ}\text{C}/\text{min}$ rate. Helium 99.999 % (Carbagas, Bern, Switzerland) further purified using a Big Universal Trap (Agilent technologies, Santa Clara, CA, USA) was used as carrier gas in a constant flow of 2 standard cm^3/min .

Chemicals. All gases except hydrogen were purchased in 99.999 % purity from Carbagas (Bern, Switzerland). hydrogen 99.9999 % was obtained from a precision hydrogen trace

generator (Peak Scientific, Glasgow, UK). Hydrogen was further purified to low ppbV contamination levels with gas purifiers (ZPure Glass H₂O/HC Filter; Chromatography Research Supplies Inc, Louisville, KY, USA). The 10 ppmV BTX gas mixture used for mass calibration and tuning was purchased from Carbagas (Bern, Switzerland). Chemicals used for reaction, fragmentation and LOD studies, i.e., benzene ($\geq 99.9\%$), toluene (99.9%), α -pinene (98%), naphthalene (99.0%), 2-decanone (98%), 2,6-ditert-butylpyridine ($\geq 97\%$), anisaldehyde ($\geq 99.9\%$) and benzophenone ($\geq 99\%$) were all purchased from MERCK/Sigma Aldrich (Buchs, Switzerland). Solutions of these analytes were made with GC grade hexane ($> 99\%$) from MERCK/Sigma Aldrich (Buchs, Switzerland). The EPA 8270 LCS mix 1 was purchased from Supelco (Bellefonte, PA, USA) and contained 100 $\mu\text{g/mL}$ of each of the 78 EPA major pollutants as acetone/methylene-Chloride (9:1 V:V) solution. The solution was further diluted in hexane to a concentration of 2.5 $\text{ng}/\mu\text{L}$.

5.1.4 Results and discussion

5.1.4.1 Reagent ion distributions

As described in the experimental section, the reagent gases nitrogen, isobutane, and methane were added downstream of the plasma region and merged with the H₃⁺/H₂ gas flow. The protonation of the reagent gases by H₃⁺ and consecutive reactions lead to the formation of reagent gas specific ions. Since the selectivity of the CI method depends on the availability of characteristic reagent ion species, detailed knowledge regarding their individual distributions is essential. It is emphasized that there is a major difference between the generation of CI reagent ions with EI and H₃⁺, respectively. Electron ionization produces mainly *radical cations* and many fragments of the reagent gas. These species potentially induce chain reactions that inevitably lead to abundant adverse neutral as well as ionic by-products. Consequently, swift CI-source contamination is one of the major drawbacks^[43,44]. In contrast, plasma generated H₃⁺ *protonates* the reagent gases, which is 1. a process known to be far less intrusive (despite the high gas phase acidity of H₃⁺ and thus exothermic protonation reaction enthalpy), and 2. ideally does not generate radical cations.

Depending on the collision number (i.e., the pressure), different ion distributions can be generated for analyte ionization. Thus, the reaction systems can be largely controlled via the source pressure. Figure 5.1.2 shows the behavior of the reagent ion distributions with

changing source pressures for all three reagent gases. These distributions are discussed in the following. Reagent ion mass spectra at 13 mbar ion source pressure are shown in Figure 8.1.1.

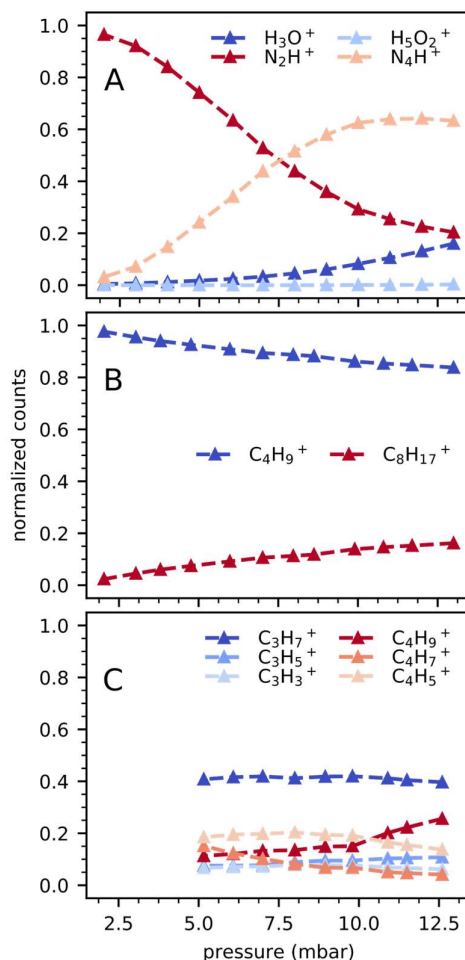
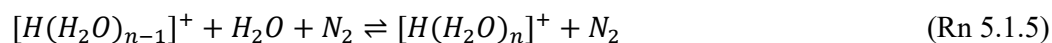


Figure 5.1.2 Reagent ion distribution as function of ionization source pressure for the reagent gases (A) nitrogen, (B) isobutane and (C) methane.

Nitrogen reaction system: As Figure 5.1.2A shows, N_2H^+ represents the main reagent ion species at low source pressures between 2 and 7.5 mbar. It is generated via proton transfer reaction from H_3^+ to N_2 (Rn 5.1.1)^[96]. Since even at very high gas purities (low ppbV level in this work) residual water is the main contaminant in bulk gases and on surfaces. Due to its chemical properties, water often plays a major role in the ion distribution in CI sources other than classical EI driven CI. The proton affinity of nitrogen compared to water is rather small ($\text{PA}(\text{N}_2) = 493.8 \text{ kJ/mol}$)^[42] and therefore water ($\text{PA}(\text{H}_2\text{O}) = 691.0 \text{ kJ/mol}$)^[42] potentially interferes with the N_2H^+ reaction system. Since H_3O^+ is the thermodynamically favored species, N_2H^+ and H_3^+ begin converting via

proton transfer reaction to H_3O^+ (Rn 5.1.3)^[96] in a medium pressure region up to 7.5 mbar. Simultaneously, the generation of N_4H^+ acting as a reservoir species for N_2H^+ proceeds in an equilibrium reaction with excess nitrogen (Rn 5.1.4)^[97]. Further increase of the pressure results in a steady growth of the H_3O^+ signal, while the N_4H^+ signal levels off. The signal of the proton bound cluster $[H(H_2O)_2]^+$ due to reaction of H_3O^+ with H_2O ^[98] does not represent a notable reagent (Rn 5.15). This is important to know, since the proton affinity increases with the $[H(H_2O)_n]^+$ cluster size and therefore the desired high reactivity (i.e., low selectivity) of the reagent ion system is only preserved at small cluster sizes^[99–101]. $[H(H_2O)_2]^+$ shows already a significantly increased proton affinity compared to H_3O^+ of approximately 140 kJ/mol^[99]. The TOF mass analyzer tolerates ionization source pressures up to 13 mbar. At this maximum pressure, N_2H^+ , N_4H^+ and H_3O^+ represent the dominant reagent ions. Note that the H_3O^+ signal is expected to be underestimated especially for higher pressures due to low mass losses in the ion transfer stages of the mass analyzer. Larger water clusters with $n > 2$ were not observed in significant amounts.



Isobutane reaction system: $C_4H_9^+$ (PA(C_4H_8) = 802.1 kJ/mol)^[42] is the main ion species using isobutane as reagent gas. $C_4H_9^+$ is produced via the reaction of H_3^+ and isobutane followed by a methane elimination and subsequent reaction with another isobutane molecule (Rn 5.1.6 - Rn 5.1.8). A different pathway reacts via hydrogen elimination (Rn 5.1.9)^[102]. Residual water does not affect the reagent ion population due to the higher proton affinity of C_4H_8 as compared to water. As shown in Figure 5.1.2B the reagent ion distribution is slightly shifted from $C_4H_9^+$ to higher $C_nH_m^+$ (e.g., $C_8H_{17}^+$) species with increasing source pressure. A pronounced change of ion distribution with the source pressure as seen for the nitrogen reaction system is not observed.





Methane reaction system: Methane as reagent gas leads to strong signals for $C_3H_7^+$ and $C_4H_9^+$. Additionally, abundant signals of $C_3H_3^+$, $C_3H_5^+$, $C_4H_5^+$ and $C_4H_7^+$ appeared even at low pressures. These ion species were also observed in studies of Field et al.^[36] at pressures up to ~2.5 mbar in low abundance. These authors used a filament-based CI source for their studies. The relative intensities of the C_3 -species did not vary strongly with the source pressure, whereas $C_4H_5^+$ and $C_4H_7^+$ decreased in favor of an increasing $C_4H_9^+$ population as the source pressure was increased. Species such as CH_5^+ and $C_2H_5^+$ represent the main reagents in classical EI driven CI^[35] and are the initial ions produced in chemical reactions following primary CH_5^+ generation at low pressures^[102]. In the present study, these species were not observed due to the fast temporal evolution of the reaction system to form higher $C_nH_m^+$ species, which are thermodynamically favored. The absence of H_3O^+ depicts the higher proton affinities of the neutral counterparts of the generated ions as compared to water. In addition to the main compounds shown in Figure 5.1.2C, higher $C_nH_m^+$ species of masses up to 200 Th were detected, however, with very low abundances. A more detailed description of the methane system can be found in the supplementary information (Section 8.1). In the presented example, reagent ion control was performed by simply regulating the pressure. Considerable shifts in the methane ion distribution were also observed upon diluting the reagent gas with argon. An accompanied change in the gas phase acidity is possible by varying this parameter. However, for definite conclusions, this effect requires further investigations.

4.1.4.2 The active reagent ion for the N_2 system with low water content

The plots in Figure 5.1.2 reflect the final charge distributions arriving at the detector, but not necessarily the distributions actively protonating the analyte. This possible deviation becomes evident when considering the relatively long 3rd reaction stage (cf. Figure 5.1.1) and the previously mentioned low mass cut off of the segmented quadrupole. The latter may lead to significant underestimation of the H_3O^+ population and its alleged role as a reagent. This issue is addressed in the following.

From PTR-MS it is well-known that the signal intensities of analytes correlate with the reaction rate coefficient of the proton transfer reaction with H_3O^+ ^[56-58,85]. However,

reaction rate coefficients for N_2H^+ and H_3O^+ differ for each compound^[103,104], which allows distinguishing the major actively protonating reagent ion species.

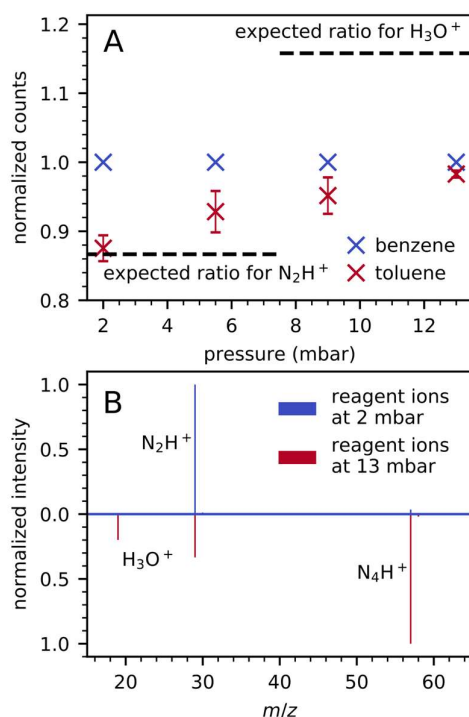


Figure 5.1.3: (A) Relative $[\text{M}+\text{H}]^+$ signal intensities of benzene and toluene sampled using GC separation at different ionization source pressures with N_2 with low water content as reagent gas. Signals were normalized to the benzene signal. Expected ratios calculated via reaction rate constants are plotted as dotted lines. Rate coefficients were taken from^[103,104]. (B) Reagent ion spectra using nitrogen with low water content as reagent gas at ion source pressures of 2 mbar and 13 mbar.

Figure 5.1.3A shows the relative $[\text{M}+\text{H}]^+$ signal intensities of benzene and toluene normalized to the benzene signal at different source pressures. For lower pressures, where N_2H^+ is the main protonating reagent ion (cf. Figure 5.1.2A), the benzene signal intensity is higher as compared to the toluene signal ($\sim 1:0.88$ benzene:toluene). This is in full agreement with the reagent ion spectra for 2 mbar shown in Figure 5.1.3B and the corresponding reaction rate coefficients, which predict a faster reaction for benzene than for toluene with N_2H^+ ^[103]. The expected protonated benzene/toluene ratios for an exclusive reaction with N_2H^+ and H_3O^+ , respectively, are shown in Figure 5.1.3A as dashed lines. With increasing pressure, the toluene signal increases relatively to the benzene signal and the maximum ratio of about 0.98:1 (toluene:benzene) is reached at 13 mbar. Since the reaction rate coefficients predict a faster reaction for H_3O^+ with

toluene as compared to benzene^[104], this finding clearly indicates an increasing contribution of H_3O^+ to the protonation process at higher source pressures. However, water still plays a minor role in the overall $[\text{M}+\text{H}]^+$ yield. This is in full accordance with the reagent ion distribution at 13 mbar given in Figure 5.1.3B.

In conclusion, to a good approximation the detected reagent ion distribution does reflect the actively protonating species and the nitrogen purity for this system is sufficiently high for N_2H^+ dominating the protonation chemistry even at the maximum source pressure.

5.1.4.3 Protonation vs photoionization and the role of the segmented quadrupole

Since the plasma glow is in line of sight with the 3rd stage (cf. Figure 5.1.1) it causes a certain generation of photoionized analyte molecules M^+ . This was generally observed with all analytes under investigation. Comparing the intensity scales in Figure 5.1.4 clearly shows that from an analytical perspective the photoion yield is rather negligible as compared to the protonated molecule yield. When operating the CI setup with an RF of $U_{\text{pp}} = 200 \text{ V}$ the $[\text{M}+\text{H}]^+$ intensity typically exceeds that of the M^+ by a factor of 50. Nevertheless, it is worth taking a closer look at both species and their dependence on the RF amplitude of the segmented quadrupole as well as the source pressure, as depicted in Figure 5.1.4. It becomes apparent that for the photoionized species only the transfer properties of the ions, formed in the 3rd stage, change with varying RF amplitude. The slopes for all pressure settings show a steep increase with a maximum transmission between approximately 80 and 120 V and level off at higher voltages to roughly 70 % of the maximum transmission. It is noted that even with 0 V M^+ ions were detected. A clearly different behavior was observed for the protonated molecule of xylene. Between 0 V and ~ 50 V at 2.5 mbar and ~80 V at 13 mbar, respectively, the $[\text{M}+\text{H}]^+$ was virtually absent. After the onsets the signal increases exponentially and levels off for 2.5, 4, and 5.5 mbar at approximately 100, 150, and 180 V, respectively. The virtually parallel progression of all slopes suggests a plateau also for the higher-pressure settings at an extrapolated higher RF amplitude. A plateau indicates that the chemistry cannot be driven further by the quadrupole field.

These significantly differing results between photoionization and protonation imply that the quadrupole not only affects the transfer properties, but also is an essential part of the 3rd stage to further drive the chemistry of the protonation step (cf. Figure 5.1.1). It is

assumed that efficient RF driven *mixing* of the reagent ions with the neutral analyte within the quadrupole field significantly amplifies the extent of ion-molecule-reactions. Additionally, the focusing effect concentrates reagent ions onto the quadrupole main axis, which leads to an increase in the rate of protonation.

Figure 5.1.4A also shows an interesting pressure dependence of the observed $[M+H]^+$ population. For example, the plateau intensity for the four lowest pressures at 200 V exhibit a perfectly linear behavior. However, an interpretation is rather difficult since the pressure affects the plasma conditions, the reagent ion formation, diffusion, the protonation step and the transfer properties. To assess each contribution, further investigation is required, which is far beyond the scope of this work. Nevertheless, the results allow to distinguish between transmission and chemistry effects and clearly demonstrate the importance of the quadrupole for the entire CI source design. Moreover, they show an optimized operational point of this stage for analytical operation at an RF amplitude of 200 V and a pressure of around 8 mbar.

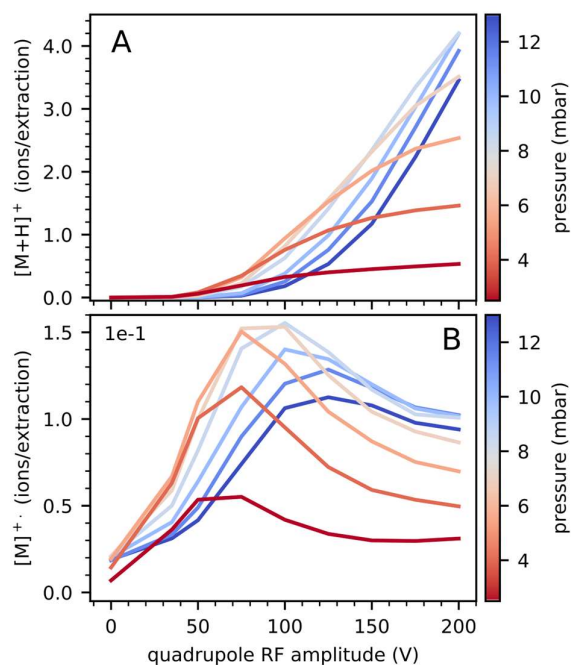


Figure 5.1.4: (A) Protonated and (B) photoionized analyte in dependence of the first quadrupole RF voltage at different ionization source pressures. A continuous sample flow of 0.5 sscm of a 10 ppmV xylene gas mixture with N_2 as reagent gas was used.

5.1.4.4 Analyte fragmentation behavior

The fragmentation behavior upon protonation with different reagent ions was exemplified with α -pinene as the analyte, which is well-known for its fragility. Figure 5.1.5 depicts the TIC normalized signal intensities for the main charged species assigned to α -pinene as a function of the source pressure. In addition to the $[M+H]^+$ at m/z 137 ($C_{10}H_{17}^+$) and the $[M-H]^+$ at m/z 135 ($C_{10}H_{15}^+$), the characteristic fragments at m/z 121 ($C_9H_{13}^+$), m/z 93 ($C_7H_9^+$) and m/z 81 ($C_6H_9^+$), which are well-known from PTR-MS^[93,105], were observed for all reagent gases to a certain extent.

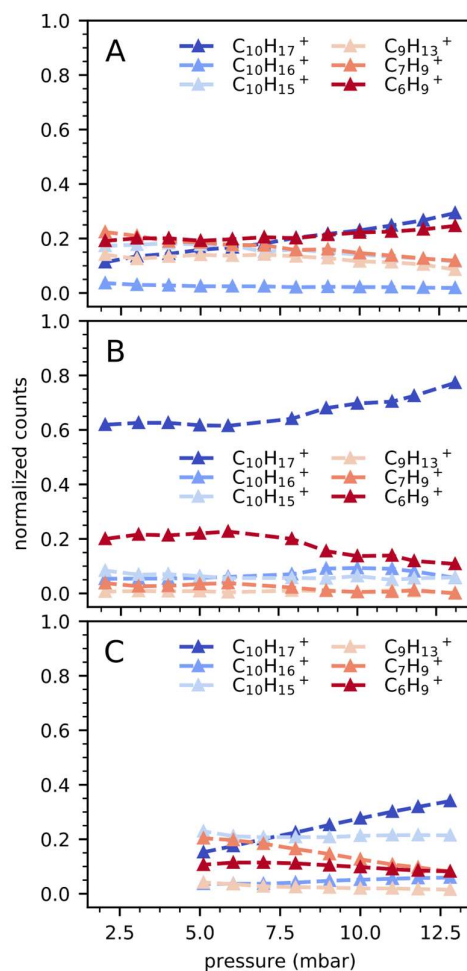


Figure 5.1.5: Pressure dependent α -pinene fragmentation behavior for (A) nitrogen, (B) isobutane and (C) methane as reagent gases. The measurements were performed with repeated GC injections of α -pinene. For comparable signal intensities, 100 μ g and 2.5 ng on column injections were used for nitrogen and isobutane/methane as reagent gases, respectively.

Figure 5.1.5 shows that the fragmentation pattern for α -pinene strongly depends on the used reagent, as expected. This result is readily rationalized by the largely differing gas phase acidities of the reagent ions, which result in also largely different excess energies for the protonation step^[52,53,87]. The RF amplitude of the segmented quadrupole was kept at 200 V. The effect of the Quadrupole RF on the extent of fragmentation is shown in Figure 8.1.2.

In case of nitrogen as reagent gas, the fragment ion pattern of α -pinene exhibits a pronounced source pressure dependence (c.f. Figure 5.1.5A). At low pressure, fragments at m/z 93 and m/z 121 are present in high abundance in addition to the well-known fragments at m/z 81 and m/z 135 ($[M-H]^+$)^[105]. Additionally, at higher pressures, H_3O^+ begins to noticeably participate in the protonation. This reduces the average excess energy deployed in the target molecule, as compared to the N_2H^+ only case. The $[M+H]^+$ ion signal increases strongly from 12 % at low pressures to 29 % at 13 mbar. This result is rationalized in terms of the changing exothermicity of the protonation step and also in higher collision numbers resulting in more effective collisional deactivation. Preliminary experiments demonstrated that careful addition of gaseous water to the pure N_2 gas flow allows for a “softer” fragmentation behavior as observed with dry nitrogen as reagent gas (cf. next paragraph). This finding potentially represents a valuable analytical method, which allows rapid in-situ switching between pure and water doped nitrogen reagent gas to swiftly adjust the exothermicity (also called *hardness* in the literature) and the degree of *selectivity* of the protonation chemistry. Using H_3O^+ in this way without the need of high field strengths, such as in PTR-MS, is subject to current research and the results will be presented in an upcoming publication.

Generally, the analyte protonation using isobutane as reagent gas shows less fragmentation as compared to pure nitrogen (cf. Figure 5.1.5B). Due to the high proton affinity of C_4H_8 and therefore lowered exothermicity of the protonation step, an abundant protonated molecule yield even at lower pressures is observed. The excess energy calculated using the difference of the proton affinities of α -pinene and the reagent ion yields $\Delta PA = 76.9$ kJ/mol for isobutane. In comparison, ΔPA for N_2H^+ (383.8 kJ/mol) and H_3O^+ (187.6 kJ/mol)^[42,106] are calculated to be approximately five and two to three times higher, respectively. The degree of fragmentation with isobutane as reagent gas decreases just slightly with increasing source pressure, yielding a relative $[M+H]^+$ abundance between 62 % and 80 %.

Methane exhibits a more complex pressure dependence of the fragmentation yield than isobutane and nitrogen (cf. Figure 5.1.5C). Notice that the lowest ionization source pressure used with methane was 5 mbar, as a consequence of reduced pumping efficiency of the H₂/CH₄ mixtures as compared to H₂/N₂ and H₂/C₄H₁₀. With methane as the reagent gas, it is striking that the [M-H]⁺ yield for α-pinene is multiple times higher as compared to isobutane and nitrogen. The most obvious explanation is the occurrence of additional hydride abstraction^[41]. It is also noticeable that with methane as reagent gas, adduct formation occurred (not shown here). Low abundance adduct ions were [M+39]⁺, [M+41]⁺, [M+43]⁺, [M+54+H]⁺ and [M+56+H]⁺ corresponding to the C_nH_m⁺ reagent ion species (cf. Figure 5.1.2).

5.1.4.5 Chromatographic performance and sensitivity

Critical GC-MS performance parameters are the overall stability of the setup/method, peak width, symmetry of the chromatographic peaks, linear ranges, and limits of detection (LOD) for diverse analytes.

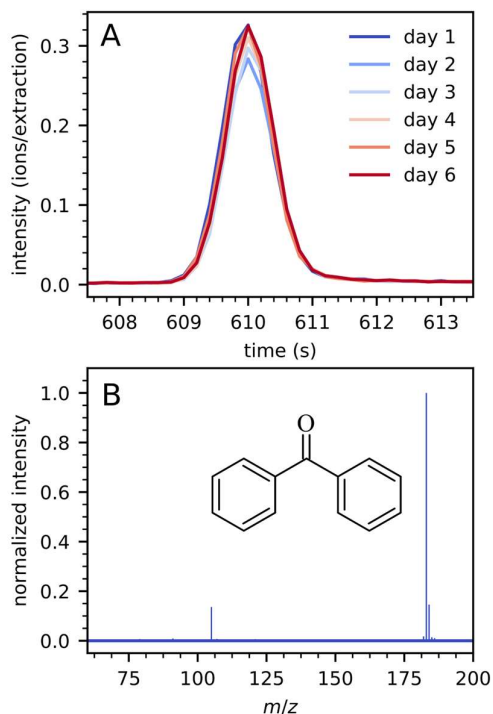


Figure 5.1.6: (A) Chromatographic peaks of multiple 100 pg benzophenone injections recorded over a period of six days. Each day represents an average of three injections. (B) Mass spectrum of a 100 pg benzophenone injection with nitrogen as reagent gas at 13 mbar ion source pressure.

For the assessment of these parameters all experiments were conducted at a total flow rate of 300 standard cm³/min. This flow was determined as the best compromise for the overall instrument performance in terms of peak shape/width (symmetrical, ~1.9 s peak width at 5 % height) and tolerable signal intensity loss due to dilution. The average asymmetry factor calculated at 10 % height^[107] for all peaks shown in Figure 5.1.6A is 1.08 and thus very close to Gaussian peak shape. The ionization source and heated transfer line temperatures were kept at 300 °C and 280 °C, respectively.

RSD determination - The performance stability is demonstrated by the relative standard deviation (RSD) of day to day injections with nitrogen as the reagent gas. For the RSD measurements, 100 pg benzophenone was injected several times over a period of six days. Figure 5.1.6A depicts the chromatographic peaks of the [M+H]⁺, each day representing the average of three GC runs. The calculated RSD based on the peak area is 4.2 %. Figure 5.1.6B exemplarily shows a mass spectrum acquired during one of the multiple benzophenone injections. The spectrum is clean and allows unambiguous compound identification.

Table 5.1.1: Limit of detections and protonated molecule yields for different compounds using nitrogen, isobutene, and methane as reagent gases, respectively.

Compound	PA (kJ/mol)	LOD (pg on column)			[M+H] ⁺ yield (%)		
		Nitrogen	Isobutane	Methane	Nitrogen	Isobutane	Methane
α-Pinene	~879 ^[106]	1.2	12.6	>25	29	63	33
Naphthalene	802.9 ^[42]	1.0	-	>25	93	-	30
2,6-Di-tert-butylp yridine	982.2 ^[42]	0.4	1.8	3.7	65	99	74
Anisaldehyde	881.1 ^[42]	0.5	0.6	2.0	82	98	84
Benzophenone	882.3 ^[42]	0.4	0.6	6.0	81	99	68
2-Decanone	n.a.	0.8	0.7	>25	91	96	77

Limits of detection and protonated molecule yields - LODs of six different analytes with all three reagent gases were determined using the calibration curve method. The LOD is defined as three times the standard deviation of the noise (3σ). For compatibility reasons and since predominantly protonated molecules are generated, the LOD calculation is done using the [M+H]⁺ signal intensity of each analyte. [M+H]⁺ yields are also used for the performance comparison between the reagent gases. Therefore, [M+H]⁺ yields were calculated as the ratio between the [M+H]⁺ - signal and the TIC of the background-

subtracted analyte mass spectra. The values calculated for each analyte and each reagent gas are summarized in Table 5.1.1. Mass spectra of the compounds presented in Table 5.1.1 are shown in Figure 8.1.6 - 8.1.8.

For the LOD determinations α -pinene, naphthalene, 2,6-di-tert-butylpyridine, anisaldehyde, benzophenone, and 2-decanone were injected in the range of 1 to 250 pg including 7 different concentrations. Most compounds showed the lowest LODs with nitrogen as reagent gas, ranging between 400 fg (for benzophenone and 2,6-di-tert-butylpyridine) and 1.2 pg (for α -pinene) on column. The protonated molecule yields for naphthalene, benzophenone, anisaldehyde, and 2-decanone with nitrogen were between 65 % and 93 %. Due to increased fragmentation, the $[M+H]^+$ yield of α -pinene is 29 %. For comparison, LODs of 2.5 pg and 3.5 pg on column for benzophenone were shown for a GC-APCI approach^[10] and for a filament-based source coupled to a Q-TOF^[108], respectively.

LODs for isobutane were recorded at 8 mbar instead of 13 mbar since the sensitivity strongly dropped at higher pressures. For isobutane as reagent gas the LODs for 2,6-di-tert-butyl-pyridine, anisaldehyde, benzophenone, and 2-decanone are comparable to N_2 . The α -pinene sensitivity, however, significantly decreased by an order of magnitude, with an LOD of only 12.6 pg. The relatively low acidity of the isobutane reagent ions is insufficient to effectively protonate naphthalene, accordingly it was not observed in this case. On the other hand, the low acidity results in significantly lower excess energies upon protonation as compared to the other two reagents, and outstanding $[M+H]^+$ yields between 95 % and 99 % were obtained. As an exception, α -pinene resulted in a protonated molecule yield of 65 %, which is attributed to its fragility as discussed earlier.

Methane as a reagent gas did not lead to acceptable LODs in the low pg on column range. Adduct ion formation and high-mass $C_nH_m^+$ reagent ions caused strong interferences with the analyte signals. Consequently, the determined LODs of three out of six analytes were higher than 25 pg on column. The lowest LOD (2 pg on column) was obtained for anisaldehyde. In addition, this compound was the only analyte with $[M+H]^+$ yields above 80 % using methane. Due to abundant $[M-H]^+$, M^+ , and adduct formation, methane generally showed the lowest $[M+H]^+$ yields of all reagent gases.

Linear ranges - The linear range spans 4.5 to 5 orders of magnitude with nitrogen and isobutane and 3 to 4 orders of magnitude with methane (Figure 8.1.3 - 8.1.5) as reagent gas. For all reagent gases, the upper limit of the linear range was limited only by the capacity of the GC. Peak fronting effects caused by GC column overload appeared at around 25 ng – 50 ng injected compound. R^2 -values were > 0.99 for all shown examples in this range.

5.1.4.6 Range of ionizable compounds

For the evaluation of the different selectivities of nitrogen, isobutane, and methane, an EPA 8270 contaminant standard mix containing 78 compounds was analyzed with each reagent gas. The same ion source parameters as for the LOD estimations were used. The results are shown in Table 5.1.2 and Figure 5.1.7. Table 8.1.1 in the supplementary section shows the detailed results for each analyte/reagent pair, as well as the compound class assignment of each analyte. Figure 5.1.7 clearly demonstrates the very good performance of nitrogen as reagent gas with 74 out of 78 detected compounds, as compared to only 41 and 62 detectable species with isobutane and methane, respectively.

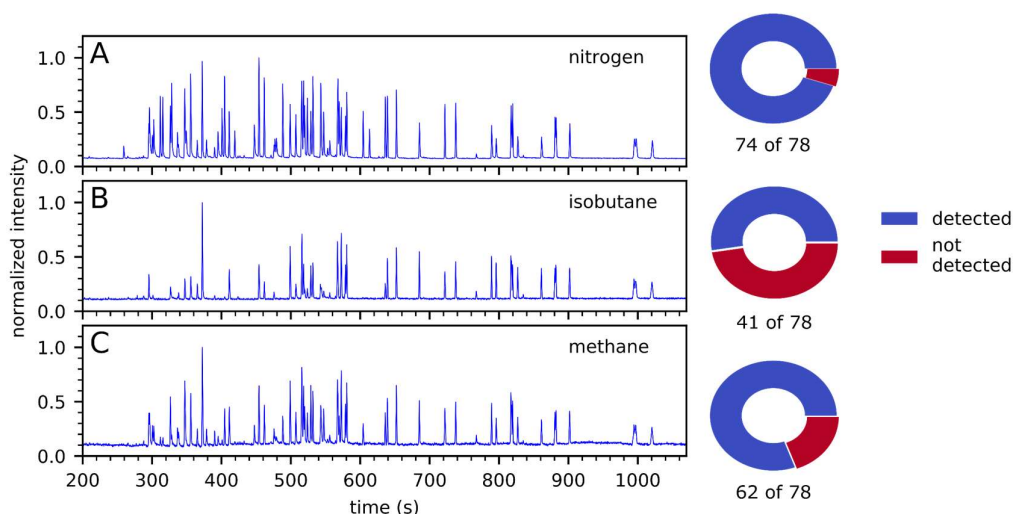


Figure 5.1.7: TICs of 2.5 ng splitless injections of an EPA 8270 LCS mix using (A) nitrogen, (B) isobutane and (C) methane as reagent gas, respectively. The pie charts illustrate the amount of detected (blue) and not detected compounds (red).

Since the sample compounds cover a broad range of chemical functionalities, the EPA 8270 mixture allows a critical assessment of the performance of the three reagent gases regarding different compounds/compound classes. For proton transfer reactions, the

proton affinity is naturally the main analyte property controlling the protonation efficiency. However, proton affinities are not available for all compounds present in the mixture. Kauppila et al.^[94] categorized the compounds into seven different classes depending on the functionalities and expected ionization behavior. Although this was done for photoionization, we apply the same categories in this work except for phenolic compounds, which are treated separately, see below.

18 compounds belong to the class of polycyclic aromatic hydrocarbons (PAH). Differently sized PAHs, some with additional methyl groups or aliphatic rings, constitute this group. Except for naphthalene (PA(Naphthalene) = 802.9 kJ/mol)^[42], all PAHs in this list exceed the proton affinity of isobutane (802.1 kJ/mol)^[42] sufficiently. Consequently, all PAHs were detected with nitrogen and methane and 17 out of 18 with isobutane, respectively. The $[M+H]^+$ ion was observed with all reagent gases and it represented the base peak for all PAH compounds using nitrogen and isobutane as reagent gas. With methane, the $[M+H]^+$ represented the base peak for most PAHs, but for some analytes also M^+ and adduct species were abundantly present.

As stated above, the compounds with phenolic-groups were treated as a separate class. It includes 17 phenolic compounds with up to two nitro- or five chlorine-substituents, respectively. The range of ionizable compounds in this group is as expected from available thermochemical data: Phenol has a proton affinity of 817.4 kJ/mol^[42]. Electron density withdrawing groups, e.g., -Cl or -NO₂, significantly increase the acidity of phenolic compounds^[109,110] and hence reduce the PA values. Therefore, neither phenol nor chlorine- and nitro-substituted phenolic compounds were ionized using isobutane as reagent gas. The three cresol isomers are special cases: The methyl group in ortho and para position pushes the respective PA values close to protonation threshold^[42,94,110]. This means that o-cresol and m-cresol are amenable to protonation with isobutane reagent ions, whereas the PA of p-cresol is slightly lower than the PA of phenol, which was not detected. However, p-cresol and m-cresol were not resolved by the chromatography, and further experiments on the individual behavior of these two compounds with the pure isomers were currently not performed. Consequently, for isobutane as reagent gas, p-cresol was denoted as “not detected”, based on the compared PA values. Nevertheless, from an analytical point of view it is interesting to distinguish between the GC unseparated m- and p-cresol by the choice of protonating reagents. With methane, seven of the 17 phenolic compounds were detected, including phenol and all cresol-isomers.

Higher substituted phenols with more than one Cl/NO₂ substituent were not detected. In stark contrast, nitrogen as reagent gas was able to protonate 14 out of 17 phenolic compounds, even with up to four chlorine- and up to one NO₂-substituent. Only 4,6-dinitro-2-methylphenol, 2,4-dinitrophenol, and pentachlorophenol were not detected.

Non-phenolic, halogenated compounds containing up to six chlorine or bromine substituents define the third class, denoted as “halogenated” in Table 5.1.2. 11 compounds of this class with either aromatic or aliphatic structure are present in the EPA 8270 mixture. Halogenated phenyl ethers are also assigned to this group, since their phenylic function is etherified. Nitrogen as reagent gas was able to ionize all constituents of this third class. For most of these compounds the [M+H]⁺ was the dominating species. Only for hexachloroethane and hexachlorocyclopentadiene the [M-Cl]⁺ represented the base peak. With methane as the reagent gas, hexachloroethane and hexachlorocyclopentadiene were not ionized at all, as well as three other compounds of this group. Therefore, six out of 11 halogenated compounds were detected with methane. Isobutane derived reagent ions were not able to ionize any of the compounds in this group.

The nitro compound class includes analytes with up to two NO₂-groups attached to aromatic rings without other substituents present. Six of the 78 compounds within the mixture are assigned to this group. Using nitrogen and methane as reagent gases, all constituents lead to [M+H]⁺, for two and four compounds, respectively, even as the base peak. None of the nitro compounds were observed with isobutane.

In addition to nitro-functionalized molecules, the EPA mixture includes 12 other compounds containing nitrogen, mainly with amine functionality. Molecules with halogens or nitro groups next to the amine functionality are also classified as members of this group.

Amine functionalities are known to strongly elevate proton affinities. Thus, amine groups are expected to have a higher impact on the protonation behavior than the presence of nitro or halogen substituents. This is clearly supported by the fact that all members of this class were observed with all three reagent gases. With isobutane, the [M+H]⁺ dominated the mass spectra in all 12 cases. With nitrogen and methane as reagent gases, 11 out of 12 compounds formed the [M+H]⁺ as the base peak.

Six phthalate- and one adipate-ester are classified as “esters”. All esters were ionized by all reagent ions. For most of them, nitrogen leads to stronger fragmentation as compared to isobutane and methane. Thus $[M+H]^+$ signals represent the base peak for only one of the seven esters with nitrogen as reagent gas. For methane and isobutene, the $[M+H]^+$ ion is the dominating species for all ester grouped compounds.

All three ethers in the mixture were observed with nitrogen and methane as reagent gases, but not with isobutane. Mostly the $[M+H]^+$ ion were the base peak, only bis(2-chloroethoxy)methane was detected as a fragment at 93 Th with nitrogen as reagent gas.

The last group defined by Kauppila et al. comprises four other oxygen (O)-containing compounds^[94]. Benzoic acid is the only analyte within this group that is not detected even with nitrogen as reagent gas. This finding is surprising, since its proton affinity is higher as compared to water and nitrogen^[42]. The assumption that benzoic acid is already lost/degraded during the chromatographic separation was supported by an additional GC-EI-TOF experiment. Nonetheless, this compound is listed as non-detected in Table 5.1.2.

Table 5.1.2: Number of detected compounds in the EPA 8270 LCS mixture, classified by functionality.

Group (Number of compounds)	Number of detected compounds (%)		
	Nitrogen	Isobutane	Methane
PAHs (18)	18 (100)	17 (94)	18 (100)
Phenols (17)*	14 (82)	2 (12)	7 (41)
Halogenated compounds (11)	11 (100)	0 (0)	6 (55)
Nitro-compounds (6)	6 (100)	0 (0)	6 (100)
Other N-containing (amines) (12)	12 (100)	12 (100)	12 (100)
Esters (7)	7 (100)	7 (100)	7 (100)
Ethers (3)	3 (100)	1 (33)	3 (100)
Other o-containing (4)	3 (75)	2 (50)	3 (75)
All (78)	74 (95)	41 (52)	62 (79)

* m-cresol and p-cresol were not separated by the GC-column and oven program. Detectability of these isomers was estimated based on their proton affinities.

Due to the lower proton affinity of benzyl-alcohol this compound was not detected with isobutane reagent gas. With nitrogen and methane only the tropylium cation was detected as a fragment at 91 Th.

5.2.5 Conclusion

This work demonstrates the outstanding analytical performance of an H_3^+ driven chemical ionization source with three sequential reaction stages for GC-TOF-MS analysis. In particular nitrogen as reagent gas and its corresponding N_2H^+ reagent ion proves to be of high analytical value. It shows excellent, wide-range ionizing capabilities, but far less pronounced fragmentation as compared to the direct protonation of analyte molecules with H_3^+ . Moreover, precise water vapor addition to the pure N_2 gas flow establishes a well-defined H_3O^+ or $[\text{H}(\text{H}_2\text{O})_2]^+$ populations without further clustering steps, which can lead to virtually equally “soft” fragmentation behavior as with isobutene as reagent gas. This finding provides a valuable analytical method, which is capable of swiftly adjusting in-situ the *hardness* and the degree of *selectivity*. Generating H_3O^+ in this way - without the need of high field strengths as applied in PTR-MS - is subject to current research and will be presented in an upcoming publication.

5.2 Parallel operation of electron ionization and chemical ionization using a single TOF mass analyzer

Steffen Bräkling^{1,2*}, Kai Kroll², Carsten Stoermer¹, Urs Rohner¹, Marc Gonin¹, Thorsten Benter², Hendrik Kersten², Sonja Klee¹

¹TOFWERK, 3645 Thun, Switzerland

²Department of Physical and Theoretical Chemistry, University of Wuppertal, Gauss Str. 20, 42119, Wuppertal, Germany

Reprint with permission from *Anal. Chem.* **2022**, *94*, 15, 6057-6064. Copyright 2022 American Chemical Society.

<https://pubs.acs.org/articlesonrequest/AOR-5GSVPK8XB5VEGKGJB5VV>

5.2.1 Abstract

This work describes a novel GC-MS (gas chromatography-mass spectrometry) system that simultaneously displays the mass spectral information of electron (EI) and chemical ionization (CI) generated ion populations for a single chromatographic peak. After GC separation, the eluent is equally split and supplied in parallel to an EI and a novel CI source, both operating continuously. Precise switching of the ion optics provides the exact timing to consecutively extract the respective ion population from both sources and transfer them into a time-of-flight (TOF) mass analyzer. This technique enables the acquisition of complementary information from both ion populations (EI and CI) within a single chromatographic run and with sufficient data points to retain the chromatographic fidelity. The carefully designed GC transfer setup, fast ion optical switching, and synchronized TOF data acquisition system provide an automatic and straightforward spectral alignment of two ion populations. With an eluent split ratio of about 50 % between the two ion sources, instrument detection limits (IDLs) of < 40 fg on column (octafluoronaphthalene) for the EI and < 2 pg (Benzophenone) for the CI source, respectively were obtained. The system performance and the additional analytical value for compound identification are demonstrated by means of different common GC standard mixtures and a commercial perfume sample of unknown composition.

5.2.2 Introduction

For decades, gas chromatography (GC) in combination with electron ionization (EI) mass spectrometry (MS) has been used as a valuable analytical tool, and still today represents the method of choice for targeted analysis of volatile and semi-volatile compounds. In general, the EI-MS detector depicts the rather narrow chromatographic peak shapes with high fidelity. The standard setting of applying 70 eV electrons offers non-selective ionization with high efficiency and produces characteristic, reproducible compound fragmentation patterns. These allow for a straightforward database matching, e.g., with the NIST/EPA/NIH Mass Spectral Library^[22] and nearly automated compound identification in targeted routine analysis. In addition, those fragmentation pattern provides valuable structural information to further confirm the molecule of interest^[28,111].

In non-target analysis, however, instrumental requirements are more elaborate due to the lack of information on the analytes prior to the analysis. Furthermore, standard samples are not always available to confirm the presence of a specific compound^[112]. In liquid chromatography (LC) coupled to mass spectrometers, non-target screening is widely established in research fields such as in water and food analysis^[62,64,65]. Some non-targeted applications have also been reported for GC-MS hyphenation using atmospheric pressure ionization^[13,70], originally designed for LC applications^[113,114]. These methods usually apply collision induced dissociation (CID) to gain the additional structural information required to confirm the presence of a compound. However, EI fragment spectra are often preferred over CID due to better reproducibility, platform-independence, and availability of comprehensive libraries. Though examples for non-targeted analysis with GC-EI-MS are available in the literature^[59], identification of the molecular ion, greatly facilitating compound assignment, is often not feasible due to extensive fragmentation immediately following the 70 eV ionization process; a complementary ionization mechanism yielding the molecular ion would therefore desirable^[75,115]. Numerous examples for “softer” ionization processes in a low-pressure ionization GC-MS system, e.g., chemical- (CI)^[7,116], photo- (PI)^[17,30], field- (FI)^[3,4], and cold electron-ionization^[24,117] have been introduced. All these techniques generate intact molecular ions. To provide both, 70 eV EI fragment and exact molecular mass information of a sample, two separate GC runs are required with most common instruments, first using EI and subsequently a “soft” ionization technique, respectively. Multiple MS vendors offer an exchangeable EI and additional (mostly) CI source. This

approach, however, increases analysis time, leads to complex data alignment, and poses the risk of sample degradation/changes between the two individual runs. Often, laborious hardware changes are necessary to exchange the ion sources. The first example for a single ion source approach was given by Brunnée^[118] in 1968 with an EI/ field ionization (FI) combination. The use of an EI and CI ionization volume within a single ion source for subsequent measurements was shown in ref [76]. Simultaneous acquisition with both ionization techniques for a single GC or even GCxGC run, requires fast and synchronized extraction, detection, and data acquisition of the two different ion populations. Quasi-simultaneous acquisition of both, “soft” and “hard” ionization methods was shown by Eschner et al.^[16] using EI/PI and by Alam et al.^[6] with rapid switching between high and low kinetic energy electrons of 70 eV and 14 eV, respectively. In all these instruments, the “soft” ionization method essentially operates in the same low-pressure region of the 70 eV EI source. In contrast, CI sources require elevated pressures to ensure sufficient reactive collisions between the analyte and the charged reagents. Quasi-simultaneous operation of EI and CI using the same ion source is limited by the required pressure adjustment between each mode change.

Consequently, efficient generation and acquisition of CI and EI information within a single chromatographic run is only possible employing two different, spatially and pressure separated ionization sources. Previously, Claflin et al.^[119] and Hejazi et al.^[73] presented approaches with two separate mass spectrometers, each equipped with an EI or CI/FI source, respectively, coupled to one chromatographic system, demonstrating the advantage of acquiring both EI and CI/FI data. Disadvantages of dual a MS setup are increased space and other resource demands, non-correlated detector shifts between the two instruments and of course the financial aspects for the required hardware.

In this work we describe a GC-MS system comprised of two spatially separated and continuously operating EI and a medium-pressure CI source within the same TOF analyzer during a single GC run.

5.2.3 Experimental

Mass spectrometer design and ionization sources. Figure 5.2.1 depicts schematically the principle of operation of the GC-dual ionization source mass spectrometer. The setup combines a medium-pressure CI source enclosed in an atmospheric pressure interfaced TOF (API-TOF; TOFWERK, Thun, Switzerland) and an EI source located in the high-

vacuum pressure stage of the API-TOF systems directly upstream of the TOF mass analyzer. The TOF mass analyzer was operated with a resolution of ~ 4500 at m/z 183 and a mass range of m/z 10 – 500. The EI source was operated with 70 eV electron energy and an emission current of 1 mA. Details on the custom CI source in combination with a GC-TOF were presented previously^[120].

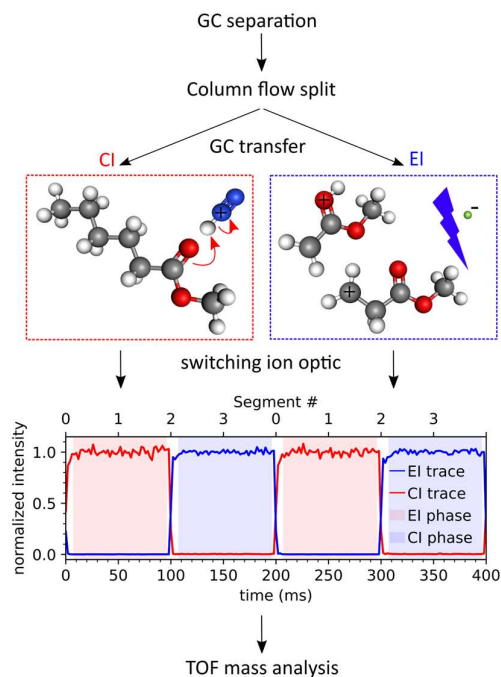


Figure 5.2.1: Schematic depicting of the dual ionization source GC-MS setup and normalized Total ion counts of the CI and EI signals during switched operation. A switching rate of 10 Hz is shown resulting in a 5 Hz temporal resolution for each ion source.

Both sources operate continuously. A custom ion optical device consecutively extracts the ion populations from each source and pulses them into the TOF analyzer. Ion optical switching ensures accurate temporal synchronization of the mass analysis and unequivocal allocation of the data. In this work a 5 Hz acquisition rate was used to sufficiently represent a one-dimensional GC peak with the corresponding EI- and CI-TOF mass spectra. The equilibration time for the mass signal to stabilize is approximately 5 ms between each cycle (cf. Figure 8.2.1). For clarity of representation and demonstrating the fast ion optical switching capability, single spectra were averaged to 500 Hz in Figure 5.2.1. Individual spectra recorded during a single ion source acquisition cycle are averaged to a spectrum leading to a 5 Hz acquisition rate. This setting was used for all studies in this work. To separate the EI and CI data, mass spectra are saved to different

segments within the data file for each time step (cf. Figure 5.2.1). An experimental arrangement is given in Figure 8.2.2.

GC hyphenation. For GC separation, an Agilent 7890A GC (Agilent Technologies, Santa Clara, CA, USA) equipped with a liquid injection inlet and a Rxi-5ms column (30 m, 0.25 mmID, 0.25 μm , Restek, Bellefonte, PA, USA) was used. The GC effluent is then equally split through a silcoNert coated Y-Splitter (Restek, Bellefonte, PA, USA) into two individual gas flows, feeding the respective ion sources. Two custom transfer lines ensure continuous heating to retain the chromatographic separation up to the ion source inlets. The custom transfer lines with a bending radius of < 15 cm were made from Ultimet Plus stainless-steel tubing (Agilent technologies, Santa Clara, Ca, USA) with an inner diameter of 0.25 mm, electrically insulated and resistively heated on the outside leading to temperatures up to 300 $^{\circ}\text{C}$. Each transfer line is connected to the MS with heated vacuum feedthroughs to the respective ionization source.

Chemicals and sample preparation. All chemicals, including the compounds of the custom 100 $\text{pg}/\mu\text{l}$ ketone/aldehyde mix (cf. Table 8.2.2), were purchased from MERCK/Sigma Aldrich (Buchs, Switzerland). A fatty acid methyl ester (FAME) C₄-C₂₄ saturated carbon mixture and an EPA 8270 LCS mix were diluted with hexane to 1 $\text{ng}/\mu\text{l}$ and 2,5 $\text{ng}/\mu\text{l}$, respectively. The CI source was operated as described in ref [120]. For the perfume analysis, 0.2 ml headspace of a brand perfume was sampled, using a manual headspace sampler (Ellutia, Ely, UK).

Gas chromatographic separation method. For the analysis of the FAMEs and the EPA 8270 LCS mix the following procedure was used: After 1 μl splitless (inlet temperature 280 $^{\circ}\text{C}$) autosampler (Agilent technologies, Santa Clara, CA, USA) injection, the temperature was held for 2 min at 43 $^{\circ}\text{C}$, followed by an oven temperature ramp rate of 20 $^{\circ}\text{C}/\text{min}$ to 250 $^{\circ}\text{C}$ and further increased to 300 $^{\circ}\text{C}$ at an oven ramp rate of 30 $^{\circ}\text{C}/\text{min}$. For the perfume headspace and the custom ketone/aldehyde standard analysis the temperature ramps were 10 $^{\circ}\text{C}/\text{min}$ and 20 $^{\circ}\text{C}/\text{min}$, respectively. A constant carrier gas flow of 1.2 sccm helium (99.9999%) was used.

5.2.4 Results and discussion

5.2.4.1 Chromatographic data alignment and GC column split characterization

The presented instrument enables unique simultaneous acquisition of EI and CI mass spectra with one mass analyzer during a single GC run. Figure 5.2.2A shows the chromatograms of a FAMES C_4 - C_{24} even carbon GC standard for the EI and CI mode, respectively. All compounds, including retention times and detected major ion signals, are listed in Table 8.2.1.

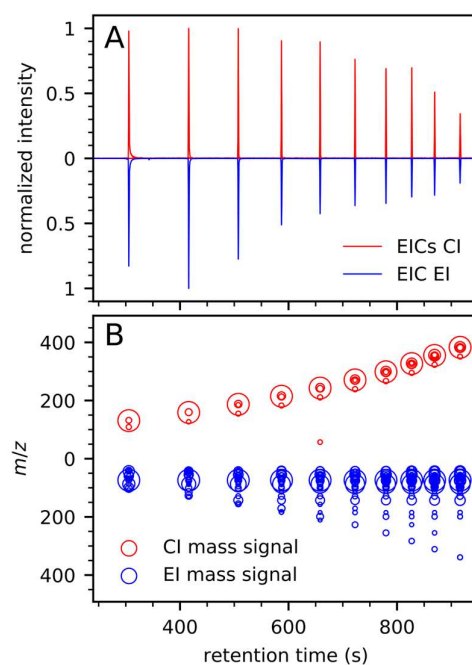


Figure 5.2.2: (A) normalized extracted ion chromatograms (EIC)s of the $[M+H]^+$ signals from CI and the fragment at m/z 74 from EI for 1 ng on column of C_4 - C_{24} saturated carbon FAMES. (B) normalized mass-signal distributions of the FAMES standard, sampled from the CI and EI source, respectively. Intensities are indicated by the marker size.

Methyl butyrate was not analyzed with EI due to the filament solvent delay. The red trace depicts the extracted ion chromatograms (EICs) of the individual $[M+H]^+$ signals from the CI source. The blue line shows the EIC of the $C_3H_5O_2^+$ fragment at m/z 74, which represents the base peak for all analyzed FAME compounds in the EI spectra^[20,121]. The corresponding mass distributions of the EI (blue) as well as the CI (red) spectra for each chromatographic peak are depicted in Figure 5.2.2B with the negative and the positive y-axis for the respective m/z scale. The circle size is proportional to the signal intensity.

It is clearly seen that in case of the CI spectra the distributions show low variance, and the center of masses are shifted to higher masses with progressing retention time. The main signals clearly represent the $[M+H]^+$ ions generated via “soft” ionization. In contrast, the EI mass spectra show the expected pronounced broadening of the mass distributions with increasing retention time and increasing mass, accordingly. Generally, a more detailed fingerprint improves the database-matching, however, all FAME compounds show identical main fragments with comparable relative intensities ($m/z = 74, 87, 43, \text{ and } 143$). This makes all EI mass spectra of these homologues look very similar and renders individual compound identification with higher uncertainty. Again, the $[M+H]^+$ signals dominate the CI mass spectra for all measured FAMEs, only minor fragment signals ($< 2.5 \%$) at $[M-31]^+$ are observed. This finding demonstrates the complementary dimension gained with CI for compound differentiation and identification.

However, the advantage of combining CI and EI data requires highly precise and constant alignment of their respective chromatograms, since the retention time essentially determines the correct assignment of both spectra types to the same compound. Therefore, close attention was paid to minimize feasible retention time deviations after the chromatographic separation step, by considering crucial design aspects, such as:

1. The correct transfer length between the GC and the respective ionization source,
2. the flow velocities within the GC-ionization source transfer,
3. different mean dwell times within the ionization sources and
4. different ion transfer times for the two ion populations (EI/CI) within the mass spectrometer.

For the characterization of the final chromatographic setup, the FAMEs standard with a broad range of compound volatility, from early eluting, e.g., methyl hexanoate to late eluting, e.g., methyl lignocerate was used. Figure 5.2.3A shows the measured deviations between the EI retention time (maximum of the chromatographic peak resembled by the EI data points) and the corresponding CI retention time (maximum of the peak resembled by the CI data points) for each FAME. These data confirm chromatographic retention time deviations $< 100 \text{ ms}$ for all compounds, which is lower than the temporal resolution of the 5 Hz acquisition rate (corresponding to 200 ms) for each ion source. Furthermore, a linear regression of the EI and CI retention times yields a correlation with an r^2 -value

of > 0.9999 and a linear function of $RT_{CI} = (1.000 \pm 6e-5) * RT_{EI} - (0.1652 \pm 0.041)$ (cf. Figure 8.2.3). Note that the combination with an atmospheric pressure CI source may require a more complex transfer setup. In addition to the retention time, the corresponding peaks of the FAMES standard recorded via EI and CI, respectively, essentially show similar shapes and widths. Figure 8.2.4 illustrates overlays from three peaks of the respective CI and EI chromatograms at different retention times, with variances at FWHM (full width half maximum) of max. 6.2% between EI and CI.

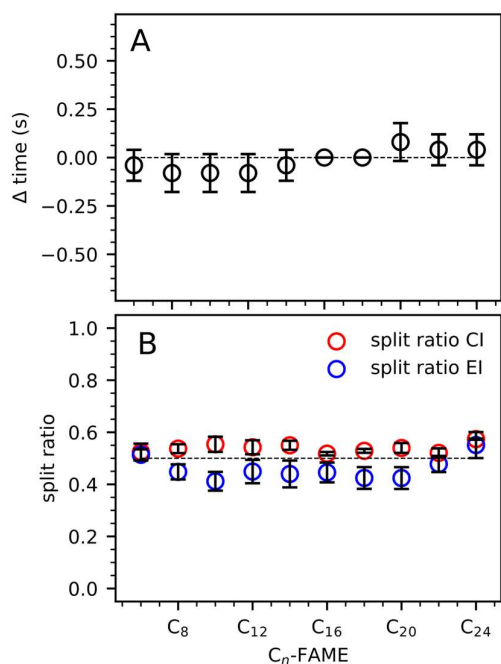


Figure 5.2.3: (A) Time deviation between CI and EI chromatogram for each FAME. (B) Measured column split ratios between CI and EI source for each FAME. In both data sets, three replicates were averaged, and the error bars indicate the respective standard deviation.

For an assessment regarding sensitivity and quantification performance, it was crucial to investigate the ratio of the split eluent. Due to the very good coincidence of CI and EI retention times, a significant discrimination was not expected. Nevertheless, to estimate the relative amount of analyte transferred to each ionization source, the Y-splitter was replaced by a straight MXT stainless steel column connector (Restek, Bellefonte, PA, USA) and each ion source was separately coupled to the GC column. In this way the entire sample was transferred only into one source and the signal intensities were compared to the acquired data using the Y-splitter. Gas flows entering the ion source were kept constant to prevent pressure differences in the ion transfer. The ratio of the

corresponding base peaks measured with the direct and the split GC flow, respectively, are depicted in Figure 5.2.3B. The results show only small deviations from the theoretically expected ratio of 50 % as indicated by the dotted line. The CI source values slightly vary between 50 % and 55 %. The EI source shows ratios slightly below 50 %, with the lowest values at around 42 %. Also, the split ratio is stable within the covered temperature range, since no explicit shift was recognized throughout the GC run.

5.2.4.2 Analytical performance

The analytical performance with regard to instrument detection limit (IDL)^[122] was determined for both ionization modes. Nine repeated GC injections of 10 pg on column benzophenone and of 200 fg on column octofluoronaphthalene (OFN) each were used for the determination of the CI- and the EI-IDL. The extracted ion chromatograms of the corresponding mass traces of the $[M+H]^+$ for benzophenone and the M^+ for OFN are depicted in Figure 8.2.5. For the EI mode an IDL of < 40 fg on column and for the CI mode an IDL < 2 pg on column were determined. These results are in good agreement with the sensitivities obtained for each ionization source operated separately. As expected, the switching method reduced the sensitivity by approximately a factor of four due to the 50% GC split and the 50% duty cycle for mass acquisition in each mode.

5.2.4.3 Spectrum quality for compound identification

For an assessment of the degree of unambiguous compound identification, the spectrum quality in both modes is essential, in particular with regard to:

1. Mass accuracy and precision of the quasi molecular ion signal $[M+H]^+$,
2. representation of the relative isotopic abundances according to the natural occurrence and
3. the matching quality of the EI fragment distribution of a compound with the corresponding database spectrum.

The latter clearly defines the reliability of compound assignment when comparing the experimental fragment signature with available databases. The quality of the first criterion defines the abundancy number of feasible molecular formulas and their errors from the true constitution. Consequently, a highly accurate and precise mass determination essentially reduces the number of feasible sum formulas and improves the correct identification probability. However, even for the inherently limited mass range rather elaborate lists of compounds are generated by the search algorithms^[123]. Despite some

general rules⁷⁸, this list can be further shortened using the information from the isotopic abundance pattern. It is noted that for the correct assignment of molecular formulas based on isotopic intensities, it is a prerequisite that the sample itself reflects the natural ratios.

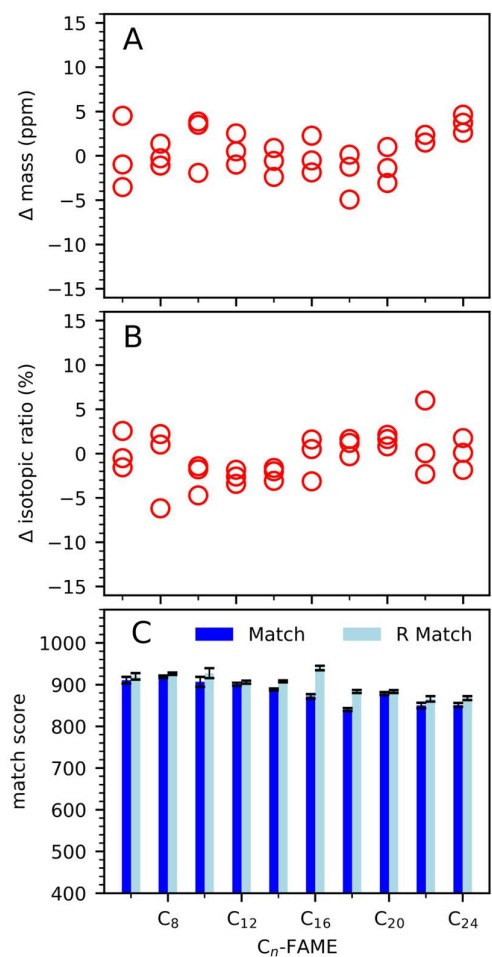


Figure 5.2.4: (A) Mass accuracy of the $[M+H]^+$ signals from the CI source and (B) the accuracy of the natural isotopic abundance on the first isotopic peak $[(M+1)+H]^+$. (C) Fragment library matching scores (Match) and reversed matching scores (R Match) of the ion distributions from the EI source.

The spectrum quality obtained with the instrument was investigated with regard to all three criteria and the results are summarized in Figure 5.2.4. Again, the FAMES standard was used with three replicates and an injected mass of 1 ng on column of each compound. The characterization of the CI mass accuracy reveals deviations < 5 ppm (cf. Figure 5.2.4A) and an RMS of all measurements of approximately 2 ppm deviation from the true masses. With this performance, an accurate determination of the third decimal of masses up to 300 m/z is possible. For evaluating the quality of the isotopic information, 1 ng on column of each FAME was used and the CI data of the corresponding

chromatographic peaks were averaged as stated. Figure 5.2.4B illustrates the deviations of the experimentally obtained intensities for the first isotopic peaks $[(M+1)+H]^+$ and the theoretically predicted intensities. The natural isotopic abundances are taken from ref [124]. The error for depicting the natural ratios is within $\pm 5\%$ for all FAMES. In most cases, this is sufficient to exclude suggested molecular formulas that already differ by two carbon atoms from the real constitution. Note that particularly for halogenated compounds, also higher isotopes should be considered.

For an assessment of the EI mass spectra quality the matching factors and reversed matching factors based on the NIST/EPA/NIH Mass Spectral Library^[22] search results are depicted in Figure 5.2.4C for all measured FAMES. The applied scale defines a match value of 1000 as a “perfect forward” as well as a “reverse” match. The plot in Figure 5.2.4C illustrates matching factors well above 840 for all compounds, which demonstrates excellent similarity of the experimental spectra with the data base.

4.2.4.4 Improved identification using EI and CI information

The performance of the present instrument and the value of the complimentary data were assessed with two different samples: a liquid injection of a custom carbonyl mixture and a headspace injection of a perfume sample. The simultaneously acquired EI and CI chromatograms are shown in Figure 5.2.5A and Figure 5.2.5B, respectively. In addition, a more complex standard sample of an EPA 8270 LCS mix is shown in Figure 8.2.7 and Figure 8.2.8. Table 8.2.2 lists the main ion signals observed for the carbonyl sample for each ionization mode, as well as the retention times, the mass errors, the $[M+H]^+ / [(M+1)+H]^+$ intensity ratios, and the EI fragment library matching factors for each compound. The carbonyl standard measurement clearly demonstrates the advantage of the complementarity of EI and CI data in the assignment of the correct elemental composition. Figure 5.2.6A-C show the simultaneously recorded CI and EI EICs of the main ion signals detected for 2-dodecanone, dodecanal and 2-tridecanone. Clearly, the 5 datapoints/s for each ion source fully retain the chromatographic fidelity. Additionally, Figure 5.2.6D-F show the corresponding mass spectra for each compound. The similarity of the EI fragmentation pattern of 2-dodecanone and 2-tridecanone is clearly discernible in Figure 5.2.6D and 5.2.6F.

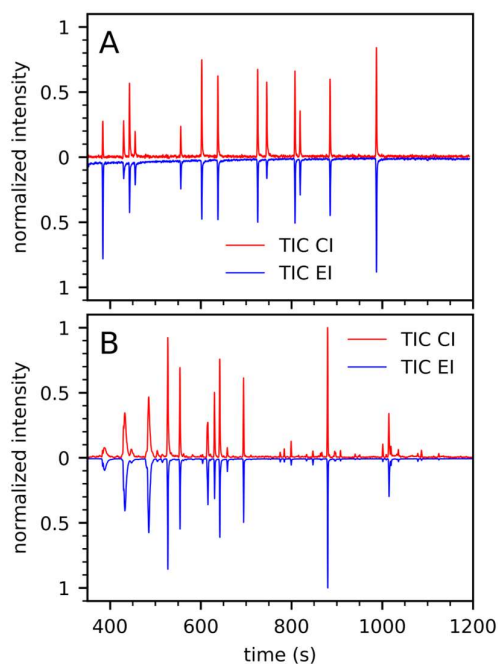


Figure 5.2.5: Total ion chromatograms (TICs) of (A) a custom-made carbonyl compound mix and (B) the headspace of a perfume sample.

The main ions, ranked in decreasing intensity, are m/z 58, 43 and 71 (cf. Table 8.2.2) with nearly identical relative signal strengths in both cases. The matching factor for each spectrum with the corresponding “wrong” database spectrum is 825 and 826, respectively. Consequently, the EI information alone still results in a fairly good match for the wrong compound. For this case, the advantage of the immediately available CI information is apparent. With virtually no fragmentation or adduct formation the CI data in Figure 5.2.6D and 5.2.6F (red traces) show significantly simplified mass spectra with intense protonated molecule signals ($[M+H]^+$) at m/z 185.1907 and m/z 199.2052, respectively. The accurate mass deviates from the corresponding molecular formulas $C_{12}H_{25}O^+$ and $C_{13}H_{27}O^+$ by -3.6 and 2.4 ppm, respectively. This lies well within the evaluated mass accuracy and precision range of ± 5 ppm. For both compounds the list of generated formulas, using the most common hetero atoms and a generous ± 10 ppm mass difference, does not yield the true elemental composition for the measured exact mass in the first place. The primary hits of the sum formula generator are listed in Table 8.2.3. However, in addition to the mass accuracy, especially the isotopic abundance pattern, besides other common rules^[78], eliminates most of the “wrong” and chemically impossible suggestions. The isotopic pattern fitting is easily implemented into an automated workflow for subsequent rating procedures. With -1.1% difference to the

theoretical abundance of the first isotope only the suggested formula $C_{12}H_{25}O^+$ lies within the evaluated $\pm 5\%$ range (cf. Figure 5.2.4B). In case of the measured exact mass of m/z 199.2047 the effect is even more pronounced. The first five hits derived by the sum formula generator lie within the allowed ± 5 ppm (cf. Table 8.2.3) accurate mass deviation and are feasible candidates. In fact, the last elemental composition $C_{11}H_{25}N_3^+$ is a realistic stable molecule found in the NIST/EPA/NIH Mass Spectral Library^[22] as N''-Hexyl-N,N,N',N'-tetramethyl -guanidine. However, neither this one, nor any of the other suggested formulas meet the 5 % isotopic ratio deviation criterium, except $C_{13}H_{27}O^+$ with 3.5 % error. Additionally, the EI spectrum strongly indicates a ketone functionality.

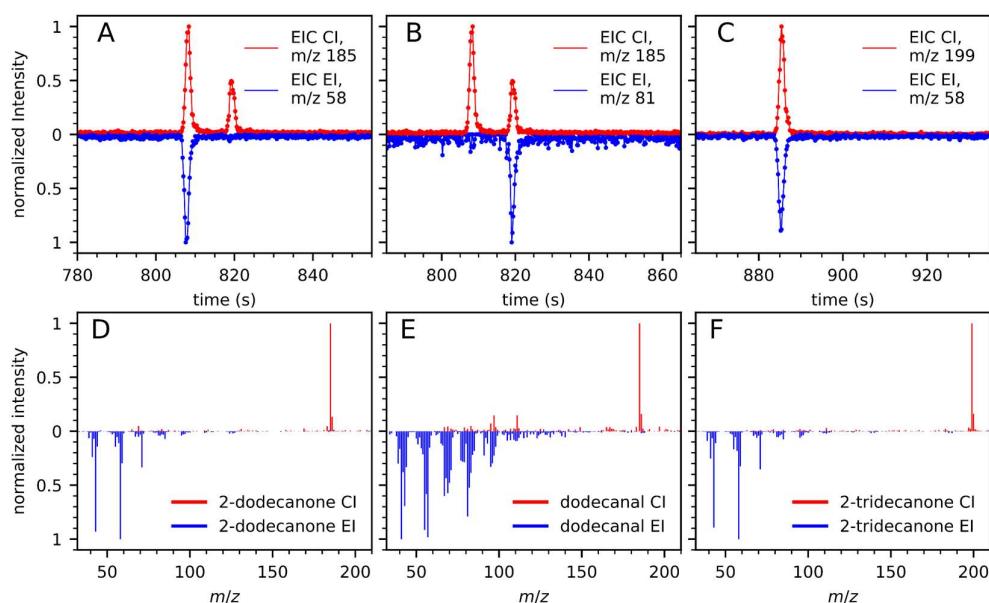


Figure 5.2.6: Enlarged chromatograms and mass spectra for three substances of the carbonylic standard mix. Chromatographic peaks of 100 pg on column (50 pg per ion source) of (A) 2-dodecanone (B) dodecanal and (C) 2-tridecanone, simultaneously recorded in CI and EI mode. Comparison of the acquired EI and CI mass spectra of (D) 2-dodecanone and (E) dodecanal and (F) 2-tridecanone.

The GC carbonyl mixture also provides an excellent example, in which the molecular ion information was insufficient for unequivocal compound identification. Figure 5.2.6D and Figure 5.2.6E display virtually the same CI spectra (red traces) of two different compounds, dodecanal and 2-dodecanone, respectively. As these are isomeric compounds, the exact mass and isotopic ratio information from the corresponding CI mass spectra are identical. In most cases, even retention times are similar and do not allow to distinguish between isomers. In the present example, they differ only by 11 seconds

(cf. Table 8.2.2). In this case the fragment information provided by the EI method is of great value: The blue mass spectra in Figure 5.2.6D and 5.2.6E show distinct different patterns for dodecanal and 2-dodecanone. This is also confirmed by the corresponding matching factors of 914 and 888 for each correct assignment.

Another illustrative example for the value of parallel recording of CI and EI data is given by the two co-eluting compounds citronellal and trans-2,cis-6-nonadienal (cf. Table 8.2.2). The incomplete chromatographic separation caused strong spectral interference, which renders deconvolution and EI fingerprint matching with standard libraries impossible for both compounds. However, the CI spectrum at 602 s retention time unambiguously shows the protonated forms of both species at m/z 155 and 139 (cf. Figure 8.2.6), respectively, and thus clearly confirms their coexistence within this chromatographic peak.

A further identification criterion that has not been discussed so far is the retention index (RI). The RI is of great benefit for compounds with clearly distinguishable differences in retention times, provided they are available in the respective GC libraries. The present work though focuses on the advantages of the complementarity of EI and CI information.

The instrument performance was further evaluated with a headspace (HS) injection of a brand perfume sample (HS-GC-EI/CI-TOFMS). Figure 5.2.7A depicts the extracted ion chromatograms of all mass signals in the CI and EI spectra of the chromatographic peak at 1184 s retention time. This compound provides a remarkable example for identification, in which case the missing RI essentially requires the additional information from the dual ionization approach. The NIST/EPA/NIH Mass Spectral Library^[22] comparison of the EI data (cf. Figure 5.2.7B) reveal several search results with matching factors well above 800, of which the first ten hits are listed in Table 5.2.1. This large set of equivalents, with only slightly differing factors, causes low matching probabilities in the range of merely 2 – 11 % for each individual hit (cf. Table 5.2.1).

Experimental RIs that may provide further evidence in the identification process are not listed in the available databases for all the proposed compounds (6 out of 10). Predicted RIs are available, however, with relatively high uncertainty. In this case, the EI-only approach is essentially failing. The simultaneously generated CI mass spectrum of the compound shows a dominant signal at mass m/z 253.2158 (cf. Figure 5.2.7B).

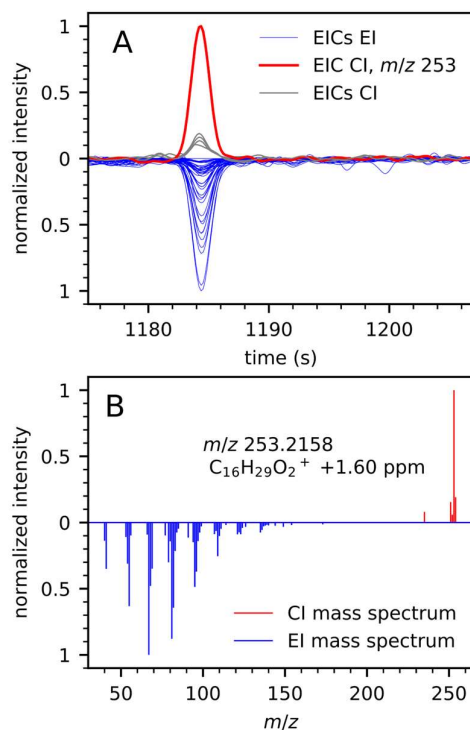


Figure 5.2.7: (A) Enlarged chromatogram of the brand perfume headspace sample. All EICs of the detected masses below the chromatographic peak at 1184 s retention time are depicted. The trace of the dominant protonated molecule in the CI mode at m/z 253 is shown in red. (B) Corresponding EI and CI mass spectra of the chromatographic peak at 1184 s.

Table 5.2.1 has only two elemental compositions ($C_{16}H_{28}O_2$ and $C_{17}H_{32}O$) in the EI hit list within the required nominal mass restrictions. The high mass accuracy and precision of the TOF analyzer can clearly further distinguish between these two sum formulas, since only the suggested $C_{16}H_{29}O_2^+$ meets the 5 ppm mass error criterion (1.6 ppm). Additionally, the isotopic ratio differs by only 2.4 %, which is well below the allowed ± 5 % and thus supports the correct assignment. In contrast, with 145 ppm mass error, the respective protonated form of the other suggested composition ($C_{17}H_{33}O^+$) is far above the accepted mass deviation. Using the additional RI information, the compound is identified with high certainty as (8Z)-oxacycloheptadec-8-en-2-one. A higher identification level would require an additional measurement of a reference standard^[125]. Nonetheless, this example clearly illustrates the strongly improved identification confidence by complementary EI, CI and RI data. An additional example from the perfume sample showing the improved identification is given in Figure 8.2.9 and Table 8.2.4.

Table 5.2.1: First compound suggestions of the fragment spectra library search in combination with the CI information for the mass spectra shown in Figure 5.2.7B.

Systematic name	Sum formula	m/z [M+H] ⁺	Δ mass (ppm)	Δ isotopic ratio (%)	EI match	Probability (%)	RI
(8Z)-oxacycloheptadec-8-en-2-one	C ₁₆ H ₂₈ O ₂	253.2162	1.6	2.4	847	10.8	1940
(9Z,12Z)-octadeca-9,12-dien-1-ol	C ₁₈ H ₃₄ O	267.2682	>1000	-8.9	831	6.2	2050
methyl (9E,12E)-octadec-9,12-dienoate	C ₁₉ H ₃₄ O ₂	295.2632	>1000	-13.7	828	5.5	n.a
(11E)-12-cyclopropyl-dodec-11-en-1-ol	C ₁₅ H ₂₈ O	225.2213	>1000	9.3	825	5.5	n.a.
(9E,12Z)-tetradeca-9,12-dien-1-ol	C ₁₄ H ₂₆ O	211.2056	>1000	17.1	824	4.9	1675
methyl (11E,13E)-icosa-11,13-dienoate	C ₂₁ H ₃₈ O ₂	323.2945	>1000	-21.8	818	3.7	2276
(14R)-14-methylhexadec-8-yn-1-ol	C ₁₇ H ₃₂ O	253.2526	145.2	-3.6	814	3.2	n.a
(9E,12E)-octadeca-9,12-dienoic acid	C ₁₈ H ₃₂ O ₂	281.2475	>1000	-8.8	814	3.2	n.a
hexadec-9-yn-1-ol	C ₁₆ H ₃₀ O	239.2369	>1000	2.7	807	2.4	n.a.
2-chloroethyl (9Z,12Z)-octadeca-9,12-dienoate	C ₂₀ H ₃₅ ClO ₂	343.2398	>1000	-18.0	805	2.2	n.a

5.2.5 Conclusion and outlook

The performance of a GC-EI/CI-TOFMS, featuring the parallel detection of ions from a 70 eV electron and a chemical ionization source was shown. The used 10 Hz mode switching provides sufficient data points to represent the original chromatographic peak shape in both modes with great fidelity for the used GC system. Several examples demonstrated the added value of the complementary CI information, gained by i.e., the accurate mass of the protonated molecule and its isotopic abundance pattern, in addition to the characteristic fragment fingerprints from the EI mode. This provides a strongly improved level of compound identification in non-targeted GC analyses.

Future work will include the further increase of the chromatographic peak capacity via multidimensional GC using a possible ion mode switching capability of 100 Hz. Furthermore, the CI source will be supplied with rapidly changeable reagent gases to add additional selectivity in the protonation process.

5.3 Gas chromatography coupled to time-of-flight mass spectrometry using parallel electron and chemical ionization with permeation tube facilitated reagent ion control for material emission analysis

Steffen Bräkling^{1,3}, Christina Hinterleitner², Luca Cappellin^{1,4}, Thorsten Benter³, Sonja Klee¹, Hendrik Kersten³

1 Tofwerk (3645 Thun, Switzerland)

2 Berner Fachhochschule BFH, Architektur, Holz und Bau (2500 Biel, Switzerland)

3 University of Wuppertal, Department of Physical and Theoretical Chemistry (42119 Wuppertal, Germany)

4 Department of Chemical Science, University of Padua, (35131 Padua, Italy)

Published in *Rapid. Commun. Mass Spectrom.* **2023**, 37, e9461.

<https://doi.org/10.1002/rcm.9461>

5.3.1 Abstract

Rationale. Volatile organic compounds (VOCs) emitted by an artificial leather part for car interiors are determined with GC-MS (gas chromatograph coupled to a mass spectrometer) using simultaneous electron and chemical ionization (EI&CI). A device for swift reagent ion switching in CI mode between consecutive runs is presented.

Methods. VOCs emitted from the investigated material were sampled onto Tenax[®] absorption tubes using micro emission chambers and subsequently injected into the GC through thermal desorption. The detector was a time-of-flight mass spectrometer (TOFMS) simultaneously operating in EI and CI mode during a single chromatographic run. A custom permeation tube setup allowed for swift selection between various reagent ions in CI mode, e.g., $[\text{N}_2\text{H}]^+$, $[\text{H}_3\text{O}]^+$, $[(\text{H}_2\text{O})_2\text{H}]^+$ and $[\text{NH}_4]^+$.

Results. Different reagent ions are swiftly selectable between single GC runs without hardware changes. Differences in molecular ion generation and the selectivity of the various reactants were carefully assessed. Several examples for the improved

identification of unknown compounds with the available complementary and comprehensive EI&CI data set are demonstrated for a relevant material emission application.

Conclusion. The presented technique provides additional value to the standard GC-EI/MS procedure commonly used for material emission characterization. It allows for a non-targeted analysis approach with moderate analysis time.

5.3.2 Introduction

Volatile Organic Compounds (VOCs) are released from many different materials and can negatively impact human health, indoor air quality, production quality or just produce unwanted odors. Prone to intense VOC emission are materials such as plastics, leather, paint, adhesives, and flooring^[126–132]. The characterization and single compound identification are necessary to evaluate the potential hazard of these complex mixtures but are still analytically challenging. Usually gas chromatography (GC) coupled to mass spectrometry (MS)^[1,2] or real time methods, e.g. proton transfer reaction (PTR) MS^[133] are applied. The latter provides higher temporal resolution and sampling rate with detection limits in the pptV to ppqV range^[58,91]. In combination with a high mass resolution analyzer the generation of sum formulas for enhanced characterization is also possible.

GC-MS in combination with electron ionization (EI) allows for improved structural information and compound identification of VOCs^[119,134]. Typically, an electron energy of 70 eV is applied, which is around the maximum of the ionization cross section curve for most molecules. Consequently, the fingerprint of the resulting fragment spectra is rather unaffected by small electron energy deviations and is thus more or less independent of the instrument used. This fact renders EI MS highly suitable for structure elucidation based on comparison with mass spectral libraries such as the NIST/EPA/NIH Mass Spectral Library^[22]. However, this standard procedure becomes less favorable in cases where extensive and unspecific fragmentation leads to ambiguous fragment spectra, absent molecular ion signals, or in cases where the correct analyte is just not listed in the database^[14,75].

Recently, a new GC-TOFMS instrument was introduced^[135]. It combines the advantages of EI allowing comprehensive database searches, and a softer chemical ionization method for acquiring high resolution molecular ion information. Data from both ionization

methods are recorded within a single GC run for rapid analysis and allows for unambiguous assignment of both sources of information to a particular chromatographic peak. This system is particularly suited for non-target analysis, which will be demonstrated in this work by means of the identification of eight VOCs from thermal desorption measurements of an artificial leather sample.

The plasma-based CI source used in combination with the EI source was presented earlier^[120]. Low hydrogen flow rates obtained from a small and laboratory-safe on-demand generator are used for ion generation. Earlier we showed that the primarily generated H_3^+ population can be specifically converted to a variety of other reagent ions, e.g., $[\text{N}_2\text{H}]^+ / [\text{N}_4\text{H}]^+$, $[\text{H}_3\text{O}]^+$ or $[\text{C}_4\text{H}_9]^+$, which enables the user to adjust the gas phase acidity and consequently balance between selectivity as well as the degree of fragmentation. In this work we also demonstrate the capabilities of a reagent gas supply unit with temperature-controlled permeation tubes to swiftly alter the acidity of the reagent ion population in between two consecutive GC runs.

5.3.3 Experimental

MS set up. The used GC-TOFMS was previously presented and characterized in detail by Bräkling et al.^[116]. Briefly, this instrument features the combined data acquisition of EI fragment spectra and the accurate molecular mass information from a CI source within a single GC run. Following the chromatographic separation, the GC effluent is equally split and fed to the EI and CI source, respectively. A fast ion optical switching device alternately delivers ion populations from the EI and the CI source into the TOF analyzer with high frequency. This allows for the mass resolved recording of a narrow GC peak with sufficient data points for both modes. The retention times are precisely aligned to facilitate unambiguous data assignment.

The CI source with its three-stage design is described in detail in reference^[120]. Briefly, in the 1st stage a low power helical resonator drives a hydrogen plasma at around 13 mbar and produces $[\text{H}_3]^+$ ions. Subsequent addition of a reagent gas allows to alter the gas phase acidity and selectivity of the protonating species in the 2nd stage. In the 3rd stage, the GC-effluent is introduced, and the charged reagents finally ionize the analyte. In contrast to the previously described setup, a modified reagent gas supply for the 2nd stage is presented. Previously, the selectivity was altered by adding different reagent gases such as nitrogen, methane and isobutane from distinct gas cylinders directly into the 2nd stage

of the CI source. In this study, a main flow of nitrogen is enriched with dopants such as water or ammonia from a temperature-controlled permeation tube setup. For the generation of protonated water and the respective proton bound water clusters, H₂O in milliQ[®] (18 MΩ) quality was filled into a 10 cm long and 1/4 inch OD Teflon[®] tubing with 0.5 mm wall thickness, plugged with Teflon[®] rods and sealed with Swagelok ferrules. For the generation of ammonium ions an identical setup was filled with a 30 % NH₃/H₂O mixture. The amount of water and ammonia diffusing through the Teflon[®] into the nitrogen sheath flow is very sensitive to temperature changes. Therefore, the permeation tubes were placed into temperature-controlled, 1/2 inch stainless steel tubes, enabling the precise regulation of the added reagent concentration. In total, three such heated assemblies were placed in parallel to the nitrogen flow (cf. Figure 5.3.1). Two were filled with water, but held at different temperatures (85 °C and 115 °C) and one contained the NH₃/H₂O mixture. A fourth line is included for the supply of pure and dry nitrogen. As shown in Figure 5.3.1, two 4-way valves mounted on each side of the four stainless steel tubes allows swift switching between the different reagents.

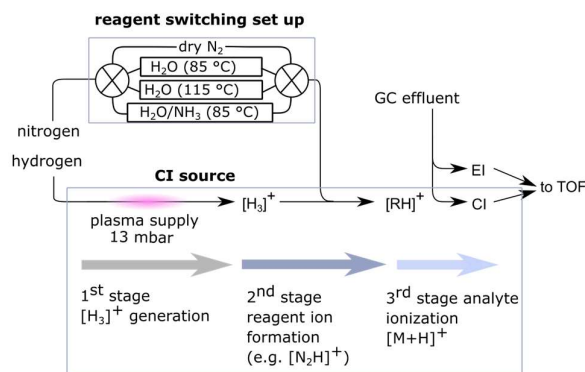


Figure 5.3.1: flow scheme of the instrumental MS set up.

Sample and sample preparation. For the present material emissions study an artificial leather sample for car interiors supplied by a car manufacturing company was used. The measurements were performed according to ISO 12219-3:2012^[2]. A piece of the artificial leather (~30 x 30 mm, ~850 mg) was placed into a stainless-steel micro emission chamber with a volume of 114 cm³ (Markes International, Offenbach am Main, Germany). The chamber temperature was held constant at 65 °C. Following an equilibrium time of 20 minutes, the VOC emission of the sample was collected for 15 minutes onto Tenax[®] TA absorption tubes (Gerstel, Mühlheim an der Ruhr, Germany) with a flow rate of 100 ml/min of dry, compressed air. For reference, this procedure was carried out with the

empty chamber prior to each sample measurement. The Tenax[®] absorption tubes were spiked with toluene d-8 as an internal standard for the GC-MS analysis.

GC Interface. The dual ionization source TOFMS was coupled to an Agilent GC (6890; Agilent technologies, Santa Clara, CA, USA) equipped with a 60 m DB-5-ms (0.25 mm ID, 25 μ m film thickness) column (Agilent technologies, Santa Clara, CA, USA). The Tenax[®] absorbed samples were introduced into the GC via a thermal desorption unit (Gerstel TDS3, KAS4; Gerstel, Mülheim an der Ruhr, Germany). The chromatographic separation was performed according to the following program: After sample introduction (inlet temperature 260 °C) the oven was held at 40 °C for 4 min. Subsequently, the oven temperature was increased by 3 °C/min to 100 °C followed by a temperature ramp of 8 °C/min to 280 °C. The final temperature was held for 2.5 min. The column flow of helium with 99.9999% purity was set to 1.2 ml/min.

Chemicals. 99.9999 % Hydrogen was generated using a hydrogen generator (Peak scientific, Inchinnan, UK). Nitrogen and helium were purchased from Carbagas (Bern, Switzerland) with a stated purity of 99.9999%. All gases were additionally purified (Big Universal Trap; Agilent technologies, Santa Clara, CA, USA) to low ppb contamination levels. Toluene d-8 and a C8-C22 alkane standard for RI estimation were purchased from Merck (Buchs, Switzerland). Custom permeation tubes were filled with milli-Q[®] water (18 m Ω) and 30 % ammonia solution (Merck, Buchs, Switzerland).

Data analysis. For chromatographic deconvolution and peak detection AnalyzerPro XD (Spectralworks, Runcorn, Cheshire, UK) was used. The postprocessing software was customized for parallel analysis of CI and EI data generated by the used instrument. EI fragment library searches were performed using the NIST MS search 2.4 program and the NIST20^[22] EI fragment library, including the MS interpreter Version 3.4.4 (National Institute of Standards and Technology; Gaithersburg, MD, USA).

4.3.3 Results and discussion

4.3.3.1 Reagent supply unit – control of the reagent ion distributions

The primary hydrogen plasma in the 1st stage (cf. Figure 5.3.1) of the CI source almost exclusively generates H₃⁺, which leads to a reagent gas with a defined proton transfer reactivity. This quantity is thermodynamically expressed as the proton affinity (PA) given for H₂ as PA = 422.3 kJ/mol^[42]. In general, the lower this value, the higher the acidity of

the CI reagent gas and the broader the accessible range of analytes (less selective). However, with increasing ΔPA between reagent gas and analyte, the excess energy available for fragmentation steps increases as well. To decrease the acidity of the CI gas in a controlled way, additional reagents can be added in the 2nd stage. As described in the experimental section, the permeation tube assembly (cf. Figure 5.3.1) allows to swiftly select between four different, predefined acidity strengths of the CI gas without laborious hardware or gas supply changes. Figure 5.3.2 (A-D) presents the corresponding reagent ion distributions (RG1-4) for each predefined setting. Previous experiments have shown that these spectra do reflect the actual composition interacting with the analyte added in the 3rd stage^[120]. It is obvious that in case of multiple reagent ions the acidity of the CI gas is not simply defined by one specific PA value but is rather described by a distribution with a weighted mean \overline{PA} value and a standard deviation representing its width. In case of Figure 5.3.2A the dry N₂ line (RG1) was opened in the 2nd stage. Three types of reagent ions are observed, [H₃O]⁺, [N₂H]⁺ and the most abundant [N₄H]⁺ with proton affinities of the neutral precursors of 691.0 kJ/mol^[42], 493.8 kJ/mol^[42] and 517.0 kJ/mol¹, respectively. Based on the relative intensities in the spectrum a mean weighted \overline{PA} of 550 kJ/mol with a standard deviation of 76 kJ/mol is calculated for this particular predefined CI gas setting. The spectra in Figure 5.3.2B and 2C display the reagent ion distributions generated by water doped nitrogen at two different mixing ratios. The water level is simply adjusted by the permeation tube temperature. In this way two different reagent gases RG2 and RG3 were generated with mean weighted proton affinities of 662 ± 117 kJ/mol and 795 ± 94 kJ/mol, respectively. Thus, a unique feature is offered by the sensitive response of the protonated water cluster distribution upon varying the permeation tube temperature (cf. Figure 8.3.1). In addition to the already discussed species [N₂H]⁺, [N₄H]⁺ and [H₃O]⁺, proton bound water clusters such as [(H₂O)₂H]⁺ (PA ~ 831 kJ/mol)^[99] and [(H₂O)₃H]⁺ (PA ~ 893 kJ/mol)^[100] appear with increasing temperature. In addition the highly acidic species [N₂H]⁺ and [N₄H]⁺ are quantitatively depleted at the maximum temperature of 130 °C. Clearly, this effect relates to the altered water mixing ratio of the reagent gas. Since each reagent ion species with its specific proton affinity contributes to the weighted mean \overline{PA} of the CI gas by its relative population, a corresponding \overline{PA} function of the permeation tube temperature is obtained.

¹ No PA value for N₄H⁺ was found in the literature. Therefore, a value of 517.9 kJ/mol was calculated using ab initio methods. This value was used for PA estimations.

This is illustrated in Figure 5.3.2E. It shows that the mean weighted proton affinity of the CI gas is continuously adjustable between 520 kJ/mol and 800 kJ/mol by simply selecting the corresponding permeation tube temperature. In this operational mode, the protonation occurs principally with more than one reagent ion type, which is leading to a PA width, represented by the standard deviation of the cluster distribution. However, the setup also allows for other dopants to be used such as NH₃. The resulting reagent ion spectrum (RG4) for a 30 % ammonia in water mixture at a permeation tube temperature of 85 °C is given in Figure 5.3.2D. With regard to the analytical applicability and sample throughput, a reasonable switching time between the different predefined acidity strengths of the CI gas is essential. Figure 5.3.2F shows the time evolution of the reagent ions between two switching cycles from RG1 to RG3 and vice versa. The equilibration times are well below 200 s and thus lie within typical GC cool down times.

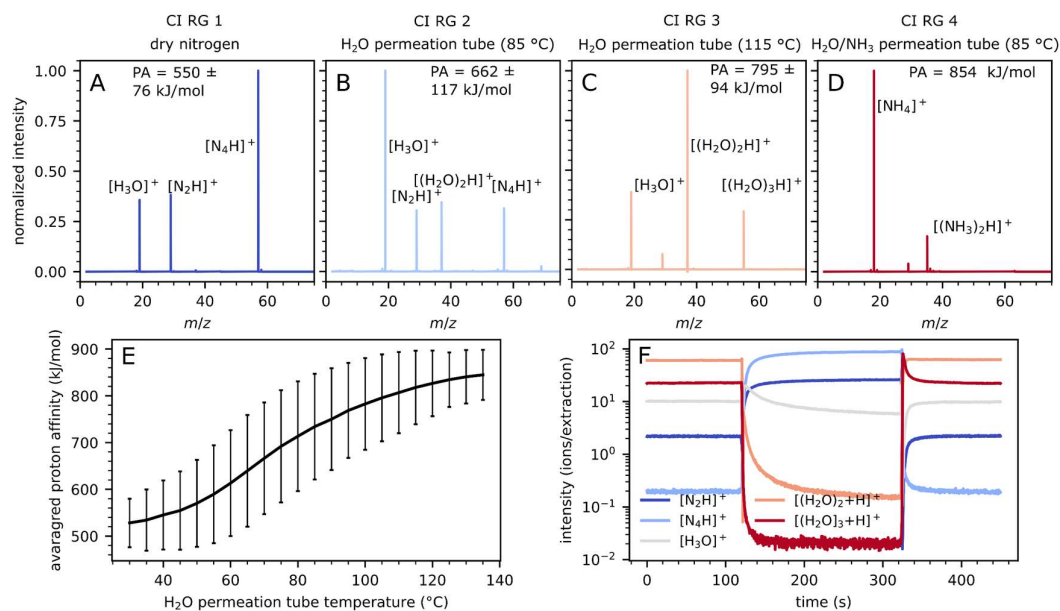


Figure 5.3.2: Reagent ion distributions generated using (A) RG1, (B) RG2, (C) RG3 and (D) RG4. (E) averaged proton affinity in dependence on the water permeation tube temperature. (F) Switching time between dry nitrogen as reagent gas and water doped nitrogen.

5.3.3.2 Reagent supply unit – control of selectivity and degree of fragmentation

As mentioned before, the presented instrument acquires CI and EI information simultaneously from one single GC run. Key to the analysis is the combination of the EI fingerprint information with the complementary exact mass of the intact compound from

the CI trace. The correct exact mass can only be derived from a mass signal unambiguously related to the intact molecule. Commonly, the degree of fragmentation during protonation decreases with increasing PA of the reagent, however, at the cost of a reduced analyte range^[52,120]. Therefore, this instrument is capable of generating a broad and swiftly selectable range of reagent acidities, as shown in the previous section. To further evaluate this feature, the effects with regard to selectivity and molecular ion yields are further characterized in the following.

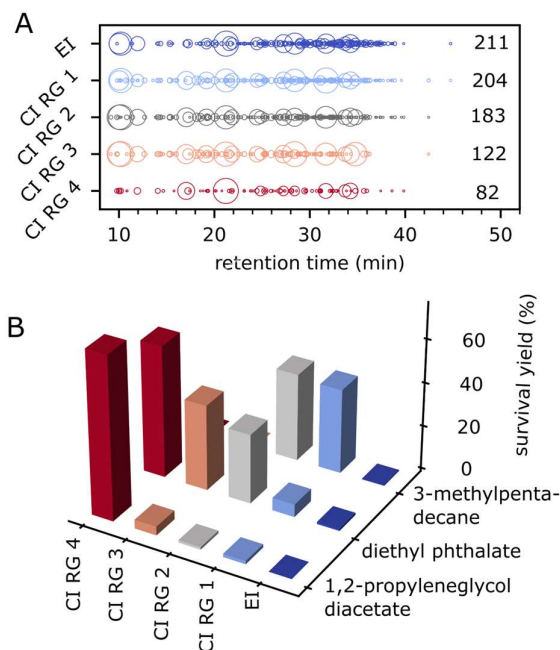


Figure 5.3.3: (A) Number of detected compounds from the artificial leather emission, depicted for EI and each CI reagent. All signals above a threshold of $1 \mu\text{g}/\text{m}^3$ toluene equivalent were used for this evaluation. The marker size represents the normalized intensities of the signals. For each ionization method the number of detected compounds is given within the Figure. (B) Comparison of survival yields of the intact parent ions using EI and the different CI reagents, exemplarily shown for compounds 3-methylpentadecane, diethyl phthalate and 1,2-propyleneglycol diacetate.

The emission of the artificial leather sample was recorded employing all different reagents available. Simultaneously, 70 eV EI was applied under identical conditions and provided structural information. The acquired chromatograms for each ionization method are shown in Figure 8.3.2. Since the EI chromatogram is identical for each reagent run, it is only displayed once (blue) within the measurements using N_2 as CI reagent (RG1).

To evaluate the “*selectivity*” of the different methods, all signals above $1 \mu\text{g}/\text{m}^3$ toluene equivalents, as stated in ISO12219^[2], are counted as detected compounds and displayed in Figure 5.3.3A. As expected, electron ionization demonstrated its unparalleled, inherent non-selective character with 211 detected compounds in the leather sample. RG1, (cf. Figure 5.3.2) with the highest gas phase acidity of all the employed reagents protonated 204 of these and thus enabled their mass spectral identification. Consecutively decreasing the acidity using RG 2 to 4 expectedly decreased the number of detected compounds to 183, 122 and 83, respectively. In this example, the large difference in selectivity between dry nitrogen and water doped nitrogen or ammonia is readily explained by the exceptional ionization efficiency of $[\text{N}_2\text{H}]^+ / [\text{N}_4\text{H}]^+$ towards alkanes. These represent an abundant compound class in the leather emission profile and are not protonated with $[\text{NH}_4]^+$ and only partially with $[\text{H}_3\text{O}]^+$ and $[(\text{H}_2\text{O})_2\text{H}]^+$.

To evaluate the “*softness*” among the different methods, the degree of fragmentation is expressed in terms of the survival yield (%) of a mass signal that unequivocally contains the sum formula information for the compound of interest. This can either be the molecular ion obtained with EI, the protonated or deprotonated molecule, or an adduct ion such as $[\text{M}+\text{NH}_4]^+$. Figure 5.3.3B illustrates the results for three different, rather fragile compound classes, each represented by exemplarily chosen compounds from the leather emission sample. Figure 8.3.3 shows the corresponding mass spectra. Clearly, using EI the molecular ion signals are virtually absent for each compound. The class of non-polar alkanes, such as 3-methylpentadecane, shows favorable protonation cross sections towards the $[\text{N}_2\text{H}]^+ / [\text{N}_4\text{H}]^+$ system using RG1 with a survival yield of 38 % for the $[\text{M}-\text{H}]^+$. For non-functionalized alkanes the $[\text{M}-\text{H}]^+$ commonly represents the main detected species from protonation reactions^[7]. Increasing the reagent gas phase water concentration for RG2 the $[\text{M}-\text{H}]^+$ yield of 3-methylpentadecane slightly improves to 40 %, however, at the cost of reduced absolute ion abundances. This effect is even more pronounced with larger water clusters or the ammonia enriched gas phase when using RG3 and RG4, respectively. In these cases, the protonation of 3-methylpentadecane becomes endergonic and thus no signal was observed.

Phthalates are the second investigated class for which diethyl phthalate was exemplarily chosen as a frequently observed emission product. In general, this class shows a characteristic and dominant fragment $[\text{C}_8\text{H}_5\text{O}_3]^+$ at m/z 149.023. Particularly for 70 eV EI it represents the base peak in virtually all phthalate mass spectra without any molecular

ion information revealed, which is also true for diethyl phthalate. In contrast, with all CI reagents the protonated intact molecule is identified. A swift and steady increase in the mean weighted proton affinity for the used reagent gases (cf. Figure 5.3.2A-D) resulted in an increasing survival yield of 6%, 31%, 39% and 60%, respectively (cf. Figure 5.3.3B). Note that for the phthalate the absolute ion current is nearly independent of the used reagent, which is in stark contrast to the previously discussed alkane example.

The $[\text{NH}_4]^+ / [(\text{NH}_3)_2\text{H}]^+$ system of RG4 (cf. Figure 5.3.2D) is the most selective one, but known for a gentle ionization behavior^[45,46]. This is in particular noticeable for the third considered compound class with acetic parts, since these represent thermodynamically favored leaving groups. An illustrative compound is 1,2-propyleneglycol diacetate, with survival yields of merely 4 % with the protonated water cluster system of RG3. In stark contrast, ammonia leads to abundant formation of stable $[\text{M}+\text{NH}_4]^+$ -adducts for this compound class. In case of 1,2-propyleneglycol diacetate an adduct yield of 75% was obtained (cf. Figure 5.3.3B and 8.3.3).

5.3.3.3 Enhanced compound identification with complementary EI and CI information

In the following, it will be demonstrated how the simultaneously recorded EI and CI data from are used for advanced compound identification. Based on an unknown artificial leather emission sample, four common scenarios with different qualitative and quantitative levels of available EI and CI information are highlighted. Each scenario will be presented in a step by step identification approach with eight exemplarily chosen compounds. For this approach, the advantage of being able to swiftly change the CI gas phase acidity will be employed as well to improve the correct compound assignment.

Scenario 1: *“The EI mass spectral information for database matching provides an appreciable first entry library hit. Chromatographic and CI information are subsequently used to increase the confidence of identification for the predicted compound.”*

The outgassing sample of the artificial leather is comprised of a vast number of abundant aliphatic compounds. Figure 5.3.4A depicts some $[\text{M}-\text{H}]^+$ traces of different higher molecular weight alkanes, ionized with the $[\text{N}_2\text{H}]^+ / [\text{N}_4\text{H}]^+$ system (RG1). As stated before, this reagent enables the analysis of various non-functionalized aliphatic

compounds with $[M-H]^+$ as the base peak^[7]. The large structural compound diversity but nonetheless similarity of the corresponding 70 eV EI mass spectra as well as chromatographic behavior is characteristic for this analyte class. Consequently, in complex samples, peaks of different compounds essentially interfere within small chromatographic time frames. Frequently, this renders the identification based on EI library searches difficult and leads to only poor identification confidence. In some cases, the RI information is misleading since branched alkanes show lower boiling points than the unbranched species as indicated for two exemplary chromatographic peaks of non-functionalized alkanes in Figure 5.3.4B, this causes the non-isomeric, unbranched $C_{16}H_{34}$ and the branched $C_{17}H_{36}$ species to overlap with close retention times/RIs. The RI calculation in the presented study using an alkane standard is shown in Figure 8.3.4.

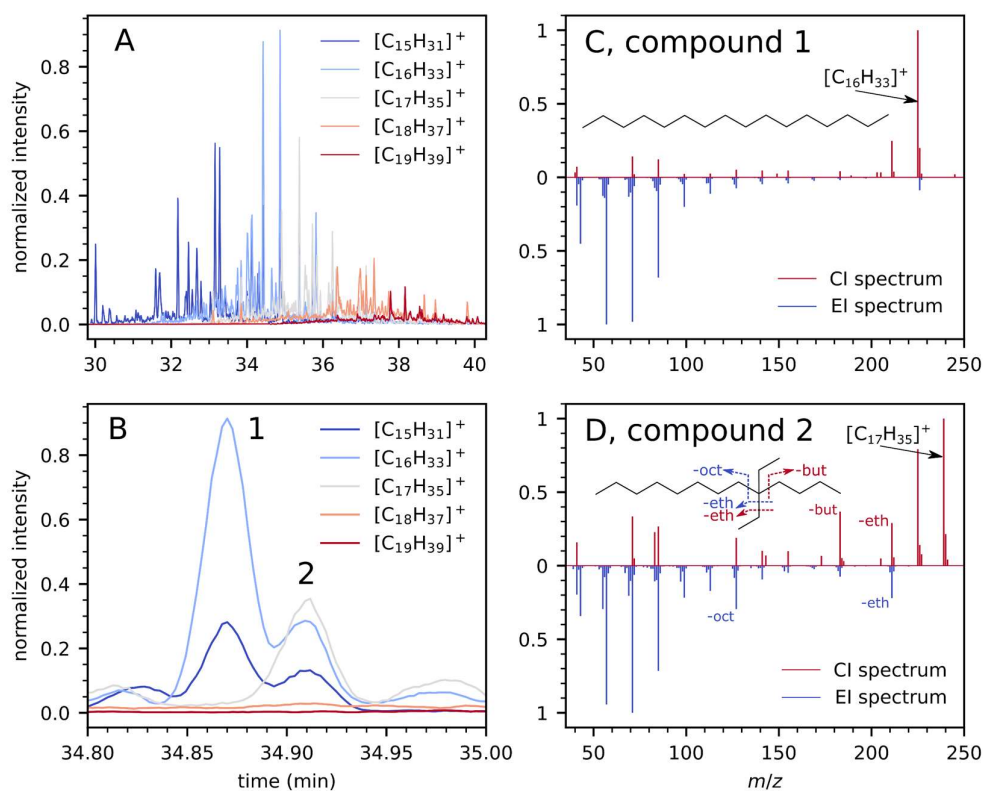


Figure 5.3.4: (A) Extracted ion chromatograms (EIC) of different alkane mass traces ionized with the CI reagent system RG1. (B) Enlarged EICs of two closely eluting signals at ~34.9 min. (C) CI and EI mass spectrum of the chromatographic signal at 31.87 min (compound 1) (D) CI and EI mass spectrum of the chromatographic signal at 31.91 min (compound 2).

The corresponding CI and EI mass spectra of compound 1 ($C_{16}H_{34}$) are shown in Figure 5.3.4C. Compound 1 is clearly unequivocally identified as hexadecane: The EI

NIST library search yields a matching factor of 909 and a reasonable probability of 33 % for hexadecane as the first hit. The CI information predicts a molecular sum formula of $C_{16}H_{34}$ with an accurate mass error of < 5 ppm. In addition, the CI mass spectrum exhibits $[M-H]^+$ as the base peak with little fragmentation, which is a strong indicator for an unbranched alkane. The RI determined for this compound is 1597 and nicely fits to the RI of hexadecane (1600). Branched alkanes with the same sum formula would have lower RIs as mentioned earlier. Consequently, the identification procedure for corresponding compounds is straight forward.

Compound 2 has almost the same calculated RI (1601) as compound 1. However, more characteristic fragmentation is noticeable for compound 2 in the EI as well as the CI mass spectrum, which indicates the presence of a branched alkane (cf. Figure 5.3.4D). Usually, the fragments in both ionization modes are complementary and characteristic for the branching positions, which supports structural elucidation of the molecule. Compound 2 was identified as 5,5-diethyltridecane as follows: The CI information predicts a molecular sum formula of $C_{17}H_{36}$ with an accurate mass error of < 5 ppm. The EI mass spectrum shows a common alkane fragmentation pattern without molecular ion but intense fingerprint. The NIST database search yielded a good first hit (matching factor 873 and 34% probability) for 5,5-diethyltridecane, which is in very good accord with the determined sum formula. Moreover, the characteristic fragments $[M-C_2H_5]^+$ and $[M-C_8H_{17}]^+$ are abundantly present. Both are marked in Figure 5.3.4D, as -eth and -oct and represent the loss of a branch and the longer part of the chain at the 5,5 position, respectively. In the $[N_2H]^+/[N_4H]^+$ CI spectrum, abundant $[M-C_2H_5]^+$ are observed as well. In addition, an intense butyl loss with the remaining ion signal $[M-C_4H_9]^+$ is observed, which is not strongly present using 70 eV. This fragment clearly indicates the loss of the smaller part of the chain with the cleavage at the 5,5 branch position (cf. Figure 5.3.4D) and finally completes the structural elucidation of 5,5-diethyltridecane. Noticeable in the CI spectrum is the presence of $[M-CH_3]^+$, which is a common fragment for all alkanes and thus not very characteristic for this specific compound. Finally, the RI for 5,5-diethyltridecane (1605) is in fairly good agreement with the calculated RI (1601) and additionally supports the identification of this compound.

Scenario 2: “The EI database search results in an inconclusive priority list. Chromatographic and CI information proves the first entry as incorrect and provides evidence for lower rated hits as more probable.”

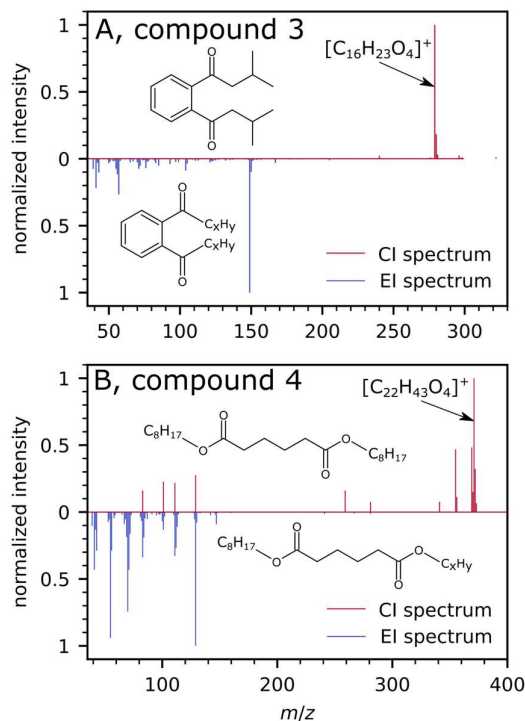


Figure 5.3.5: (A) CI (RG4) and EI mass spectra of the chromatographic signal at 38.60 min (compound 3) (B) CI (RG2) and EI mass spectra of the chromatographic signal at 44.80 min (compound 4). The molecular structures in each spectrum are derived from the respective MS information. In EI details on certain hydrocarbon branches are not available and assigned with C_xH_y, respectively.

In GC-MS analysis of complex samples the comparison with an EI fragment library frequently remains inconclusive. Multiple reasons, such as missing compounds within the library or loss of structural information due to unspecific fragmentation, are conceivable^[14]. In the latter case, the library search shows multiple hits with reasonable matching factors but reduced probability for each suggested compound. Here the RI values (if available), but in particular the molecular ion information significantly reduces the list of candidates. Two examples illustrating this situation are presented in the following.

Figure 5.3.5A shows the EI and CI spectrum of the third example (compound 3) from the leather analysis at a retention time of 38.6 min. For reasons already discussed, the use of less acidic reagents for compounds with high proton affinities is more favorable

(cf. Figure 5.3.3B). In this case the acidity strength of RG4 was sufficient to record sufficiently high $[M+H]^+$ signal intensities and a survival yield of nearly 100 % was obtained. In the EI spectrum the dominant signal at m/z 149 strongly suggests the presence of a phthalate with its typical $[C_8H_{15}O_3]^+$ fragment. However, this class rarely reveals the molecular ion or any other characteristic fingerprint in EI-MS, which implies strong similarity among spectra and renders specific identification difficult if possible at all. Expectedly, the first hit of the NIST library search, suggest butyl undecyl phthalate ($C_{23}H_{36}O_4$), with a probability of only 8.4 %. The CI spectrum, however, leads to a sum formula of $C_{16}H_{22}O_4$ with a mass accuracy of approximately 1 ppm. Only three entries in the EI search list match this molecular mass: The 5th (di-isobutyl phthalate), 16th (dibutyl phthalate), and 29th (butyl isobutyl phthalate) list entry with probabilities of 3.4 %, 1.9 % and, 1.3 %, and ratings of 799, 785 and, 775, respectively. These three isomers can further be distinguished by means of the additional chromatographic information, with RIs of 1870, 1944 and 1965, respectively. Finally, the compound 3 in Figure 5.3.5A is unambiguously assigned to diisobutyl phthalate (measured RI = 1863).

A second example for scenario 2 is given in Figure 5.3.5B - a compound of the artificial leather sample recorded at 44.8 min retention time (compound 4). The CI spectrum was acquired with RG2. The NIST database comparison of the EI fingerprint suggests mono-2-ethylhexyl adipate ($C_{14}H_{26}O_4$) with 50.9 % certainty for the first search list entry. The CI spectrum clearly reveals the $[M+H]^+$ as the most abundant signal, with a derived sum formula of $C_{22}H_{42}O_4$ at a mass accuracy < 1 ppm. Consequently, the first EI search list is wrong. Only two lower rated entries on 2nd and 4th place, bis(2-ethylhexyl) adipate ($C_{22}H_{42}O_4$) and dioctyl adipate ($C_{22}H_{42}O_4$) with probabilities of 18.6 % and 12.7 %, respectively, match the determined sum formula. In addition, both molecules are listed with corresponding experimental RI values of 2400 and 2398 and match well with the calculated RI in this data set. In conclusion, with a high degree of confidence compound 4 is narrowed down to these two molecules. Due to the proximity of the RI values and rather unspecific fragment patterns in the EI and CI spectra, a further differentiation is not possible based on the available data. Finally, it should be noted that the obvious mismatch in the EI database search for this example is readily explained by the high degree of similarity in the fragment fingerprint of the mono and bi-esters. The CI information, however, unambiguously predicts one of the bi-esters as identified compound.

Scenario 3: “The 70 eV NIST identity data base search shows **no reasonable match, but some suggested compounds and the unknown share fragmentation similarities**. CI information is used for the NIST hybrid-similarity search^[26] to further improve the compound identification process.”

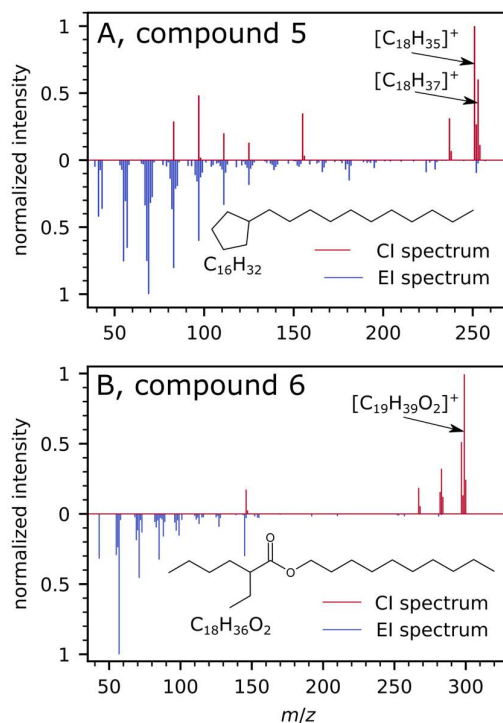


Figure 5.3.6: The CI and EI mass spectra used for similarity search approaches were recorded at (A) 38.66 min (compound 5) and (B) 39.49 min (compound 6) retention time. The depicted substances in the EI mass spectra are the compounds predicted by the NIST hybrid search, but do not match the CI information.

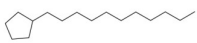
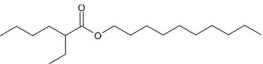
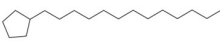
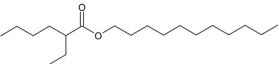
In the previous examples, the additional CI information facilitated the identification of compounds as obtained by a common EI identity spectral database search. However, GC-EI/MS libraries (NIST/EPA/NIR) are far from reflecting the entire molecular diversity nature provides. Nevertheless, in cases of missing compounds, chances are that databases provide at least entries with certain structural similarities to the molecule of interest. Given that the EI fragment patterns resemble this relation, the additional molecular mass information from the CI trace allows for hybrid similarity searches^[26], provided in the NIST search program to identify the unknown. This scenario is illustrated with compounds 5 and 6, found in the leather emission sample at retention times of 38.66 min and 39.49 min, respectively. Figure 5.3.6A and B show the corresponding EI and CI mass spectra and Table 5.3.1 summarizes the important identification steps.

For the NIST identity search the EI mass spectrum of compound 5 (cf. Figure 5.3.6A) scores low matching factors between 700 and 800 for the first couple of list entries, indicating that the correct molecule is not listed. The CI spectrum recorded with RG1 shows the $[M-H]^+$ with an exact molecular mass of 251.2740 Da and a mass error of 2.8 ppm. With high confidence the sum formula of compound 5 is $C_{18}H_{36}$. In accordance with this carbon/-hydrogen ratio is the presence of an abundant $[M+H]^+$ signal, an indicator for the presence of one double bond equivalent (DBE) in the aliphatic structure. However, the CI information does not allow to differentiate the DBE of a ring structure or an unsaturated position along the carbon chain. An additional NIST hybrid-search was performed, with the EI spectrum shown in Figure 5.3.6B and the CI derived nominal mass (252 Da) as an additional input parameter. Note that even though the NIST database only works with nominal masses, it is advantageous to verify the hybrid similarity search with the exact mass information. Undecyl-cyclopentane with a sum formula of $C_{16}H_{32}$ (224 Da) was ranked, scoring a matching factor of 900, but differing by a C_2H_4 group (28 Da) to the CI derived sum formula. Additional entries were alcoholic compounds considering a potential H_2O loss for RG 1. However, this group can be excluded since compound 5 was not detected with less acidic reagents. Nevertheless, the hybrid similarity search hit list provided an essential information concerning the raised DBE question. Since most entries were cyclopentane derivatives with different length of the aliphatic side chain, it is reasonable to assume the same structure for compound 5, with simply the alkyl part extended by an additional C_2H_4 group. Consequently, we propose that compound 5 is tridecyl-cyclopentane. This is further supported by the chromatographic information. The RI difference of 200 between undecyl-cyclopentane and compound 5 is reasonable for a C_2H_4 -elongation of the side chain. Moreover, neither the EI nor the CI mass spectrum shows fragments that indicate a differently branched isomer.

The EI mass spectrum of compound 6 (cf. Figure 5.3.6B) also scores low matching factors (< 650) with the normal NIST identity search. Therefore, the same hybrid similarity search was applied adding the nominal m/z value of 298 derived from the protonated molecule of the CI spectrum. The highest matching factor of 845 for this approach was obtained for decyl-2-ethylhexanoate ($C_{18}H_{36}O_2$). It differs by a CH_2 unit from the sum formula $C_{19}H_{38}O_2$ given by the accurate mass of the $[M+H]^+$ derived from the CI spectrum. The position of the additional CH_2 unit is subsequently obtained from the EI

mass spectrum. As shown in Figure 8.3.5, the NIST software indicates the fragments in the library spectrum that are shifted by a mass to charge ratio of 14 (CH₂) as compared to the spectrum of compound 6. The NIST interpreter tool allows to identify the hydrocarbon branch carrying this CH₂ group in the structurally similar molecule. Undecyl-2-ethylhexanoate is finally assigned to compound 6. As listed in Table 5.3.1, also the DBE and the additional RI information is in accordance with this result.

Table 5.3.1: Results for a similarity search approach using EI and complementary CI information for the spectra in Figure 5.3.6.

	compound A	compound B
CI information	C ₁₈ H ₃₆ (DBA = 1)	C ₁₉ H ₃₈ O ₂ (DBA = 1)
EI library result		
Original match	757	>650
library RI	1660	1914 ± 201 (95%)
measured RI	1869	1965
Hybrid match	900	843
Δ mass (hybrid search)	+28 (C ₂ H ₄)	+14 (CH ₂)
suggested formula		

Scenario 4: “*The EI mass spectral information does not provide any reasonable search result. Only CI information is used for the elementary identification process.*”

In the leather emission sample compounds were detected without any useable EI library search result at all. Although, the EI information does not result in any compound identification, the empirical sum formula is often available via the CI spectrum. Compound 7 and compound 8 represent two such examples and are discussed in the following. Their EI and CI spectra are shown in Figure 5.3.7A and B, recorded at retention time 29.37 min and 30.24 min, respectively. In this context the benefit of CI information from runs with different reagents will be shown.

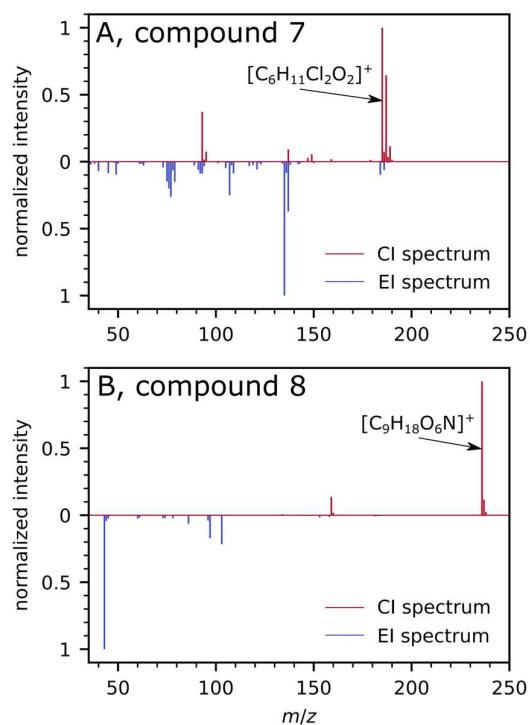


Figure 5.3.7: CI and EI spectra of (A) compound 7 and (B) compound 8 at retention times 29.37 min and 30.24 min, respectively. In both cases no reasonable EI library search result is obtained but the corresponding CI spectra provide the molecular formula.

The CI mass spectrum of compound 7 in Figure 5.3.7A was acquired with the reagent system RG2. The isotopic pattern (cf. Figure 8.3.6) suggests the presence of two chlorine atoms, which is in accordance with the sum formula $C_6Cl_2H_{10}O_2$ as derived from the exact mass of the protonated mono isotopic signal. With the more acidic RG1 HCl elimination was observed yielding the corresponding fragment $C_6ClH_{10}O_2^+$. Despite the characteristic Cl- pattern of the $C_5ClH_8O_2^+$ fragment at m/z 135 in the EI spectrum, neither the normal identity nor the NIST hybrid similarity search result in hits reflecting chlorine containing compounds (1282). However, the chemical composition of the compound at least allows for level 4 compound identification according to Schymanski et al.^[125].

The EI spectrum of compound 8 is shown in Figure 5.3.7B does not provide any search results with matching factors above 600 and also the molecular ion information is not present. On the contrary, the corresponding CI data obtained with RG4 clearly reveal the ammonium adduct $[M+NH_4]^+$. This allows to derive the adduct sum formula $C_9H_{18}O_6N$ and the respective molecular formula $C_9H_{14}O_6$ with a mass error < 4ppm. Common online compound databases^[136] suggest triacetin as the most probable molecule. This is further

supported by the strong ammonium adduct formation process, which is characteristic for acetate esters as shown previously. Triacetin is listed in the NIST/EPA/NIR library but was not suggested in the EI search results. This finding is readily explained by the deconvolution process in the data post processing software. In GC-MS analysis it is common to process raw data of the EI as well as CI traces for automated compound peak picking through such a software. Figure 8.3.7B depicts the deconvoluted experimental and the database triacetin EI spectra for comparison. They are mostly identical, except the two mass signals at m/z 116 and 145, which are virtually absent in the processed spectrum. A closer look at the extracted ion chromatograms of the EI traces (cf. Figure 8.3.7A) reveals co-elution with dominant fragments at m/z 116 and 145 between 30.20 and 30.27 min. In addition, the common m/z 43 fragment is strong and without distinct structure within these two seconds, which renders the correct automatic peak picking in this EI section rather difficult for the software. In contrast, from the more selective CI mass spectra the software extracted the m/z 236 trace with a well-defined compound peak for the triacetin at 30.24 min. This then suggested the detailed inspection of the EI data at this retention time. With regard to the EI mismatch, it was eventually found that the algorithm automatically assigned the two masses (m/z 116.062 and m/z 145.050) only to the earlier eluting compound and eliminated them from the deconvoluted triacetin spectrum. Through this substantial modification of the EI raw data by the post processing, triacetin was not recognized as a viable candidate for the subsequent NIST library search. In an additional standard reference measurement triacetin could clearly be assigned to compound 8. Similar examples for improved and more elaborate chromatographic analysis with the complementary EI and CI traces were previously given by Bräkling et al.^[135].

4.4 Conclusion

The material emission of an artificial leather sample for car interiors investigated using a non-targeted analysis approach with an EI&CI-TOFMS. The importance of simultaneously deriving the exact mass of the intact molecule from CI, as well as the fragment fingerprint from EI is clearly demonstrated. Several examples highlight different levels of improved compound identification based on the available information. In additions to the retention time index, the normal and similarity EI library search, the molecular formula, CI reagent specific reactions and fragmentations were used for

compound identification. In this context, the benefit of a reagent ion control unit with adjustable gas phase acidities is demonstrated.

6 Summary

The aim of this work was the development of a mass spectrometer hyphenated to a gas chromatograph which is capable of operating electron ionization and chemical ionization in parallel. The instrumental set up was intended to facilitate and improve the use of GC methods for non-targeted analysis. Special attention was paid to the development of the chemical ionization source and the corresponding GC coupling to both ionization sources.

This work demonstrates the advantages of combining EI and CI mass spectra and the resulting possibilities for GC analysis. The set up operating two ion sources (EI and CI) on a single TOF mass analyzer delivers highly complementary molecular information about the analytes. A carefully designed GC transfer enables the straightforward assignment of the corresponding EI and CI data due to low time deviations of chromatographic peaks within the corresponding chromatograms. Maintaining the EI mass spectral information is important due to its many advantages (i.e., instrumental independence, reproducibility, sensitivity, and low ionization selectivity). The possibility, and benefits of the instantaneous acquisition of additional CI mass spectra is highlighted and shown to be of great value. The identification probabilities and possibilities are greatly improved whilst avoiding tedious data alignment, hardware changes, system equilibrium times and time-consuming additional GC experiments.

During this work the impression was intensified that the use of the right CI reagent is essential for obtaining the precursor ions of analytes with the necessary quality and sensitivity. The knowledge regarding a well characterized and controllable CI source strongly facilitates the correct determination of the empirical sum formula. In addition to established CI reagent gases as methane and isobutane, protonated nitrogen (N_2H^+ and N_4H^+) was used at first. During this work however, a reagent supply unit using swiftly selectable permeation tubes for reagent ion variation rather than (flammable) reagent gases from compressed gas cylinders was developed. This allowed a stepwise selectivity variation from N_2H^+ (used for its broad ionization capability) to selective reagents as NH_4^+ (suitable for strongly fragmenting analytes). This is achieved by a controlled three-staged ionization source design enabling a stepwise reduction of the reagent gas phase acidity.

The combination of both, the parallel acquisition of 70 eV EI mass spectra and the CI mass spectra originating from a well characterized and controlled CI mechanism, has

been shown to be a powerful instrumental method for targeted, suspected, and non-targeted analysis approaches as demonstrated for material emission measurements of car interior parts. Uncertainties from unspecific fragmentation and coelution could be reduced. In addition, unknown identification was improved compared to EI only approaches.

Additional work was performed showing various applications using the developed instrument. An article about perfume authenticity measurements using additional statistical tools such as principle component analysis (PCA) for the analytical differentiation of an original brand perfume and corresponding generics was published^[137]. In addition, an application note about a flavor profile comparison between cheese and its vegan equivalent was published^[138]. A study investigating battery aging products, using the instrument described in this work, was published as an application note^[139]. The possibility of swift reagent adjustments of the developed CI source was of particular value for this application. Oligomeric carbonates, representing the main aging products, show a pronounced tendency to fragment but are measured as precursor ions using NH_4^+ reagent ions. On the other hand, the low selectivity of $\text{N}_2\text{H}^+/\text{N}_4\text{H}^+$ for the ionization of an alkane standard mixture in combination to EI was published in a white paper^[140].

As an alternative to the mode of operation summarized above, (EI and the CI sources coupled to the same GC), the CI interface can be also used for ambient sampling. A PTR reactor^[58] was used for real time monitoring of volatile organic compounds. A pine needle burning experiment was carried out demonstrating the advantages of both, real time PTR and GC-EI-MS^[134]. Fast changes in the sample composition were measured using real time PTR with a time resolution of 5 Hz. A sample from the plume was taken at a certain point of the experiment and used for GC-EI-MS analysis allowing for a more detailed insight to the sample during the same experiment.

7 Literature

- (1) ISO 16000-6:2021 Determination of Volatile Organic Compounds (VVOC, VOC, SVOC) in Indoor and Test Chamber Air by Active Sampling Sorbent Tubes, Thermal Desorption and Gas Chromatography Using MS or MS-FID.
- (2) ISO 12219-3:1012 Interior Air of Road Vehicles - Part 3: Screening Method for the Determination of the Emissions of Volatile Organic Compounds from Vehicle Interior Parts and Materials - Micro-Scale Chamber Method.
- (3) Beckey, H. D. Determination of the Structures of Organic Molecules and Quantitative Analyses with the Field Ionization Mass Spectrometer. *Angew. Chemie Int. Ed.* **1969**, *8*, 623–639.
- (4) Lattimer, R. P.; Schulten, H.-R. Field Ionization and Field Desorption Mass Spectrometry: Past, Present, and Future. *Anal. Chem.* **1989**, *61*, 1201–1215.
- (5) Ludányi, K.; Dallos, A.; Kühn, Z.; Vékey, K. Mass Spectrometry of Very Large Saturated Hydrocarbons. *J. Mass Spectrom.* **1999**, *34*, 264–267.
- (6) Alam, M. S.; Stark, C.; Harrison, R. M. Using Variable Ionization Energy Time-of-Flight Mass Spectrometry with Comprehensive GC×GC to Identify Isomeric Species. *Anal. Chem.* **2016**, *88*, 4211–4220.
- (7) Munson, M. S. B.; Field, F. H. Chemical Ionization Mass Spectrometry. I. General Introduction. *J. Am. Chem. Soc.* **1966**, *88*, 2621–2630.
- (8) Hejazi, L.; Ebrahimi, D.; Hibbert, D. B.; Guilhaus, M. Compatibility of Electron Ionization and Soft Ionization Methods in Gas Chromatography/Orthogonal Time-of-Flight Mass Spectrometry. *Rapid Commun. Mass Spectrom.* **2009**, *23*, 2181–2189.
- (9) Horning, E. C.; Horning, M. G.; Carroll, D. I.; Dzidic, I.; Stillwell, R. N. New Picogram Detection System Based on a Mass Spectrometer with an External Ionization Source at Atmospheric Pressure. *Anal. Chem.* **1973**, *45*, 936–943.
- (10) Lipok, C.; Uteschil, F.; Schmitz, O. J. Development of an Atmospheric Pressure Chemical Ionization Interface for GC-MS. *Molecules* **2020**, *25*, 3253.

- (11) Driscoll, J. N.; Clarici, J. B. Ein Neuer Photoionisationsdetektor Für Die Gas-Chromatographie. *Chromatographia* **1976**, *9*, 567–570.
- (12) Kersten, H.; Kroll, K.; Haberer, K.; Brockmann, K. J.; Benter, T.; Peterson, A.; Makarov, A. Design Study of an Atmospheric Pressure Photoionization Interface for GC-MS. *J. Am. Soc. Mass Spectrom.* **2016**, *27*, 607–614.
- (13) Portolés, T.; Mol, J. G. J.; Sancho, J. V.; Hernández, F. Advantages of Atmospheric Pressure Chemical Ionization in Gas Chromatography Tandem Mass Spectrometry: Pyrethroid Insecticides as a Case Study. *Anal. Chem.* **2012**, *84*, 9802–9810.
- (14) Stein, S. Mass Spectral Reference Libraries: An Ever-Expanding Resource for Chemical Identification. *Anal. Chem.* **2012**, *84*, 7274–7282.
- (15) Hübschmann, H. J. Introduction. In *Handbook of GC-MS: Fundamentals and Applications*. 3rd ed.; Wiley-VCH Verlag GmbH & Co. KGaA: Weinheim, 2015; pp 1–4.
- (16) Eschner, M. S.; Gröger, T. M.; Horvath, T.; Gonin, M.; Zimmermann, R. Quasi-Simultaneous Acquisition of Hard Electron Ionization and Soft Single-Photon Ionization Mass Spectra during GC/MS Analysis by Rapid Switching between Both Ionization Methods: Analytical Concept, Setup, and Application on Diesel Fuel. *Anal. Chem.* **2011**, *83*, 3865–3872.
- (17) Eschner, M. S.; Welthagen, W.; Gröger, T. M.; Gonin, M.; Fuhrer, K.; Zimmermann, R. Comprehensive Multidimensional Separation Methods by Hyphenation of Single-Photon Ionization Time-of-Flight Mass Spectrometry (SPI-TOF-MS) with GC and GC×GC. *Anal. Bioanal. Chem.* **2010**, *398*, 1435–1445.
- (18) Gross, J. H. Ionization Efficiency and Ionization Cross Section. In *Mass Spectrometry A textbook*. 3rd ed.; Springer Cham: Cham, 2017; pp 314–315.
- (19) Märk, T. D. Fundamental Aspects of Electron Impact Ionization. *Int. J. Mass Spectrom. Ion Phys.* **1982**, *45*, 125–145.
- (20) McLafferty, F. W. Mass Spectrometric Analysis: Molecular Rearrangements.

Anal. Chem. **1959**, *31*, 82–87.

- (21) Stein, S. E.; Heller, D. N. On the Risk of False Positive Identification Using Multiple Ion Monitoring in Qualitative Mass Spectrometry: Large-Scale Intercomparisons with a Comprehensive Mass Spectral Library. *J. Am. Soc. Mass Spectrom.* **2006**, *17*, 823–835.
- (22) NIST/NIH/EPA Mass Spectral Library, Standard Reference Database 1, NIST 20. Standard Reference Data program, National Institute of Standards and Technology: Gaithersburg, MD, USA 2020.
- (23) Stein, S. E.; Scott, D. R. Optimization and Testing of Mass Spectral Library Search Algorithms for Compound Identification. *J. Am. Soc. Mass Spectrom.* **1994**, *5*, 859–866.
- (24) Amirav, A.; Fialkov, A. B.; Gordin, A.; Elkabets, O.; Margolin Eren, K. J. Cold Electron Ionization (EI) Is Not a Supplementary Ion Source to Standard EI. It Is a Highly Superior Replacement Ion Source. *J. Am. Soc. Mass Spectrom.* **2021**, *32*, 2631–2635.
- (25) Maney, J. P.; Miller, C.; Comeau, J. k; van Wyck, N. E.; Fencyl, M. K. Misidentification of Organophosphate Esters during GC and GC/MS Analysis. **1995**, *29*, 2147–2149.
- (26) Moorthy, A. S.; Wallace, W. E.; Kearsley, A. J.; Tchekhovskoi, D. V.; Stein, S. E. Combining Fragment-Ion and Neutral-Loss Matching during Mass Spectral Library Searching: A New General Purpose Algorithm Applicable to Illicit Drug Identification. *Anal. Chem.* **2017**, *89*, 13261–13268.
- (27) Elie, M. P.; Elie, L. E.; Baron, M. G. Keeping Pace with NPS Releases: Fast GC-MS Screening of Legal High Products. *Drug Test. Anal.* **2013**, *5*, 281–290.
- (28) Stein, S. E. Chemical Substructure Identification by Mass Spectral Library Searching. *J. Am. Soc. Mass Spectrom.* **1995**, *6*, 644–655.
- (29) Gross, J. H. Electron Ionization Mass Spectra. In *Mass Spectrometry A textbook. 3rd ed.*; Springer Cham: Cham, 2017; pp 314–315.
- (30) Butcher, D. J. Vacuum Ultraviolet Radiation for Single-Photoionization Mass

Spectrometry: A Review. *Microchem. J.* **1999**, *62*, 354–362.

- (31) Tal’Rose V. L.; Frankevitch, E. L. Determination of Proton Affinity and Bond Dissociation Energy by Ion Impact Method. *J. Am. Chem. Soc.* **1958**, *80*, 2344–2345.
- (32) Hansel, A.; Jordan, A.; Holzinger, R.; Prazeller, P.; Vogel, W.; Lindinger, W. Proton Transfer Reaction Mass Spectrometry: On-Line Trace Gas Analysis at the Ppb Level. *Int. J. Mass Spectrom. Ion Process.* **1995**, *149–150*, 609–619.
- (33) Gross, J. H. Chemical Ionization Sources. In *Mass Spectrometry A textbook. 3rd ed.*; Springer Cham: Cham, 2017; pp 440–441.
- (34) Gross, J. H. Formation of Ions in Positive-Ion Chemical Ionization. In *Mass Spectrometry A textbook. 3rd ed.*; Springer Cham: Cham, 2017; pp 440–441.
- (35) Munson, B. Chemical Ionization Mass Spectrometry: Theory and Applications. In *Encyclopedia of Analytical Chemistry*; John Wiley & Sons, Ltd, 2000.
- (36) Field, F. H.; Munson, M. S. Reactions of Gaseous Ions. XIV. Mass Spectrometric Studies of Methane at Pressures to 2 Torr. *J. Am. Chem. Soc.* **1965**, *87*, 3289–3294.
- (37) Munson, M. S. B.; Field, F. H. Chemical Ionization Mass Spectrometry. II. Esters. *J. Am. Chem. Soc.* **1966**, *88*, 4337–4354.
- (38) Munson, M. S. B.; Field, F. H. Chemical Ionization Mass Spectrometry. IV. Aromatic Hydrocarbons. *J. Am. Chem. Soc.* **1967**, *89*, 1047–1052.
- (39) Wai, T. C.; Harrison, A. G. Effect of Chain Length on the Chemical Ionisation Mass Spectra of Methyl N-Alkanoates. *J. Chem. Soc., Perkin Trans.* **1975**, *2*, 1718–1722.
- (40) Dzidic, I.; McCloskey, J. A. Influence of Remote Functional Groups in the Chemical Ionization Mass Spectra of Long-Chain Compounds. *J. Am. Chem. Soc.* **1971**, *93*, 4955–4956.
- (41) Field, F. H.; Munson, M. S. B. Chemical Ionization Mass Spectrometry. V. Cycloparaffins. *J. Am. Chem. Soc.* **1967**, *89*, 4272–4280.

- (42) Hunter, E. P. L.; Lias, S. G. Evaluated Gas Phase Basicities and Proton Affinities of Molecules: An Update. *J. Phys. Chem. Ref. Data* **1998**, *27*, 413–656.
- (43) Newsome, G. A.; Steinkamp, F. L.; Giordano, B. C. Isobutane Made Practical as a Reagent Gas for Chemical Ionization Mass Spectrometry. *J. Am. Soc. Mass Spectrom.* **2016**, *27*, 1789–1795.
- (44) Allan, A. R.; Roboz, J. Neopentane as a Possible Replacement for Isobutane in Chemical Ionization Mass Spectrometry. *Rapid Commun. Mass. Spectrom.* **1988**, *2*, 235–237.
- (45) Dzidic, I.; McCloskey, J. A. Chemical Ionization Mass Spectrometry Using Ammonia Reagent Gas. Selective Protonation of Conjugated Ketones. *Org. Mass Spectrom.* **1972**, *6*, 939–940.
- (46) Westmore, J. B.; Alauddin, M. M. Ammonia Chemical Ionization Mass Spectrometry. *Mass Spectrom. Rev.* **1986**, *5*, 381–465.
- (47) Vairamani, M.; Mirza, U. A.; Srinivas, R. Unusual Positive Ion Reagents in Chemical Ionization Mass Spectrometry. *Mass Spectrom. Rev.* **1990**, *9*, 235–258.
- (48) Cappiello, A.; Termopoli, V.; Palma, P.; Famigliini, G.; Saeed, M.; Perry, S.; Navarro, P. Liquid Chromatography–Electron Capture Negative Ionization–Tandem Mass Spectrometry Detection of Pesticides in a Commercial Formulation. *J. Am. Soc. Mass Spectrom.* **2022**, *33*, 141–148.
- (49) Derpmann, V.; Mueller, D.; Bejan, I.; Sonderfeld, H.; Wilberscheid, S.; Koppmann, R.; Brockmann, K. J.; Benter, T. Capillary Atmospheric Pressure Electron Capture Ionization (CAPECI): A Highly Efficient Ionization Method for Nitroaromatic Compounds. *J. Am. Soc. Mass Spectrom.* **2014**, *25*, 329–342.
- (50) Munson, M. S. B. Proton Affinities and the Methyl Inductive Effect. *J. Am. Chem. Soc.* **1965**, *87*, 2332–2336.
- (51) Herman, J. A.; Harrison, A. G. Energetics and Structural Effects in the Fragmentation of Protonated Esters in the Gas Phase. *Can. J. Chem* **1981**, *59*, 2133–2145.
- (52) Herman, J. A.; Harrison, A. G. Effect of Protonation Exothermicity on The

- Chemical Ionization Mass Spectra of Some Alkylbenzenes. *Org. Mass Spectrom.* **1981**, *16*, 423–427.
- (53) Herman, J. A.; Harrison, A. G. Effect of Reaction Exothermicity on the Proton Transfer Chemical Ionization Mass Spectra of Isomeric C5 and C6 Alkanols. *Can. J. Chem* **1981**, *59*, 2125–2132.
- (54) Munson, M. S. B.; Field, F. H. Reactions of Gaseous Ions. XVI. Effects of Additives on Ionic Reactions in Methane. *J. Am. Chem. Soc.* **1965**, *87*, 4242–4247.
- (55) Klee, S.; Derpmann, V.; Wißdorf, W.; Klopotoski, S.; Kersten, H.; Brockmann, K. J.; Benter, T.; Albrecht, S.; Bruins, A. P.; Dousty, F.; Kauppila, T. J.; Kostianen, R.; O'Brien, R.; Robb, D. B.; Syage, J. A. Are Clusters Important in Understanding the Mechanisms in Atmospheric Pressure Ionization? Part 1: Reagent Ion Generation and Chemical Control of Ion Populations. *J. Am. Soc. Mass Spectrom.* **2014**, *25*, 1310–1321.
- (56) Sekimoto, K.; Li, S.-M.; Yuan, B.; Koss, A.; Coggon, M.; Warneke, C.; de Gouw, J. Calculation of the Sensitivity of Proton-Transfer-Reaction Mass Spectrometry (PTR-MS) for Organic Trace Gases Using Molecular Properties. *Int. J. Mass Spectrom.* **2017**, *421*, 71–94.
- (57) Cappellin, L.; Karl, T.; Probst, M.; Ismailova, O.; Winkler, P. M.; Soukoulis, C.; Aprea, E.; Märk, T. D.; Gasperi, F.; Biasioli, F. On Quantitative Determination of Volatile Organic Compound Concentrations Using Proton Transfer Reaction Time-of-Flight Mass Spectrometry. *Environ. Sci. Technol.* **2012**, *46*, 2283–2290.
- (58) Krechmer, J.; Lopez-Hilfiker, F.; Koss, A.; Hutterli, M.; Stoermer, C.; Deming, B.; Kimmel, J.; Warneke, C.; Holzinger, R.; Jayne, J.; Worsnop, D.; Fuhrer, K.; Gonin, M.; De Gouw, J. Evaluation of a New Reagent-Ion Source and Focusing Ion-Molecule Reactor for Use in Proton-Transfer-Reaction Mass Spectrometry. *Anal. Chem.* **2018**, *90*, 12011–12018.
- (59) Guillevic, M.; Guillevic, A.; Vollmer, M. K.; Schlauri, P.; Hill, M.; Emmenegger, L.; Reimann, S. Automated Fragment Formula Annotation for Electron Ionisation, High Resolution Mass Spectrometry: Application to

- Atmospheric Measurements of Halocarbons. *J. Cheminform.* **2021**, *13*, 78.
- (60) Sheldon, L. S.; Hites, R. A. Organic Compounds in the Delaware River. *Environ. Sci. Technol.* **1978**, *12*, 1188–1194.
- (61) Jungclaus, G. A.; Lopez-Avila, V.; Hites, R. A. Organic Compounds in an Industrial Wastewater: A Case Study of Their Environmental Impact. *Environ. Sci. Technol.* **1978**, *12*, 88–96.
- (62) Hollender, J.; Schymanski, E. L.; Singer, H. P.; Ferguson, P. L. Nontarget Screening with High Resolution Mass Spectrometry in the Environment: Ready to Go? *Environ. Sci. Technol.* **2017**, *51*, 11505–11512.
- (63) Sobus, J. R.; Wambaugh, J. F.; Isaacs, K. K.; Williams, A. J.; McEachran, A. D.; Richard, A. M.; Grulke, C. M.; Ulrich, E. M.; Rager, J. E.; Strynar, M. J.; Newton, S. R. Integrating Tools for Non-Targeted Analysis Research and Chemical Safety Evaluations at the US EPA. *J. Expo. Sci. Environ. Epidemiol.* **2018**, *28*, 411–426.
- (64) Krueve, A. Semi-Quantitative Non-Target Analysis of Water with Liquid Chromatography/High-Resolution Mass Spectrometry: How Far Are We? *Rapid Commun. Mass Spectrom.* **2019**, *33*, 54–63.
- (65) Kunzelmann, M.; Winter, M.; Åberg, M.; Hellenäs, K. E.; Rosén, J. Non-Targeted Analysis of Unexpected Food Contaminants Using LC-HRMS. *Anal. Bioanal. Chem.* **2018**, *410*, 5593–5602.
- (66) Kaufmann, A. The Current Role of High-Resolution Mass Spectrometry in Food Analysis. *Anal. Bioanal. Chem.* **2012**, *403*, 1233–1249.
- (67) Vogel, A. L.; Lauer, A.; Fang, L.; Arturi, K. R.; Bachmeier, F.; Dällenbach, K. R.; Käser, T.; Vlachou, A.; Pospisilova, V.; Baltensperger, U.; El Haddad, I.; Schwikowski, M.; Bjelić, S. A Comprehensive Nontarget Analysis for the Molecular Reconstruction of Organic Aerosol Composition from Glacier Ice Cores. *Environ. Sci. Technol.* **2019**, *53*, 12565–12575.
- (68) Misra, B. B.; Olivier, M. High Resolution GC-Orbitrap-MS Metabolomics Using Both Electron Ionization and Chemical Ionization for Analysis of Human

Plasma. *J. Proteome Res.* **2020**, *19*, 2717–2731.

- (69) Andra, S. S.; Austin, C.; Patel, D.; Dolios, G.; Awawda, M.; Arora, M. Trends in the Application of High-Resolution Mass Spectrometry for Human Biomonitoring: An Analytical Primer to Studying the Environmental Chemical Space of the Human Exposome. *Environ. Int.* **2017**, *100*, 32–61.
- (70) Li, X.; Dorman, F. L.; Helm, P. A.; Kleywegt, S.; Simpson, A.; Simpson, M. J.; Jobst, K. J. Nontargeted Screening Using Gas Chromatography–Atmospheric Pressure Ionization Mass Spectrometry: Recent Trends and Emerging Potential. *Molecules* **2021**, *26*, 6911.
- (71) Portolés, T.; Mol, J. G. J.; Sancho, J. V.; Hernández, F. Use of Electron Ionization and Atmospheric Pressure Chemical Ionization in Gas Chromatography Coupled to Time-of-Flight Mass Spectrometry for Screening and Identification of Organic Pollutants in Waters. *J. Chromatogr. A* **2014**, *1339*, 145–153.
- (72) Wanless, G. G.; Glock Jr., G. A. Simplified Mass Spectra by Means of a Dual Field Ionization/Electron Impact Source. *Anal. Chem.* **1967**, *39*, 2–13.
- (73) Hejazi, L.; Guilhaus, M.; Hibbert, D. B.; Ebrahimi, D. Gas Chromatography with Parallel Hard and Soft Ionization Mass Spectrometry. *Rapid Commun. Mass Spectrom.* **2015**, *29*, 91–99.
- (74) Muhlberger, F.; Saraji-Bozorgzad, M.; Gonin, M.; Fuhrer, K.; Zimmermann, R. Compact Ultrafast Orthogonal Acceleration Time-of-Flight Mass Spectrometer for on-Line Gas Analysis by Electron Impact Ionization and Soft Single Photon Ionization Using an Electron Beam Pumped Rare Gas Excimer Lamp as VUV-Light Source. *Anal. Chem.* **2007**, *79*, 8118–8124.
- (75) Portolés, T.; Pitarch, E.; López, F. J.; Hernández, F.; Niessen, W. M. A. Use of Soft and Hard Ionization Techniques for Elucidation of Unknown Compounds by Gas Chromatography/Time-of-Flight Mass Spectrometry. *Rapid Commun. Mass Spectrom.* **2011**, *25*, 1589–1599.
- (76) Lebedev, A. T.; Mazur, D. M.; Artaev, V. B.; Tikhonov, G. Y. Better Screening of Non-Target Pollutants in Complex Samples Using Advanced

- Chromatographic and Mass Spectrometric Techniques. *Environ. Chem. Lett.* **2020**, *18*, 1753–1760.
- (77) Gross, J. H. Relativistic Mass Defect. In *Mass Spectrometry A textbook. 3rd ed.*; Springer Cham: Cham, 2017; p 117.
- (78) Kind, T.; Fiehn, O. Seven Golden Rules for Heuristic Filtering of Molecular Formulas Obtained by Accurate Mass Spectrometry. *BMC Bioinformatics* **2007**, *8*, 150.
- (79) Amad, M. H.; Houk, R. S. High-Resolution Mass Spectrometry with a Multiple Pass Quadrupole Mass Analyzer. *Anal. Chem.* **1998**, *70*, 4885–4889.
- (80) Yang, L.; Amad, M.; Winnik, W. M.; Schoen, A. E.; Schweingruber, H.; Mylchreest, I.; Rudewicz, P. J. Investigation of an Enhanced Resolution Triple Quadrupole Mass Spectrometer for High-Throughput Liquid Chromatography/Tandem Mass Spectrometry Assays. *Rapid Commun. Mass Spectrom.* **2002**, *16*, 2060–2066.
- (81) Gross, J. H. Velocity of Ions and Time-of-Flight. In *Mass Spectrometry A textbook. 3rd ed.*; Springer Cham: Cham, 2017; pp 157–159.
- (82) Bräkling, S.; Kroll, K.; Kersten, H.; Benter, T. Development of a Flexible GC Transfer Line for a Field-Deployable GC-EI / MS; Proceedings of the 67th ASMS Conference on Mass Spectrometry and Allied Topics: Atlanta (GA), 2019.
- (83) Martinsen, D. P.; Song, B.-H. Computer Applications in Mass Spectral Interpretation: A Recent Review. *Mass Spectrom. Rev.* **1985**, *4*, 461–490.
- (84) Warr, W. A. Computer-Assisted Structure Elucidation. Part 2: Indirect Database Approaches and Established Systems. *Anal. Chem.* **1993**, *65*, 1087–1095.
- (85) Warneke, C.; De Gouw, J. A.; Kuster, W. C.; Goldan, P. D.; Fall, R. Validation of Atmospheric VOC Measurements by Proton-Transfer-Reaction Mass Spectrometry Using a Gas-Chromatographic Preseparation Method. *Environ. Sci. Technol.* **2003**, *37*, 2494–2501.
- (86) Niazi, K.; Lichtenberg, A. J.; Lieberman, M. A.; Flamm, D. L. Operation of a

- Helical Resonator Plasma Source. *Plasma Sources Sci. Technol.* **1994**, *3*, 482–495.
- (87) Bowen, R. D.; Harrison, A. G. Chemical Ionization Mass Spectra of Selected C₃H₆O Compounds. *Org. Mass Spectrom.* **1981**, *16*, 159–166.
- (88) Shahin, M. M. Mass-Spectrometric Studies of Corona Discharges in Air at Atmospheric Pressures. *J. Chem. Phys.* **1966**, *45*, 2600–2605.
- (89) Kebarle, P.; Searles, S. K.; Zolla, A.; Scarborough, J.; Arshadi, M. The Solvation of the Hydrogen Ion by Water Molecules in the Gas Phase. Heats and Entropies of Solvation of Individual Reactions: H⁺(H₂O)_{n-1}+H₂O -> H⁺(H₂O)_n. *J. Am. Chem. Soc.* **1967**, *89*, 6393–6399.
- (90) Klee, S.; Brockhaus, A.; Wißdorf, W.; Thinius, M.; Hartmann, N.; Benter, T. Development of an Ion Activation Stage for Atmospheric Pressure Ionization Sources. *Rapid Commun. Mass Spectrom.* **2015**, *29*, 143–154.
- (91) Lindinger, W.; Hansel, A.; Jordan, A. On-Line Monitoring of Volatile Organic Compounds at Pptv Levels by Means of Proton-Transfer-Reaction Mass Spectrometry (PTR-MS) Medical Applications, Food Control and Environmental Research. *Int. J. Mass Spectrom. Ion Process.* **1998**, *173*, 191–241.
- (92) Breitenlechner, M.; Fischer, L.; Hainer, M.; Heinritzi, M.; Curtius, J.; Hansel, A. PTR3: An Instrument for Studying the Lifecycle of Reactive Organic Carbon in the Atmosphere. *Anal. Chem.* **2017**, *89*, 5824–5831.
- (93) Tani, A.; Hayward, S.; Hewitt, C. N. Measurement of Monoterpenes and Related Compounds by Proton Transfer Reaction-Mass Spectrometry (PTR-MS). *Int. J. Mass Spectrom.* **2003**, *223–224*, 561–578.
- (94) Kauppila, T. J.; Kersten, H.; Benter, T. Ionization of EPA Contaminants in Direct and Dopant-Assisted Atmospheric Pressure Photoionization and Atmospheric Pressure Laser Ionization. *J. Am. Soc. Mass Spectrom.* **2015**, *26*, 1036–1045.
- (95) Kutsch, T.; Kroll, K.; Haberer, K.; Benter, T.; Kersten, H. H₂ Plasma for the Generation of Protonation Reagents with a Standart APPI Power Supply; Proceedings of the 65th ASMS Conference on Mass Spectrometry and Allied

Topics: Indianapolis, IN, 2017.

- (96) Anicich, V. G. Evaluated Bimolecular Ion-Molecule Gas Phase Kinetics of Positive Ions for Use in Modeling Planetary Atmospheres, Cometary Comae, and Interstellar Clouds. *J. Phys. Chem. Ref. Data* **1993**, *22*, 1469–1569.
- (97) Hiraoka, K.; Saluja, P. P. S.; Kebarle, P. Stabilities of Complexes $(\text{N}_2)_n\text{H}^+$, $(\text{CO})_n\text{H}^+$, and $(\text{O}_2)_n\text{H}^+$ for $n = 1$ to 7 Based on Gas Phase Ion-Equilibria Measurements. *Can. J. Chem* **1979**, *57*, 2159–2166.
- (98) Good, A.; Durden, D. A.; Kebarle, P. Ion-Molecule Reactions in Pure Nitrogen and Nitrogen Containing Traces of Water at Total Pressures 0.5-4 Torr. Kinetics of Clustering Reactions Forming $\text{H}^+(\text{H}_2\text{O})_n$. *J. Chem. Phys.* **1970**, *52*, 212–221.
- (99) Midey, A. J.; Williams, S.; Arnold, S. T.; Viggiano, A. A. Reactions of $\text{H}_3\text{O}^+(\text{H}_2\text{O})_{0,1}$ with Alkylbenzenes from 298 to 1200 K. *J. Phys. Chem. A* **2002**, *106*, 11726–11738.
- (100) Cheng, H.-P. Water Clusters: Fascinating Hydrogen-Bonding Networks, Solvation Shell Structures, and Proton Motion. *J. Phys. Chem. A* **1998**, *102*, 6201–6204.
- (101) Goebbert, D. J.; Wentold, P. G. Water Dimer Proton Affinity from the Kinetic Method: Dissociation Energy of the Water Dimer. *Eur. J. Mass Spectrom.* **2004**, *10*, 837–846.
- (102) Aquilanti, V.; Volpi, G. G. Ion-Molecule Reactions between H_3^+ and Saturated Hydrocarbons. *J. Chem. Phys.* **1966**, *44*, 2307–2313.
- (103) Milligan, D. B.; Wilson, P. F.; Freeman, C. G.; Meot-Ner (Mautner), M.; McEwan, M. J. Dissociative Proton Transfer Reactions of H_3^+ , N_2H^+ , and H_3O^+ With Acyclic, Cyclic, and Aromatic Hydrocarbons and Nitrogen Compounds, and Astrochemical Implications. *J. Phys. Chem. A* **2002**, *106*, 9745–9755.
- (104) Španěl, P.; Smith, D. Selected Ion Flow Tube Studies of the Reactions of H_3O^+ , NO^+ , and O_2^+ with Several Aromatic and Aliphatic Hydrocarbons. *Int. J. Mass Spectrom.* **1998**, *181*, 1–10.
- (105) Maleknia, S. D.; Bell, T. L.; Adams, M. A. PTR-MS Analysis of Reference and

- Plant-Emitted Volatile Organic Compounds. *Int. J. Mass Spectrom.* **2007**, *262*, 203–210.
- (106) Solouki, T.; Szulejko, J. E. Bimolecular and Unimolecular Contributions to the Disparate Self-Chemical Ionizations of α -Pinene and Camphene Isomers. *J. Am. Soc. Mass Spectrom.* **2007**, *18*, 2026–2039.
- (107) Farooq Wahab, M.; Armstrong, D. W.; Patel, D. C. Peak Shapes and Their Measurements: The Need and Concept Behind Total Peak Shape Analysis. *LCGC North Am.* **2017**, *35*, 846–853.
- (108) Lopez-Avila, V.; Nieto, S.; Prest, H.; Kernan, J.; Yefchak, G.; Clark, R.; Eno, N.; Oppenheimer, J.; Russ, B. *Combination of Chemical Ionization (CI) and Low Energy Ionization (EI) Capabilities with High-Resolution Q-TOF GC/MS*. Application Note. <https://www.agilent.com/cs/library/applications/application-%0Achemical-ionization-7250-gc-qtof-5994-0290en-agilent.pdf>. Accessed: Aug. 2021.
- (109) Vianello, R.; Maksić, Z. B. Triadic Analysis of Substituent Effects - Gas-Phase Acidity of Para-Substituted Phenols. *Tetrahedron* **2006**, *62*, 3402–3411.
- (110) McIver Jr., R. T.; Silvers, J. H. Gas-Phase Acidity of Monosubstituted Phenols. *J. Am. Chem. Soc.* **1973**, *95*, 8462–8464.
- (111) McLafferty, F. W. *Interpretation of Mass Spectra*, 1st ed.; W. A. Benjamin Inc.: New-York-Amsterdam, 1966.
- (112) Hamilton, J. F.; Webb, P. J.; Lewis, A. C.; Hopkins, J. R.; Smith, S.; Davy, P. Partially Oxidised Organic Components in Urban Aerosol Using GCXGC-TOF/MS. *Atmos. Chem. Phys.* **2004**, *4*, 1279–1290.
- (113) McEwen, C. N.; McKay, R. G. A Combination Atmospheric Pressure LC/MS:GC/MS Ion Source: Advantages of Dual AP-LC/MS:GC/MS Instrumentation. *J. Am. Soc. Mass Spectrom.* **2005**, *16*, 1730–1738.
- (114) Schiewek, R.; Lorenz, M.; Giese, R.; Brockmann, K.; Benter, T.; Gäb, S.; Schmitz, O. J. Development of a Multipurpose Ion Source for LC-MS and GC-API MS. *Anal. Bioanal. Chem.* **2008**, *392*, 87–96.

- (115) Abate, S.; Ahn, Y. G.; Kind, T.; Cataldi, T. R. I.; Fiehn, O. Determination of Elemental Compositions by Gas Chromatography/Time-of-Flight Mass Spectrometry Using Chemical and Electron Ionization. *Rapid Commun. Mass Spectrom.* **2010**, *24*, 1172–1180.
- (116) Munson, B. Chemical Ionization Mass Spectrometry. *Anal. Chem.* **1971**, *43*, 28A-43A.
- (117) Amirav, A.; Danon, A. Mass Spectrometry in Supersonic Molecular Beams. *Int. J. Mass Spectrom. Ion Process.* **1990**, *97*, 107–113.
- (118) Brunnée, C. A Combined Field Ionisation/Electron Impact Ion Source for High Molecular Weight Samples of Low Volatility. *Z. Naturforsch.* **1967**, *22 b*, 121–123.
- (119) Claflin, M.; Pagonis, D.; Finewax, Z.; Handschy, A.; Day, D.; Brown, W.; Jayne, J.; Worsnop, D.; Jimenez, J.; Ziemann, P.; de Gouw, J.; Lerner, B. An in Situ Gas Chromatograph with Automatic Detector Switching between Vocus PTR-TOF-MS and EI-TOF-MS: Isomer Resolved Measurements of Indoor Air. *Atmos. Meas. Tech.* **2021**, *14*, 133–152.
- (120) Bräkling, S.; Kroll, K.; Klee, S.; Benter, T.; Kersten, H. Hydrogen Plasma-Based Medium Pressure Chemical Ionization Source for GC-TOFMS. *J. Am. Soc. Mass Spectrom.* **2022**, *33*, 499–509.
- (121) Mjøs, S. A. The Prediction of Fatty Acid Structure from Selected Ions in Electron Impact Mass Spectra of Fatty Acid Methyl Esters. *Eur. J. Lipid Sci. Technol.* **2004**, *106*, 550–560.
- (122) Wells, G.; Prest, H.; Russ IV, C. W. *Signal , Noise , and Detection Limits in Mass Spectrometry*. Application Note.
<https://www.agilent.com/cs/library/technicaloverviews/public/5990-7651EN.pdf>.
Accessed: Feb. 2022.
- (123) Kind, T.; Fiehn, O. Metabolomic Database Annotations via Query of Elemental Compositions: Mass Accuracy Is Insufficient Even at Less than 1 Ppm. *BMC Bioinformatics* **2006**, *7*, 234.

- (124) de Laeter, J. R.; Böhlke, J. K.; de Bièvre, P.; Hidaka, H.; Peiser, H. S.; Rosman, K. J. R.; Taylor, P. D. P. Atomic Weights of the Elements: Review 2000 (IUPAC Technical Report). *Pure Appl. Chem.* **2003**, *75*, 683–800.
- (125) Schymanski, E. L.; Jeon, J.; Gulde, R.; Fenner, K.; Ruff, M.; Singer, H. P.; Hollender, J. Identifying Small Molecules via High Resolution Mass Spectrometry: Communicating Confidence. *Environ. Sci. Technol.* **2014**, *48*, 2097–2098.
- (126) Jones, A. P. Indoor Air Quality and Health. *Atmos. Environ.* **1999**, *33*, 4535–4564.
- (127) Brooks, B. O.; Utter, G. M.; Debroy, J. A.; Schimke, R. D. Indoor Air Pollution: An Edifice Complex. *Clin. Toxicol.* **1991**, *29*, 315–374.
- (128) Missia, D. A.; Demetriou, E.; Michael, N.; Tolis, E. I.; Bartzis, J. G. Indoor Exposure from Building Materials: A Field Study. *Atmos. Environ.* **2010**, *44*, 4388–4395.
- (129) Knudsen, H. N.; Kjaer, U. D.; Nielsen, P. A.; Wolkoff, P. Sensory and Chemical Characterization of VOC Emissions from Building Products: Impact of Concentration and Air Velocity. *Atmos. Environ.* **1999**, *33*, 1217–1230.
- (130) Wallace, L. A.; Pellizzari, E.; Leaderer, B.; Zelon, H.; Sheldon, L. Emissions of Volatile Organic Compounds from Building Materials and Consumer Products. *Atmos. Environ.* **1987**, *21*, 385–393.
- (131) Faber, J.; Brodzik, K.; Gołda-kopek, A.; Łomankiewicz, D. Air Pollution in New Vehicles as a Result of VOC Emissions from Interior Materials. *Pol. J. Environ. Stud.* **2013**, *22*, 1701–1709.
- (132) Chien, Y. C. Variations in Amounts and Potential Sources of Volatile Organic Chemicals in New Cars. *Sci. Total Environ.* **2007**, *382*, 228–239.
- (133) Zhu, L.; Tan, W.; Li, R. *Separation and Quantification of Trace Chemical Emissions from Packaging Materials Using the Vocus PTR-TOF*. Application Note. <https://www.tofwerk.com/wp-content/uploads/2020/08/TOFWERK-Vocus-Packaging-Materials-Emissions.pdf>. Accessed: Feb. 2022.

- (134) Klee, S.; Braekling, S.; Koss, A. *Simultaneous Real-Time CI-MS and GC-EI-MS Analysis using the EC-TOF*. Application Note. <https://www.tofwerk.com/wp-content/uploads/TOFWERK-Simultaneous-Real-Time-CI-MS-and-GC-EI-MS-App-Note-1.pdf>. Accessed: Sep. 2022.
- (135) Bräkling, S.; Kroll, K.; Stoermer, C.; Rohner, U.; Gonin, M.; Benter, T.; Kersten, H.; Klee, S. Parallel Operation of Electron Ionization and Chemical Ionization for GC-MS Using a Single TOF Mass Analyzer. *Anal. Chem.* **2022**, *94*, 6057–6064.
- (136) National Center for Biotechnology Information (2022). *PubChem Compound Summary for CID 5541, Triacetin*. <https://pubchem.ncbi.nlm.nih.gov/compound/Triacetin>. Accessed: Sep. 2022.
- (137) Klee, S.; Bräkling, S.; Vetter, M.; Bieber, S.; Letzel, T. Nontargeted Screening for the Verification of Allergenic Ingredients and Perfume Authenticity by GC-EcTOF-MS. *LCGC North Am.* **2022**, *40*, 439–444.
- (138) Vetter, M.; Bräkling, S.; Klee, S. *Flavor Profiling with the ecTOF – Volatilomic Comparison of Vegan and Non-Vegan Cheeses*. Application Note. <https://www.tofwerk.com/wp-content/uploads/2022/11/TOFWERK-ecTOF-App-note-Cheese-Flavor-Profiling.pdf>. Accessed: Nov. 2022.
- (139) Vetter, M.; Bräkling, S.; Klee, S. *Non-Target Screening of Battery Aging Products Using the ecTOF*. Application Note. <https://www.tofwerk.com/wp-content/uploads/TOFWERK-ecTOF-Battery-Aging-Application-Note.pdf>. Accessed: Sep. 2022.
- (140) Klee, S.; Braekling, S. *Simultaneous Electron Ionization & Chemical Ionization with the EC-TOF for GC-MS*. White Paper. <https://www.tofwerk.com/wp-content/uploads/TOFWERK-EC-TOF-for-GC-MS-White-Paper-1.pdf>. Accessed: Okt. 2022.
- (141) Smolinsky, G.; Vasile, M. J. Ionic and Neutral Products of an RF Discharge in Methane. *Int. J. Mass Spectrom. Ion Physics* **1975**, *16*, 137–149.
- (142) Herod, A. A.; Harrison, A. G. Bimolecular Reactions of Ions Trapped in an Electron Space Charge. *Int. J. Mass Spectrom. Ion Phys.* **1970**, *4*, 415–431.

8 Appendix

8.1 Supporting information: Hydrogen plasma-based medium pressure chemical ionization source for GC-TOFMS

Reagent ion spectra

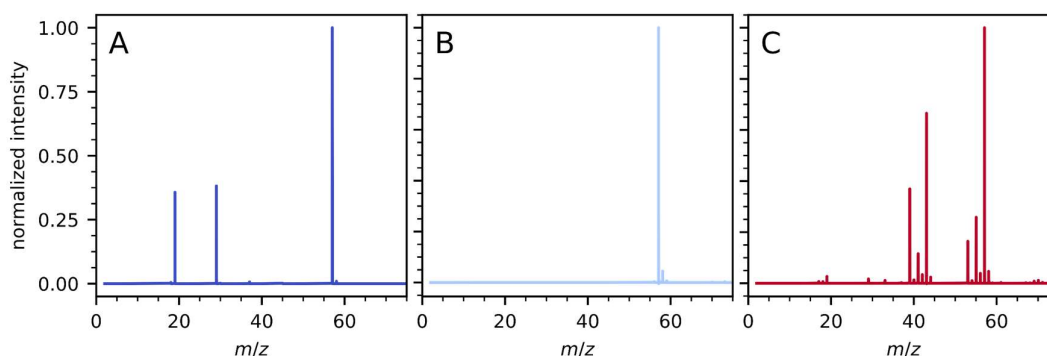


Figure 8.1.1: Reagent gas spectra at 13 mbar ion source pressure for (A) nitrogen, (B) isobutane, (C) methane as reagent gas

methane reagent ion system

The methane reagent gas spectrum is rather complex involving extensive ion chemistry. The reaction of H_3^+ with methane is shown in reaction (Rn 8.1.1-8.1.3)^[102]. An alternative mechanism for the protonation of methane via H_3^+ (Rn 8.1.4-Rn 8.1.5) is also shown by Aquilanti and Volpi (1966)^[102].



$C_2H_5^+$ is the product of the reaction between CH_3^+ and excess of neutral methane^[102].



Possible pathways for the generation of the mainly observed C₃ and C₄ species are described in detail by Field et al.^[36] using classical filament based chemical ionization at lower pressures and reaction times. However, not all species available in filament-based methane CI sources^[7,36] are expected for the reaction of Hydrogen with methane e.g., CH₂⁺. Interference into the ion chemistry by e.g., back diffusion into the plasma or the afterglow region could increase the complexity of the system. Spectra of gas discharges in methane are shown by Smolinsky et al 1975^[141]. This can also lead to the formation of radical and neutral hydrocarbons adding the possibility of further rich chemistry to the system^[142]. The formation of C₃ and C₄ species are also shown by Aquilanti et al.^[102] for the reaction of higher C_nH_m species with H₂. Low abundance C_nH_m⁺ species up to 200 Th indicating further condensation reactions. The complete interpretation of the methane reagent ion spectra is rather complex and far beyond the aim this work and therefore not completely discussed.

RF dependency on fragmentation

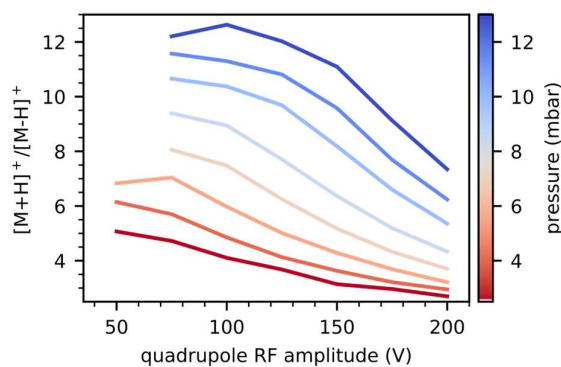


Figure 8.1.2: Fragmentation behavior of *o*-xylene on the quadrupole RF amplitude for different pressures. The ratio of the $[M-H]^+$ (fragment) and the $[M+H]^+$ increases with higher RF and lower pressures. A continuous sample flow of 0.5 standard cm³/min of a 10 ppmV xylene gas mixture with N₂ as reagent gas was used.

Linear ranges

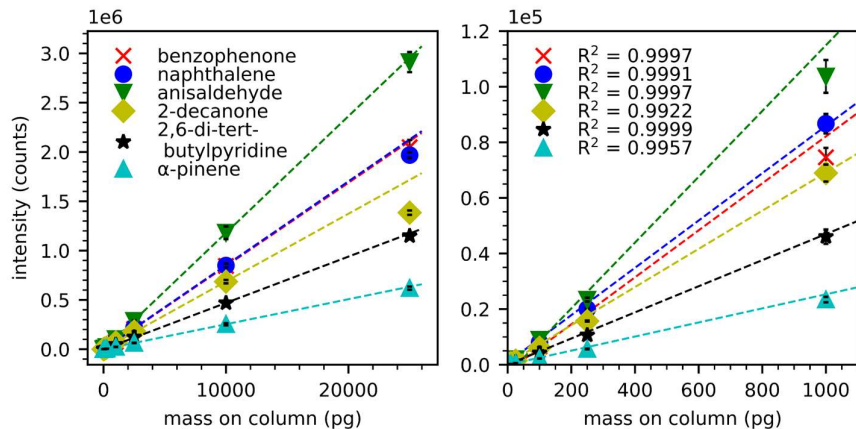


Figure 8.1.3: Range of linearity for benzophenone, naphthalene, anisaldehyde, 2-decanone, 2,6-di-tert-butylamine, and α -pinene using nitrogen as reagent gas. Left: Entire linearity range probed, right: expanded lower mass region.

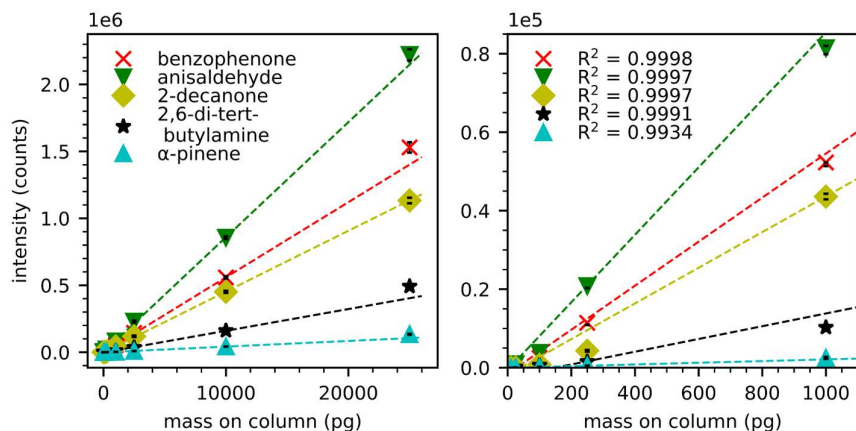


Figure 8.1.4: Range of linearity for benzophenone, naphthalene, anisaldehyde, 2-decanone, 2,6-di-tert-butylamine, and α -pinene using isobutane as reagent gas. Left: complete linearity range, right: expanded lower mass region.

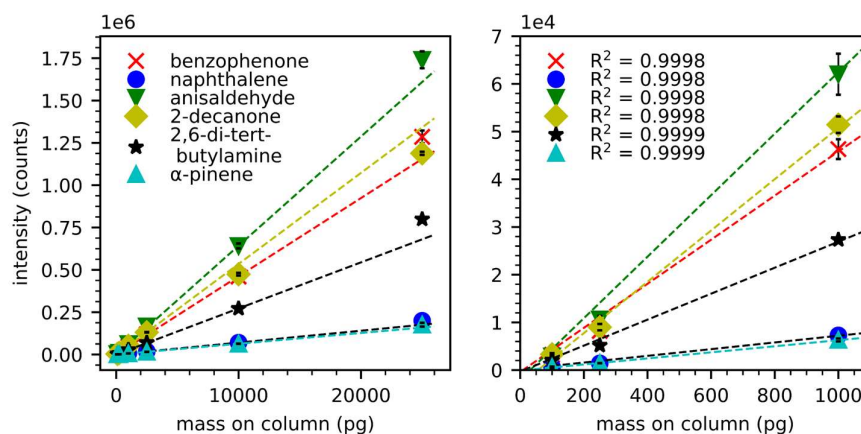


Figure 8.1.5: Range of linearity for benzophenone, naphthalene, anisaldehyde, 2-decanone, 2,6-di-tert-butylamine, and α -pinene using methane as reagent gas. Left: complete linearity range, right: expanded lower mass region.

Analyte mass spectra

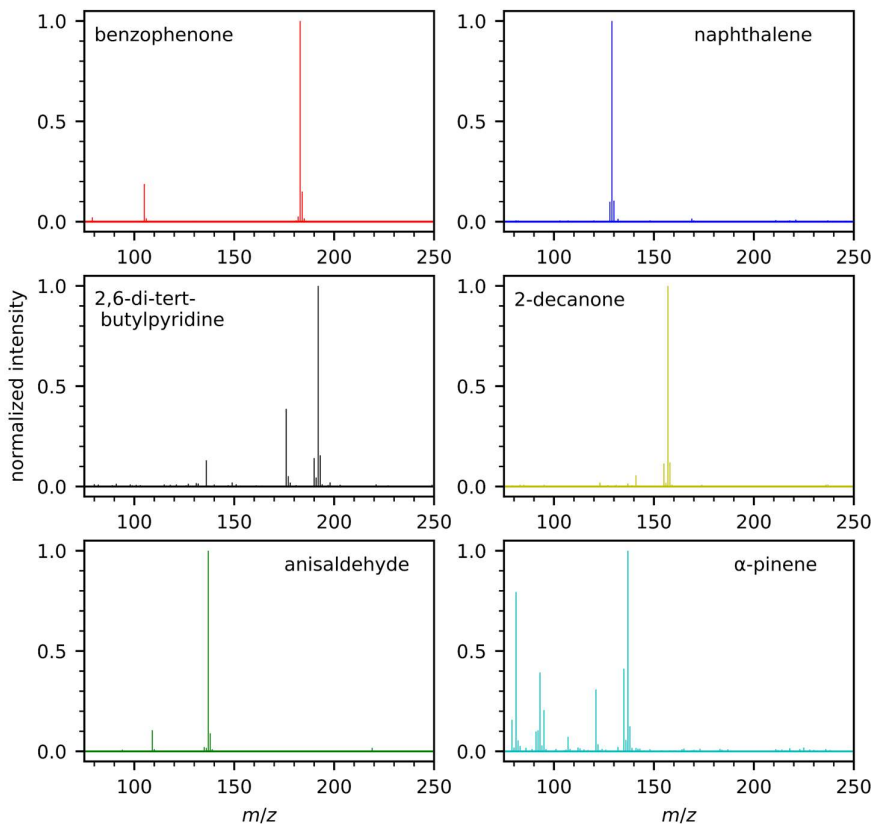


Figure 8.1.6: Mass spectra of benzophenone, naphthalene, anisaldehyde, 2-decanone, 2,6-di-tert-butylamine, and α -pinene using nitrogen as reactant gas at 13 mbar.

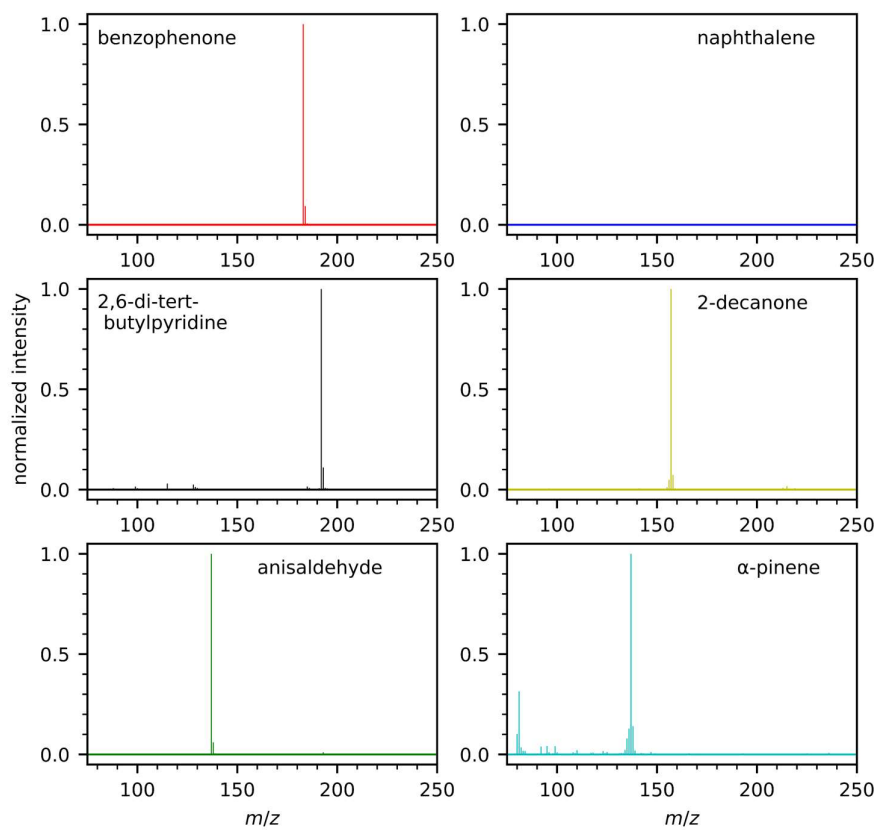


Figure 8.1.7: Mass spectra of benzophenone, naphthalene, anisaldehyde, 2-decanone, 2,6-di-tert-butylamine, and α -pinene using isobutane as reagent gas at 8 mbar.

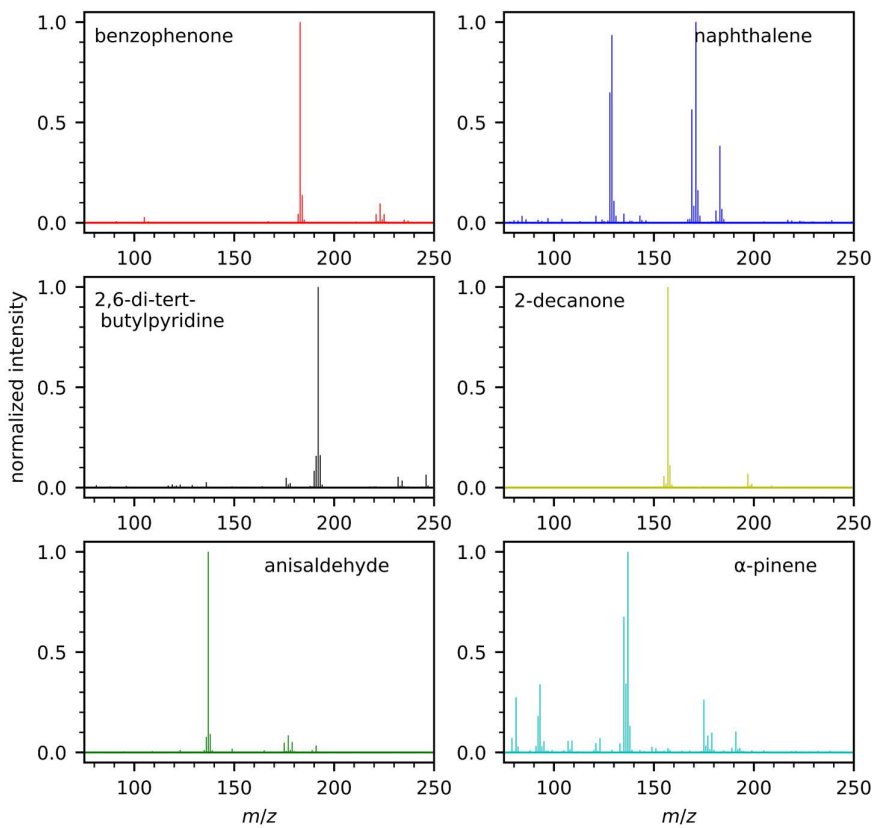


Figure 8.1.8: *Mass spectra of benzophenone, naphthalene, anisaldehyde, 2-decanone, 2,6-di-tert-butylamine, and α-pinene using methane as reagent gas at 13 mbar.*

Detailed list of compounds in the EPA 8270 LCS mix

Table 8.1.1: Compounds present in the EPA 8270 LCS mix, proton affinities, and the m/z of the base peak observed nitrogen, isobutane and methane as reagent gas.

compound	PA (kJ/mol) ^[94]	nitrogen	isobutane	methane	group
N-nitrosodimethylamine	-	[M+H] ⁺	[M+H] ⁺	[M+H] ⁺	N-containing
pyridine	930.1	[M+H] ⁺	[M+H] ⁺	[M+H] ⁺	N-containing
phenol	817.3	[M+H] ⁺	-	[M+H] ⁺	phenolic
aniline	882.5	[M+H] ⁺	[M+H] ⁺	[M+H] ⁺	N-containing
bis(2-chloroethyl)ether	n.a	[M+H] ⁺	-	[M+H] ⁺	ether
2-chlorophenol	n.a	[M+H] ⁺	-	[M+H+42] ⁺ ([M+H] ⁺ ~65 %)	phenolic
1,3-dichlorobenzene(a)	n.a	[M+H] ⁺	-	[M+H] ⁺	halogenated
1,4-dichlorobenzene (a)	n.a	[M+H] ⁺	-	[M+H] ⁺	halogenated
1,2-dichlorobenzene (a)	n.a	[M+H] ⁺	-	[M+H] ⁺	halogenated
o-cresol (a)	832.0	[M+H] ⁺	[M+H] ⁺	[M+H] ⁺	phenolic
benzyl alcohol	778.6	91	-	91	O-containing
m-cresol (a,b)	841.0	[M+H] ⁺	[M+H] ⁺	[M+H] ⁺	phenolic
p-cresol (ab)	814.0	[M+H] ⁺	-	[M+H] ⁺	phenolic
bis(2-chloroisopropyl)ether	n.a	77 ([M+H] ⁺ ~5 %)	[M+H] ⁺	[M+H] ⁺	ether
N-nitroso-di-n-propylamine	n.a	BP:72 ([M+H] ⁺ ~48 %)	[M+H] ⁺	72 ([M+H] ⁺ ~47 %)	N-containing
hexachloroethane	n.a	[M-Cl] ⁺	-	-	halogenated
nitrobenzene	800.3	94 ([M+H] ⁺ ~85 %)	-	94 ([M+H] ⁺ ~36 %)	nitro-group
isophorone	893.5	[M+H] ⁺	[M+H] ⁺	[M+H] ⁺	O-containing
2-nitrophenol	n.a	[M+H] ⁺	-	[M+H] ⁺	phenolic
2,4-dimethylphenol	n.a	[M+H] ⁺	-	-	phenolic
benzoic acid	821.1	-	-	-	O-containing
bis(2-chloroethoxy)methane	n.a	93	-	[M+H] ⁺	ether
2,4-dichlorophenol	n.a	[M+H] ⁺	-	-	phenolic
1,2,3-trichlorobenzene	n.a	[M+H] ⁺	-	-	halogenated

naphthalene	802.9	[M+H] ⁺	-	[M+H] ⁺	PAH
4-chloroaniline	873.8	[M+H] ⁺	[M+H] ⁺	[M+H] ⁺	N-containing
hexachloro-1,3-butadiene	n.a	[M-CL] ⁺ ([M+H] ⁺ ~80 %)	-	-	halogenated
4-chloro-3-methylphenol	n.a	[M+H] ⁺	-	[M+H] ⁺	phenolic
2-methylnaphthalene(a)	834.8	[M+H] ⁺	[M+H] ⁺	[M+H] ⁺	PAH
1-methylnaphthalene(a)	831.9	[M+H] ⁺	[M+H] ⁺	[M+H] ⁺	PAH
hexachlorocyclopentadiene	n.a	[M-Cl] ⁺	-	-	halogenated
2,4,6-trichlorophenol (a)	n.a	[M+H] ⁺	-	-	phenolic
2,4,5-trichlorophenol (a)	n.a	[M+H] ⁺	-	-	phenolic
2-chloronaphthalene	n.a	[M+H] ⁺	-	[M+H+42] ⁺ ([M+H] ⁺ ~75%)	halogenated
2-nitroaniline (a)	n.a	[M+H] ⁺	[M+H] ⁺	[M+H] ⁺	N-containing
1,4-dinitrobenzene (a)	n.a	109 ([M+H] ⁺ ~56 %)	-	[M+H] ⁺	nitro-group
1,3-dinitrobenzene (a)	n.a	109 ([M+H] ⁺ ~57 %)	-	[M+H] ⁺	nitro-group
1,2-dinitrobenzene(a)	n.a	109 ([M+H] ⁺ ~72%)	-	[M+H] ⁺	nitro-group
dimethyl phthalate	n.a	163 ([M+H] ⁺ ~1.5 %)	M+H	[M+H] ⁺	ester
acenaphthylene	861.1	[M+H] ⁺	[M+H+56] ⁺ ([M+H] ⁺ ~15 %)	[M+H] ⁺	PAH
2,6-dinitrotoluene (a)	n.a	[M+H] ⁺	-	[M+H] ⁺	nitro-group
3-nitroaniline (a)	n.a	[M+H] ⁺	M+H	[M+H] ⁺	N-containing
acenaphthene	851.7	[M+H] ⁺	M+H	[M+H] ⁺	PAH
2,4-dinitrophenol	n.a	-	-	-	phenolic
4-nitrophenol	n.a	108 ([M+H] ⁺ ~72 %)	-	-	phenolic
dibenzofuran	n.a	[M+H] ⁺	M+H	[M+H+42] ⁺ ([M+H] ⁺ ~81 %)	O-containing
2,4-dinitrotoluene (a)	n.a	[M+H] ⁺	-	[M+H] ⁺	nitro-group
2,3,5,6-tetrachlorophenol(a)	n.a	[M+H] ⁺	-	-	phenolic
2,3,4,6-tetrachlorophenol(a)	n.a	[M+H] ⁺	-	-	phenolic

diethylphthalate	n.a	177 ([M+H] ⁺ ~9%)	M+H	[M+H] ⁺	ester
Fluorene	831.5	[M+H] ⁺	[M+H] ⁺	[M+H] ⁺	PAH
4-chlorophenylphenylether	n.a	[M+H] ⁺	-	[M+H+42] ⁺ ([M+H] ⁺ ~70 %)	halogenated
4-nitroaniline (a)	866.0	[M+H] ⁺	[M+H] ⁺	[M+H] ⁺	N-containing
4,6-dinitro-2-methylphenol (dinitro-o-cresol)	n.a	-	-	-	phenolic
N-nitrosodiphenylamine (diphenylamine)	n.a	[M+H] ⁺	[M+H] ⁺	[M+H] ⁺	N-containing
1,2-dDiphenylhydrazine (azobenzene)	n.a	[M+H] ⁺	[M+H] ⁺	[M+H] ⁺	N-containing
4-bromophenylphenylether	n.a	[M+H] ⁺	-	[M+H+42] ⁺ ([M+H] ⁺ ~68 %)	halogenated
hexachlorobenzene	n.a	[M+H] ⁺	-	-	halogenated
pentachlorophenol	n.a	-	-	-	phenolic
anthracene (a)	877.4	[M+H] ⁺	[M+H] ⁺	[M+H] ⁺	PAH
phenanthrene (a)	825.7	[M+H] ⁺	[M+H] ⁺	[M+H] ⁺	PAH
carbazole	940.0	[M+H] ⁺	[M+H] ⁺	[M+H] ⁺	N-containing
dibutylphthalate	n.a	149 ([M+H] ⁺ ~15 %)	[M+H] ⁺	[M+H] ⁺	ester
fluoranthene (a)	869.2	[M+H] ⁺	[M+H+57] ⁺ ([M+H] ⁺ ~95 %)	[M+H] ⁺	PAH
pyrene (a)	n.a	[M+H] ⁺	[M+H] ⁺	[M+H] ⁺	PAH
benzylbutylphthalate	n.a	91 ([M+H] ⁺ ~11 %)	[M+H] ⁺	[M+H] ⁺	ester
bis(2-ethylhexyl)adipate	n.a	[M+H] ⁺	[M+H] ⁺	[M+H] ⁺	ester
benzo(a)anthracene (a)	n.a	[M+H] ⁺	[M+H] ⁺	[M+H] ⁺	PAH
chrysene (a)	840.9	[M+H] ⁺	[M+H] ⁺	[M+H] ⁺	PAH
3,3-dichlorobenzidine	n.a	[M+H] ⁺	[M+H] ⁺	[M+H] ⁺	N-containing
bis(2-ethylhexyl)phthalate	n.a	149 ([M+H] ⁺ ~26 %)	[M+H] ⁺	[M+H] ⁺	ester
di-n-octylphthalate	n.a	149 ([M+H] ⁺ ~27 %)	[M+H] ⁺	[M+H] ⁺	ester
benzo(k)fluoranthene (a)	n.a	[M+H] ⁺	[M+H] ⁺	[M+H] ⁺	PAH
benzo(b)fluoranthene (a)	n.a	[M+H] ⁺	[M+H] ⁺	[M+H] ⁺	PAH

benzo(a)pyrene (a)	n.a	[M+H] ⁺	[M+H] ⁺	[M+H] ⁺	PAH
indeno(1,2,3-cd)pyrene (a)	n.a	[M+H] ⁺	[M+H] ⁺	[M+H] ⁺	PAH
dibenz(a,h)anthracene	876.0	[M+H] ⁺	[M+H] ⁺	M ⁺ , ([M+H] ⁺ ~64%)	PAH
benzo(g,h,i)perylene (a)	n.a	[M+H] ⁺	[M+H] ⁺	[M+H] ⁺	PAH

a The elution order was assumed to be the same as reported in^[94]

b m-cresol and p-cresol were not separated by the GC-column and oven program. Detectability was estimated by comparing proton affinities

8.2 Supporting Information: Parallel operation of electron ionization and chemical ionization using a single TOF mass analyzer

Mode switching time

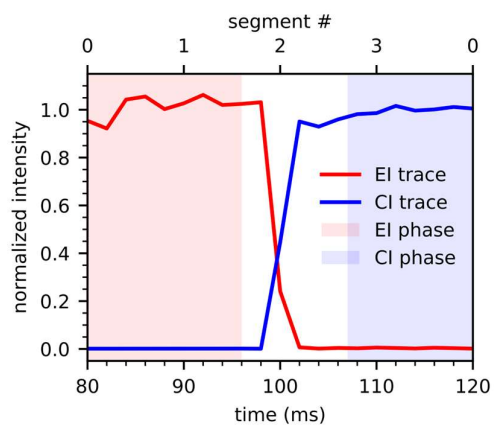


Figure 8.2.1: Time response of the switching ion optics between the CI and EI source. Single spectra were averaged to 500 Hz.

Experimental arrangement

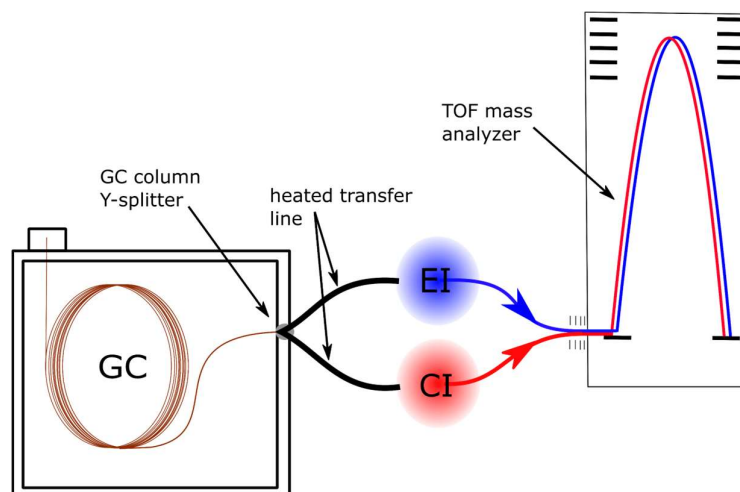


Figure 8.2.2: Instrumental arrangement.

C4 – C24 even carbon FAMES standard

Table 8.2.1: Compounds of the C4-C24 even carbon FAMES GC standard mix.

compound	retention time (s)	CI detected as	<i>m/z</i> of EI main ions
methyl butyrate	-	C ₅ H ₁₁ O ₂ ⁺	n.a.
methyl hexanoate	305	C ₇ H ₁₅ O ₂ ⁺	74, 87, 55
methyl octanoate	416	C ₉ H ₁₉ O ₂ ⁺	74, 87, 55
methyl decanoate	507	C ₁₁ H ₂₃ O ₂ ⁺	74, 87, 55
methyl laurate	587	C ₁₃ H ₂₇ O ₂ ⁺	74, 87, 55
methyl tetradecanoate	658	C ₁₅ H ₃₁ O ₂ ⁺	74, 87, 55
methyl palmitate	722	C ₁₇ H ₃₅ O ₂ ⁺	74, 87, 55
methyl octadecanoate	779	C ₁₉ H ₃₉ O ₂ ⁺	74, 87, 55
methyl arachidate	827	C ₂₁ H ₄₃ O ₂ ⁺	74, 87, 55
methyl docosanoate	869	C ₂₃ H ₄₇ O ₂ ⁺	74, 87, 55
methyl lignocerate	916	C ₂₅ H ₅₁ O ₂ ⁺	74, 87, 43

Retention time correlation

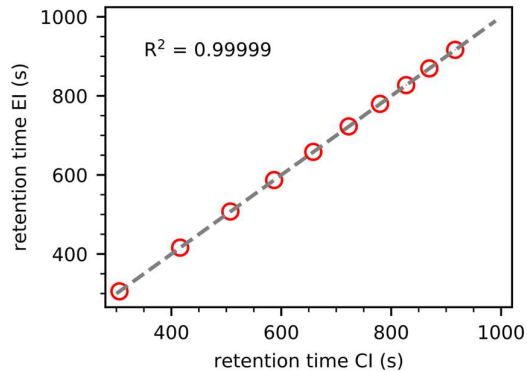


Figure 8.2.3: Linear regression of CI and EI retention times.

Peak shape comparison

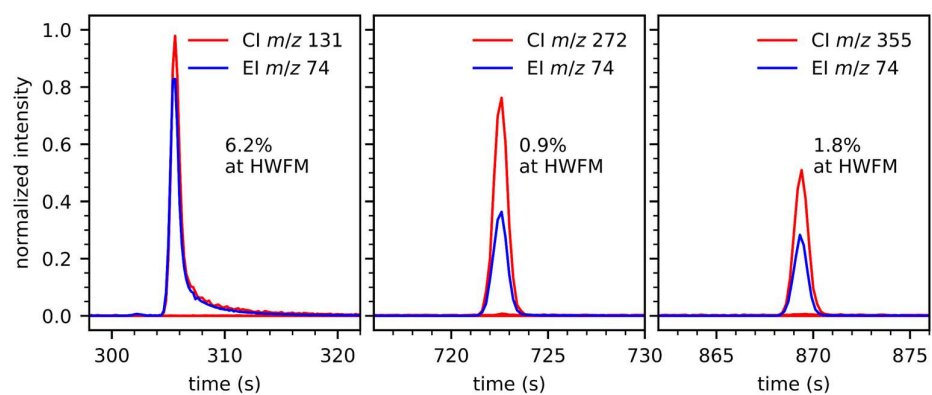


Figure 8.2.4: Peak shape comparison of different compounds of the FAMES GC standard. The relative peak with difference is measured at full width half maximum (FWHM) of the corresponding peaks.

Instrument detection limit (IDL) measurements

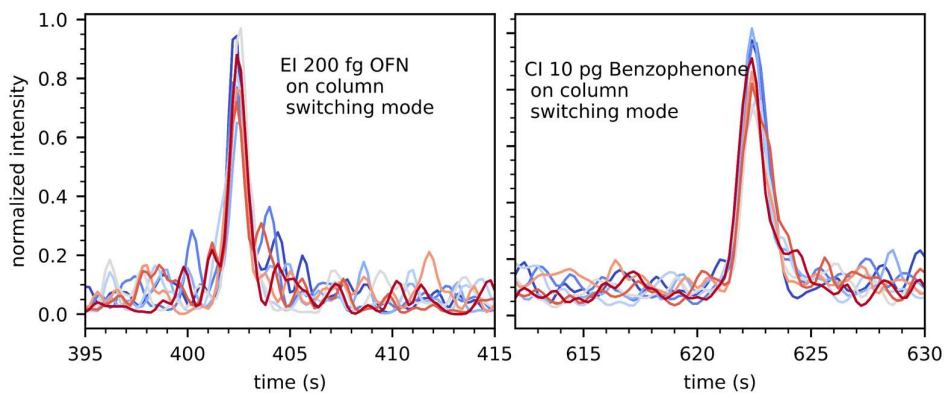


Figure 8.2.5: Nine repeated GC injections of benzophenone and octafluoronaphthalene for IDL calculations.

Custom ketone and aldehyde mix

Table 8.2.2: Compounds of the custom carbonyl mix.

compound	retention time (s)	CI detected as	m/z of EI main ions	Δ mass (ppm)	Δ isotopic ratio (%)	EI match
1-octen,3-one	430	C ₈ H ₁₅ O ⁺	70, 55	1.4	4.3	774
2-octanone	443	C ₈ H ₁₇ O ⁺	43, 58, 71	1.7	4.2	850
octanal	455	C ₈ H ₁₇ O ⁺	43, 44, 56	0.6	4.0	856
nonanal	556	C ₉ H ₁₉ O ⁺	57, 41, 43	-1.2	4.4	887
trans-2,cis-6- nonadienal	602	C ₉ H ₁₅ O ⁺	41, 69, 70	3.0	-0.3	n.a(a)
citronellal	602	C ₁₀ H ₁₉ O ⁺	41, 69, 95	3.7	2.2	n.a(a)
2-decanone	638	C ₁₀ H ₂₁ O ⁺	58, 43, 71	-0.7	4.8	865
2-undecanone	726	C ₁₁ H ₂₃ O ⁺	58, 43, 71	3.2	2.2	887
trans,trans-2,4- decadienal	746	C ₁₀ H ₁₇ O ⁺	81, 41, 39	-0.1	-4.2	n.a(b)
2-dodecanone	808	C ₁₂ H ₂₅ O ⁺	58, 43, 71	-3.7	-1.1	888
dodecanal	819	C ₁₂ H ₂₅ O ⁺		1.8	-1	914
2-tridecanone	885	C ₁₃ H ₂₇ O ⁺	58, 43, 71	2.4	3.5	882
benzophenone	987	C ₁₃ H ₁₁ O ⁺	105, 77, 182	-1.4	2.6	930

(a) Was not found using the NIST library due to strong co-elution.

(b) Was not found in the NIST library due to unknown reasons.

Table 8.2.3: Sum formulas generated with the common hetero atoms and an allowed mass difference of ± 10 ppm for the measured exact values of m/z 185.1907 and m/z 199.2052, respectively.

sum formula	exact mass	mass difference (ppm)	Δ isotopic ratio (%)
C ₉ ClH ₂₈ N ⁺	185.1905	-1.0	-11.4
C ₁₂ H ₂₅ O ⁺	185.1900	-3.6	-1.1
H ₂₉ N ₂ O ₈ ⁺	185.1918	6.4	842.0
C ₁₃ H ₃₆ N ₂ O ⁺	185.1888	-10.2	989.6
C ₁₀ H ₂₃ N ₃ ⁺	185.1886	-10.9	9.0
H ₁₅₄ N ₂ O ⁺	199.2056	2.0	475.6
C ₁₃ H ₂₇ O ⁺	199.2056	2.4	3.5
CCl ₃ H ₃₈ N ₂ O ⁺	199.2044	-3.7	545.2
C ₁₁ H ₂₅ N ₃ ⁺	199.2043	-4.3	18.8
C ₁₀ ClH ₃₀ N ⁺	199.2061	4.8	29.3

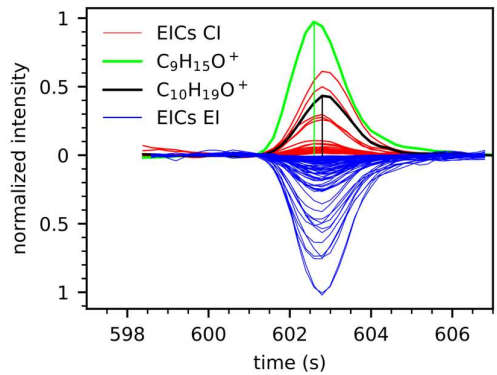


Figure 8.2.6: Chromatograms of co eluting compounds (*trans*-2,*cis*-6-nonadienal ($C_9H_{14}O$) and citronellal ($C_{10}H_{18}O$)).

Chromatograms of an EPA 8270 LCS mix

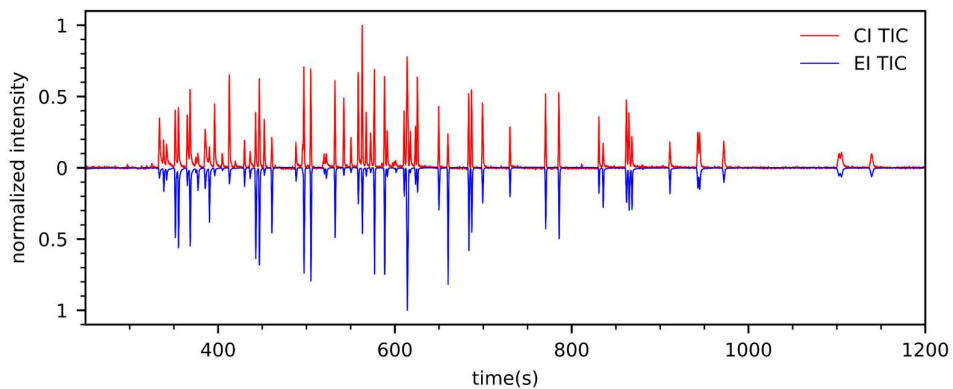


Figure 8.2.7: Chromatogram of a 2.5 ng spitless injection of an EPA 8270 LCS mix.

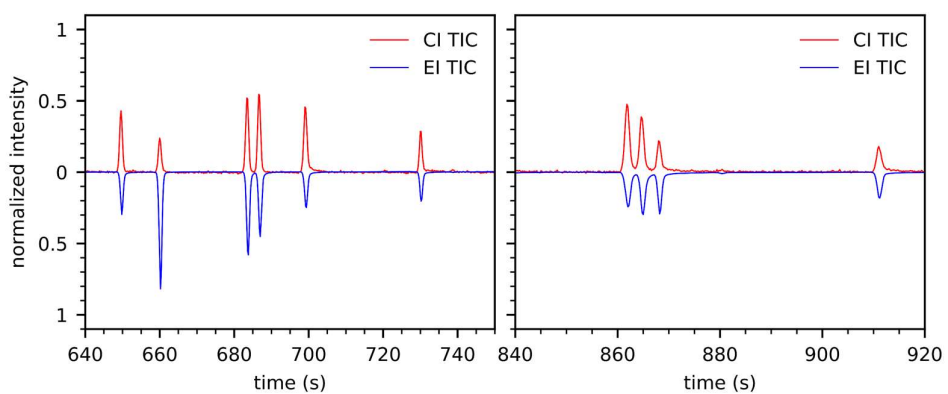


Figure 8.2.8: Enlarged chromatogram of the EPA 8270 LCS mix.

Additional example for improved compound identification

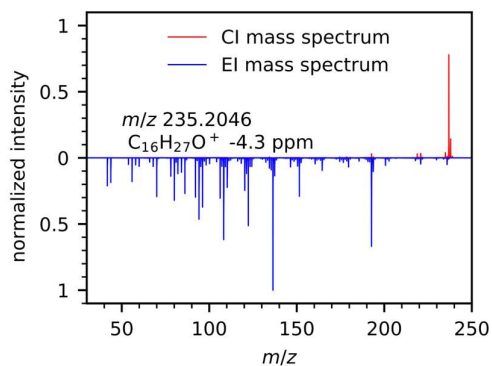
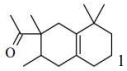
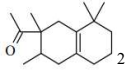
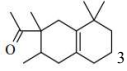
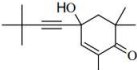
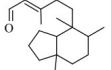
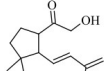
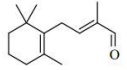
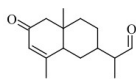
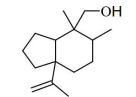
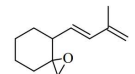


Figure 8.2.9: EI and CI mass spectrum of a chromatographic peak within the perfume sample at 1035 s.

Table 8.2.4: First compound suggestions of the fragment spectra library search in combination with the CI information for the mass spectra shown in Figure 8.2.9

structure	sum formula	m/z [M+H] ⁺	Δ mass (ppm)	Δ isotopic ratio (%)	EI match	probability (%)	RI
	C ₁₆ H ₂₆ O	235.2056	4.3	1.6	819	10.9	1649
	C ₁₆ H ₂₆ O	235.2056	4.3	1.6	817	9.2	1658
	C ₁₆ H ₂₆ O	235.2056	4.3	1.6	811	7.8	1664
	C ₁₅ H ₂₂ O ₂	235.1693	-150.5	8.3	778	6.8	n.a.
	C ₂₀ H ₃₂ O	289.2526	>1000	-18.6	762	3.8	n.a.
	C ₁₄ H ₂₂ O ₂	223.1693	>1000	15.9	747	2.9	n.a.
	C ₁₄ H ₂₂ O	207.1743	>1000	16.2	746	2.5	1584

	C ₁₅ H ₂₂ O ₂	235.1693	-150.5	8.3	746	2.2	2521
	C ₁₅ H ₂₆ O	223.2056	>1000	8.0	746	1.88	n.a.
	C ₁₄ H ₂₂ O	207.1743	>1000	15.9	743	1.74	n.a.

¹Isomere 2, ²Isomere 1, ³Isomere 3

The EI mass spectrum library search results for the EI mass spectrum given in Figure 8.2.9 shows probabilities of ~ 3-11 % for the first 6 suggestions. Experimental retention time information are not available for all compounds. The CI spectra reveals a dominant protonated molecule. The CI spectrum strongly indicates a sum formula of C₁₆H₂₆O via the given mass accuracy and isotopic pattern. Therefore, even suggestion with the same nominal mass can be excluded from the suggestion list.

8.3 Supporting Information: Gas chromatography coupled to time-of-flight mass spectrometry using parallel electron and chemical ionization with permeation tube facilitated reagent ion control for material emission analysis

Permeation tube temperature dependence of the reagent ion distribution

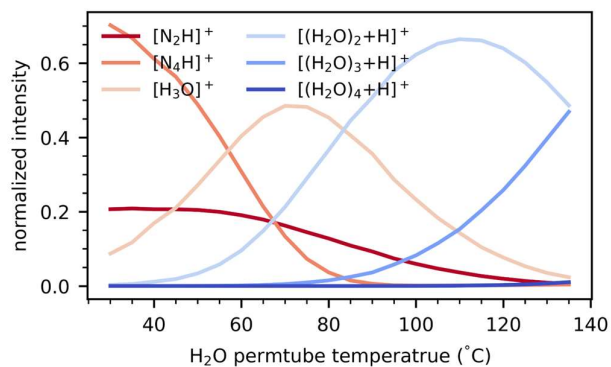


Figure 8.3.1: Dependence of the reagent ion distribution on the water filled permeation tube temperature.

Chromatograms of the material emission measurement

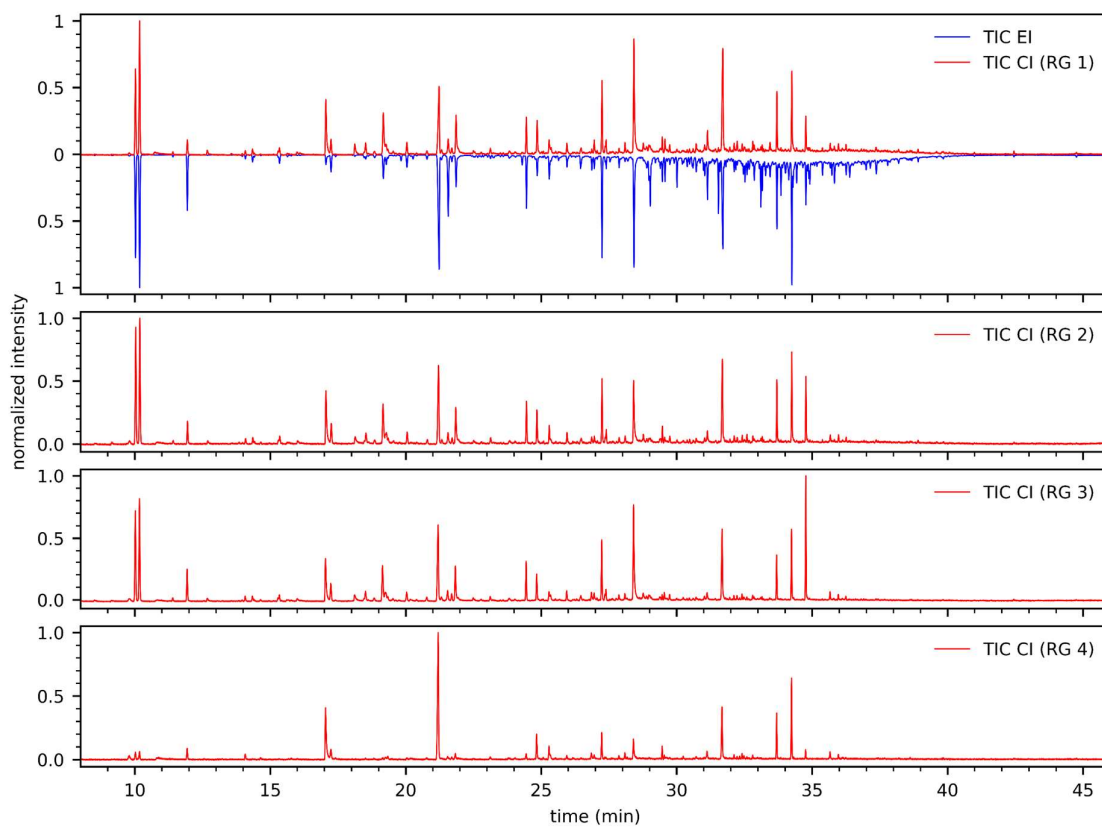


Figure 8.3.2: CI chromatograms of the artificial leather emission measured with dry N_2 (RG1), H_2O doped nitrogen at a permeation tube temperature of $85\text{ }^\circ\text{C}$ (RG2), H_2O doped nitrogen at a permeation tube temperature of $115\text{ }^\circ\text{C}$ (RG3), and H_2O/NH_3 doped nitrogen at permeation tube temperature of $85\text{ }^\circ\text{C}$ (RG4). The simultaneously recorded EI chromatograms were identical for each CI reagent run and are therefore displayed just once.

Mass Spectra for compounds of Figure 4.3.3B

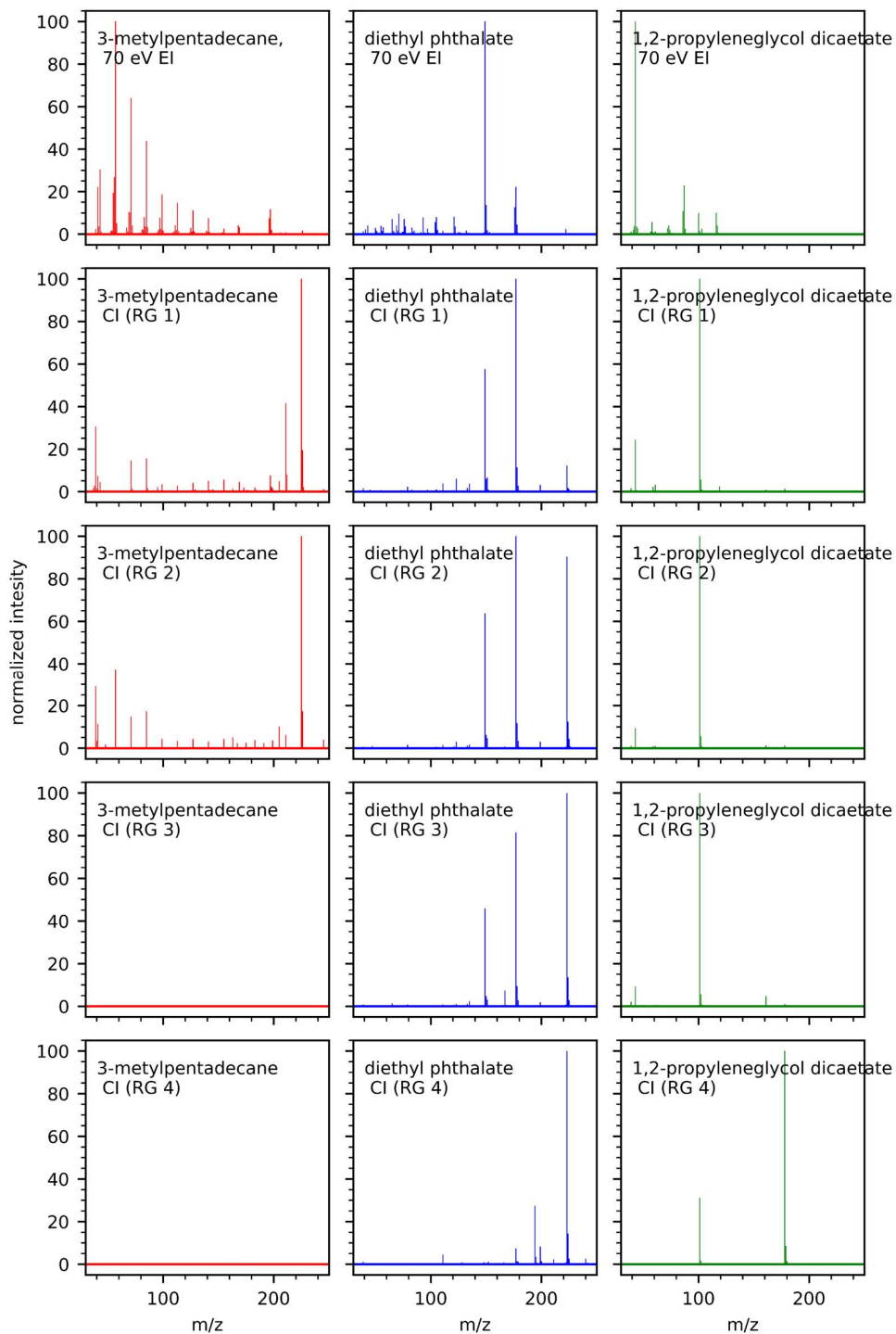


Figure 8.3.3: Mass spectra of diethyl phthalate, 1,2-propyleneglycol diacetate and 3-methylpentadecane recorded with EI and each CI reagent system.

Retention time indices

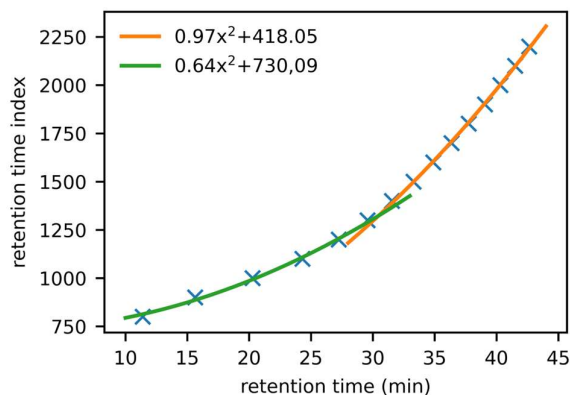


Figure 8.3.4: Retention time index function of the alkane standard for retention indices assignment.

NIST hybrid similarity search for compound 6 (Figure 4.3.6B)

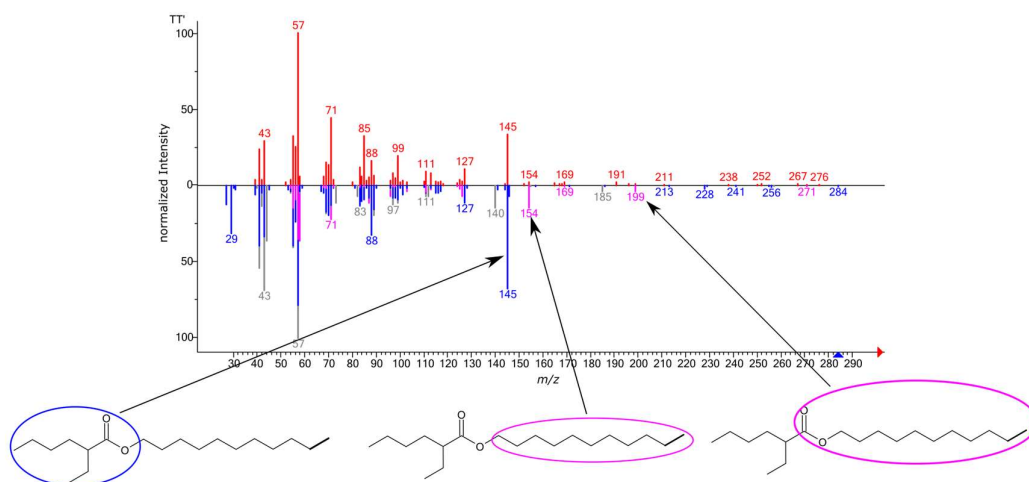


Figure 8.3.5. NIST hybrid similarity search results for compound 6 shown in Figure 5.3.6B. The measured spectrum is shown in red compared to the library spectrum in blue. Peaks present in the library spectrum but not in the measured spectrum are indicated in grey. The pink colored peaks assign signals that are present in the measured spectrum but not in the library spectrum and that additionally show a mass difference of 14 (CH_2 -group) with respect to the peaks indicated in grey.

CI spectrum of compound 7 (Figure 4.3.7A)

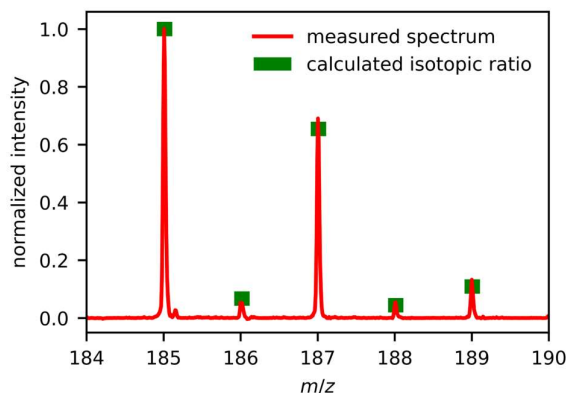


Figure 8.3.6: Isotopic pattern of $C_6Cl_2H_{11}O_2$.

Deconvolution of compound 8 (Figure 4.3.7.B)

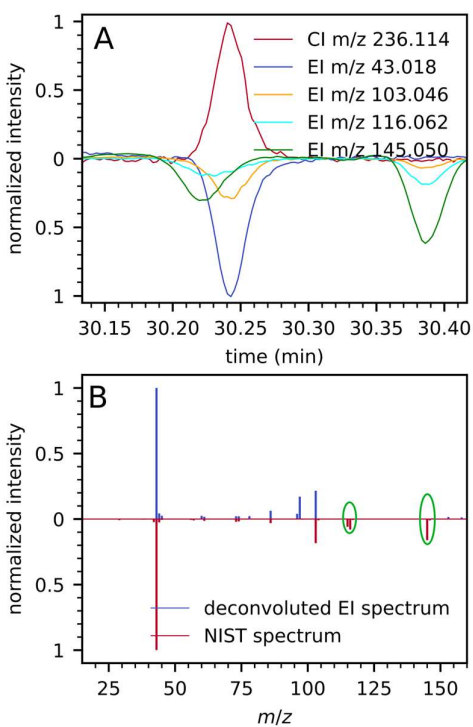


Figure 8.3.7: (A) Deconvoluted extracted ion chromatograms of triacetin showing a strong coelution on m/z 145.050 and m/z 116.062. (B) These mass signals are therefore lost in the processed and deconvoluted mass spectrum compared to the library spectrum.